DETERMINATION OF CONVECTIVE FILM COEFFICIENTS UNDER SIMULATED PYROLYSATE EVOLUTION

A THESIS

Presented to

The Faculty of the Division of Graduate

Studies and Research

By

Gregory L. Wedel

In Partial Fulfillment

of the Requirements for the Degree

Master of Science in Mechanical Engineering

Georgia Institute of Technology

August, 1974

DETERMINATION OF CONVECTIVE FILM
COEFFICIENTS UNDER SIMULATED
PYROLYSATE EVOLUTION

Approved:

P. Durbetaki, Co-Chairman

W. Wulff, Co-Chairman

L. Bangert

W. Black

Date approved by Co-Chairmen: 10/29/1974

ACKNOWLEDGMENTS

I would like to extend my sincere appreciation to Dr. Pandeli Durbetaki for his help, interest, and suggestions during the course of this thesis. I would also like to thank Dr. W. Wulff for this thesis problem and Dr. William Z. Black and Dr. Louis Bangert for their comments and concern.

I wish to express my appreciation to the School of Mechanical Engineering for the opportunity to conduct this research and to the faculty and staff for their invaluable assistance. I would also like to express my gratitude to Bob Acree for his many contributions throughout the development and finalization of this thesis.

I would also like to thank the National Science Foundation for its partial support during this investigation.

Special permission was received from the Division of Graduate Studies to vary the numbering system of tables and figures to meet the special requirements of this thesis.

To my wife, Jennifer, I extend my warmest and most sincere appreciation for her help, understanding, and continued support, without which this thesis would not have been possible.

TABLE OF CONTENTS

LIST OF TABLES

Table Page

LIST OF ILLUSTRATIONS

NOMENCLATURE

A	projected area
b	burner
Bi	Biot number
C	convection parameter
C_p	specific heat at constant pressure
D	burner diameter
d	hydraulic diameter of cloth thread interstices
E	activation energy
ex	Reynolds number exponent
Fo	Fourier number
$F_{s\infty}$	average view factor with respect to its environment
g	gravity
Gr	Grashof number
$h_1, h_2, 2\bar{h}$	convective film coefficient
Δi	reaction enthalpy
K	permeability
k	thermal conductivity
k_g, k_d	frequency factor
L	burner-cloth spacing
ℓ	characteristic linear dimension
M	mesh number
$\dot{m}$	mass flow rate
n	reaction order

Nu	Nusselt number
P	porosity
p	pressure
Pr	Prandtl number
q*	normalized heat flux
q	conductive heat flux, volumetric flow rate
R	screen radius, universal gas constant
Re	burner Reynolds number
$(Re)_o$	injection Reynolds number
r,θ	coordinates
T	temperature
U	specific internal energy
V	velocity
w	injection parameter
x,y,z	coordinates
α	fraction of open area, absorptance
β	coefficient of thermal expansion
δ	cloth thickness
ε,λ	mass fraction
μ	dynamic viscosity
ν	kinematic viscosity
ρ	density
ρδ	mass per unit area
π	scaling group
σ	Stephan-Boltzmann constant
θ	dimensionless temperature

$\bar{\bar{\tau}}$ stress tensor

τ time

ϕ stoichiometric equivalence ratio

Subscripts

a ambient

b burner

c calibration

d desorption

f flame

g gasification

i ignition

l laboratory

m mean

mf mean film

o injection, initial

p porosity

r reference

s screen or fabric

∞ rear surface free stream

1 front cloth surface

2 rear cloth surface

Superscripts

- nondimensional

* normalized

° ideal

$\rightarrow$ vector

SUMMARY

This thesis was part of a research endeavor undertaken at the Georgia Institute of Technology, School of Mechanical Engineering, in an effort to produce relevant and reasonable criteria for fabric flammability standards.

The primary objective of this thesis is to describe fabric flame interaction through determination and evaluation of the convective film coefficients on convectively heated, fine mesh wire screens, with simulated pyrolysate evolution. The screens were exposed to a premixed flame by the Convective Ignition Time Apparatus (CITA) formerly used for determining the ignition time of fabrics. The same geometric configuration was used in the film coefficient determination tests as was used in the determination of fabric ignition time.

The set of process parameters investigated consists of the screen-burner separation distance, injection air temperature and flow rate, screen mesh, and the heat flux intensity. The results of these tests are given in dimensionless form using a reference temperature to evaluate the transport properties.

These convective film coefficients were then used to predict the ignition time of fabrics, and these times were compared with the ignition times of the fabrics measured with CITA.

This work was supported by a grant from the National Science Foundation.

CHAPTER I

INTRODUCTION

Significance of Flammability Research

Per capita, the United States leads all other major industrialized nations in both fire deaths and economic losses related to fires. The number of lives lost annually in fires has climbed to nearly 12,000 and the cost of fires has been conservatively estimated at over $11 billion [1].* Of these losses, 4,000 lives, $250 million and 200,000 injuries have been associated with fabric fires [2].

Two of the major contributors to this poor fire record have been cited as ignorance and indifference, both on the private level and on the professional level. For this reason, the fire problem has been attacked from two directions: education and regulation. One of the first major Federal efforts in this direction was the Flammable Fabrics Act of 1953 which was later amended in 1967. Under this act, authorization was given for research in the area of fabric flammability. The research was initiated in November, 1969, and monitored through December, 1972, by the Government-Industry Research Committee on Fabric Flammability (GIRCFF), the membership representing the National Science Foundation,

*The numbers in brackets refer to the references given in the Bibliography.

the National Bureau of Standards, the American Textile Manufacturers Association, the Cotton Council of America, and the Man-Made Fiber Producers Association [3]. Under the auspices of this committee, the Georgia Institute of Technology received sponsorship for its research from the National Science Foundation (NSF) under the RANN program (Research Applied to National Needs), Grant No. GK-27189. Since January, 1972, the research has been continued under the sponsorship and administration of NSF as Grant No. GI-31882 [3,4].

Previous Efforts and Accomplishments

In order that relevant and reasonable standards may be established for fabric flammability, it is necessary to relate the behavior of a fabric under laboratory test methods to the hazard that it presents in actual use.

It was first proposed by Tribus [5] that a fabric or garment fire hazard be related through the partial probabilities associated with all the events leading from fabric certification via all conceivable hazardous situations to burn injury. These intermediate events include the stochastic human behavior as well as the deterministic material response to the fire.

Two of these partial probabilities are of primary importance and have been selected by GIRCFF to be determined through research endeavors. They are: (i) the probability

of ignition for a given exposure, P(I/E), and (ii) the probability of a burn injury for a given ignition, P(B/I).

The efforts at Georgia Tech have been directed toward the determination of the first probability, P(I/E). This probability can be expressed in terms of the ratio of the exposure time to the fabric ignition time [4]. An experimental and analytical program, initiated in November, 1969, has been carried out under NSF Grants GK-27189 and GK-31882 to predict the fabric ignition time as a function of exposure parameters and fabric properties.

Through this research, the thermophysical properties required in the analysis of fabric ignition have been determined for the twenty fabrics selected by GIRCFF. A modeling analysis was developed to predict the fabric ignition times and these times were then compared to those determined experimentally for both the radiative and convective heating modes.

The convective heat transfer coefficients used in this analysis were evaluated from measurements using an inert 200 mesh wire cloth exposed to a convective heat source. The convective heat source was a premixed methane-air flame which had been characterized by both the temperature profiles and CO_2 and O_2 concentration profiles [6]. The screen, which represented an average fabric porosity, was made to form one leg of a thermocouple junction and the temperature response of this screen was used to determine the convective heat

transfer rate to the fabric.

However, ignition times predicted with these measured convective film coefficients were shorter than the measured ignition times. Much of the discrepancy has been attributed to the insulating effect of the pyrolysate produced by the desorption and gasification of the fabric. These effects were not accounted for in the inert model, nor were they simulated in the determination of the heat transfer coefficients.

The porosity has also been cited by Heskestad as a major parameter affecting the convective heat transfer to fabrics [7]. The porosity of the 20 fabrics selected by GIRCFF has been measured by Factory Mutual and reported in Reference [8].

The inert heat transfer model was expanded to include the effects of gasification in order that a more accurate prediction of fabric ignition time be made [3], and now the heat transfer coefficients must be made to account for the possible effects of transpiration. Consideration will now be given to previous efforts in similar endeavors.

The experimental determination of the convective heat transfer coefficients is generally accomplished in one of four ways. The first is primarily used to determine convective cooling rates. A guarded hot plate is subjected to the external flow conditions being investigated and the power input to the plate, the plate temperature, and the

temperatures are used to determine the heat transfer coefficient.

The second method involves the use of a heat flux meter or "circular foil heat-flow meter" [9]. The heat flow meter is mounted in the body with its sensing surface flush with the surface across which the rate of heat transfer is to be measured. The emf output of the meter is calibrated to give the heat flux directly, from which the film coefficient may be determined.

The third method is used to determine convective heating rates with transpiration cooling [10]. The net heat transfer rate is calculated from measuring the steady state coolant injection flow rate and the excess surface temperature above the environmental temperature.

A fourth method which is frequently employed to determine the transient convective heat transfer coefficient involves the use of a Mach-Zehnder interferometer [11]. The operation of the interferometer is based on the refraction coefficient of the fluid changing with temperature. Interference fringes are produced by this instrument as the result of temperature gradients in the fluid. Hence, the spacing of these fringes is a direct measure of the temperature distribution.

However, due to the large temperature differences encountered in heat transfer from a turbulent methane flame and the requirement of low injection flow rates, none of the

above methods are feasible for this study. The first method excludes the possibility of convective heating. The second method does not allow gas injection at the heat flux meter surface. The third method generally requires a spherically symmetric geometry to avoid severe end effects. Finally, the last method mentioned is practical only when small temperature differences are encountered, when the level of turbulence is low, and when there is no mass injection.

Consequently, the standard techniques of determining the convective heat transfer are not applicable in this study. Fortunately, the previously mentioned technique was developed [6] in which a fine mesh wire cloth is made to form a thermocouple junction. The cloth simulates a fabric surface while allowing for gas injection. Furthermore, the cloth is thermally thin and the temperature gradients across the cloth width can be neglected. The temperature rise of the cloth can be monitored and used directly to determine the convective film coefficient. This method will be employed in this investigation.

Having investigated methods of determining the film coefficient experimentally, consideration will be given in the next section to results of other investigations of similar external flow configurations.

Heat Transfer of Impinging Air Jets

Since the thermodynamic and transport properties of

the combustion products of methane are closely approximated by those of air [7] and, since the combustion process is complete at less than one centimeter from the burner, the external flow may be considered to be that of a hot air jet impinging normally on a plane surface. In this consideration the possible difference in the temperature distribution of the premixed flame and the hot air jet is neglected but the qualitative comparison of the heat transfer results is allowed.

The heat transfer of impinging air jets has received extensive investigation both for circular jets [12,13,14,15, 16,17] and for slot jets [13,16]. These results will be briefly discussed.

In the above studies, the external flow is described by the Reynolds number

$$Re = \frac{\rho VD}{\mu} \tag{1}$$

in which the characteristic velocity V is generally taken to be the jet exit velocity and the characteristic length D is taken to be the nozzle diameter or the slot width. The heat transfer is then correlated in terms of the Nusselt number

$$Nu = \frac{hR}{k} \tag{2}$$

in which the characteristic length R is taken to be the distance from the stagnation point.

The heat transfer rates were found to invariably increase with jet exit velocities. However, no such monotonic dependence of the heat transfer rate on nozzle-to-plate spacing L was reported. The heat transfer rates were found to both increase and decrease with L depending on the jet diameter, the jet velocity, and the turbulence level. For circular jets, the local heat transfer rate has been reported to reach a minimum at about L/D = 0.5. At this spacing, one is dealing with a "wall jet" rather than an impinging jet [15]. A maximum heat transfer rate is then found to occur at L/D between 6 and 8, [15,17,18], and the rate decreases systematically for larger L/D. The second trend (a maximum occuring at L/D $\simeq$ 7) is found with both slot jets and circular jets, but only at large Reynolds numbers. As the jet Reynolds number decreases, this peak begins to flatten out. For a Reynolds number less than about 1000 [17,18], the flow is laminar and the Nusselt number is constant for nozzle-to-plate spacing L shorter than the potential core and diminishes in proportion to L^{-1} beyond that [17,19]. The deviation of the behavior of other jets from this pattern is ascribed to the high levels of turbulence inherent in the spreading of submerged jets.

An accurate description of these flow conditions, even for the low Reynolds numbers (less than 1000) encountered

in this study, is complicated by several coupled processes. The first of these is that of air drag. There is an entrainment of air with the associated decrease in the mixing zone velocity. The decrease of centerline velocity in the developed profile has been reported to be proportional to 1/L [20] for both laminar and turbulent circular jets. (However, this proportionality is valid only for spacings greater than the length of the potential core. As was pointed out by Daane [16], for nozzle-to-plate spacing less than three nozzle diameters neither the center-line velocity of the jet nor its size vary as a simple function of the spacing.) Since this study is concerned with the spacing less than three jet diameters, i.e. within the potential core region, the simple 1/L correlation is not directly applicable.

The large temperature differences which exist between the hot gases and the ambient air (~1000°C) give rise to two additional effects. The first of these is the decrease in jet bulk temperature. A hot jet discharging into a cooler atmosphere experiences a lowering of its temperature due to mixing, both before and after impingement. The center-line temperature excess of an axially symmetric hot jet was found to decrease to half its initial value in only ten jet diameters [19,21]. Accordingly, the effective temperature difference for heat transfer now also depends on the distance between nozzle and plate. (In the present study, the burner-

to-cloth spacing is less than three burner diameters, and the excess temperature drop was less than 15%.)

The second effect of the temperature difference is the buoyancy force. These forces are often negligible with respect to the inertia forces since the jet velocities normally encountered are relatively large. The velocities under consideration in this study are much lower than those considered in many of the above references and the buoyancy effects can not be neglected, except at close proximity to the nozzle.

The level of turbulence in the external flow is also a significant parameter in determining the heat transfer characteristics of impinging jets [17,19]. The turbulence level has been used to account for secondary peaks in the heat flux profiles about the stagnation point.

To account for these coupled processes associated with the nozzle-to-plate spacing, the external flows are generally described by one of two methods. In the first method, one attempts to relate the heat transfer to an approach velocity [15,19]. This method involves the use of a semi-empirical relation for the velocity profile and is generally used for $L/D>8$.

In the second method of correlation, one uses the nozzle exit flow conditions as a basis for the Reynolds number [14,16,17]. The effects associated with the nozzle-to-plate spacing are then described using the dimensionless

distance L/D. The shortcoming of this method is that the L/D effect is not established independently of the heat transfer rate. However, the jet exit Reynolds number and the ratio L/D uniquely describe the external flow conditions without requiring the determination of the approach velocity. Furthermore, the Reynolds number based on jet exit velocity can be determined within 2.2% using the mixture mass flow rate of the methane and air, whereas the Reynolds number based on the approach velocity can be determined within 6%, at best, using stagnation pressure measurements. Consequently, the second method of correlation will be employed in this investigation.

Thesis Objectives

Decomposition gases emerging from the heated surface of a cellulosic material effectively protect this surface from impinging gas flames. The material porosity, however, may allow some of the impinging gas flames to bleed through to the unexposed side, thereby increasing the rate of heat transfer to the material.

The first objective of this thesis is to describe the fabric-flame interaction through the determination and evaluation of the film coefficients on fine mesh wire screens under simulated fabric porosity and pyrolysate evolution, and to express these results in terms of the governing nondimensional parameters. The second objective is to use

the results of these tests to predict the ignition times of fabrics exposed to the same heat flux source, and to compare these times to the fabric ignition times measured using the Convective Ignition Time Apparatus (CITA).

The fabric geometry is simulated by inert stainless steel wire cloths. The action of the emerging pyrolysates is simulated through the injection of preheated air, and the effect of fabric porosity is simulated by the suction of air through the screen.

Since the ultimate objective of this thesis is the prediction of fabric ignition times, the ranges of process parameters to be covered by this thesis are determined by fabric exposure conditions encountered in actual garment use. Specifically, the same laboratory exposure conditions will be investigated in this thesis as were used in the experimental determination of fabric ignition times under convective heating [3].

CHAPTER II

ANALYSIS

As outlined in the thesis objectives, the interaction between the fabric and flame is to be determined through the use of fine mesh wire screens under simulated fabric porosity and pyrolysis. However, dynamic similarity between the film coefficient determination tests and the fabric ignition time measurements is not possible. Consequently, the change in the film coefficient due to the variations in aerodynamic boundary conditions must be determined. This is achieved through modeling analysis.

The modeling analysis, then, is used (1) to describe the convective heating of a fabric and a screen, to derive the governing dimensionless groups which correlate the heat transfer data and to provide criteria for similarity between the fabric and the screen tests, (2) to introduce the fabric porosity and decomposition rate into the description of the heat transfer process, and (3) to predict the ignition time of fabrics in terms of the material properties and convective heating conditions.

The phenomena associated with the convective heating of a fabric are first presented qualitatively in the formulation of the problem. Secondly, the equations which

describe the fabric-flame interaction are presented along with their associated boundary conditions. Finally, a summary is presented of the governing equations describing the convective heating of a fabric and the closed form solutions to these equations.

Problem Formulation

During the fabric ignition time measurements under convective heating, the primary mode of heat transfer to and from the fabric was convection: forced convective heating of the fabric front surface and natural convective cooling of the fabric rear surface. The interaction between the heated fabric surface and the environmental gases is described in terms of convective film coefficients.

To assess both the heat transfer in the screen tests and the heat transfer in the fabric ignition time tests, the overall convective heat transfer is described by two film coefficients: one for the cloth rear surface, h_2, and a second for the cloth front surface, h_1. These two coefficients are not equal and their respective heat fluxes depend on different free stream temperatures. Specifically, the environmental temperature for the forced convective heating of the front surface is the free stream gas flame temperature, T_f, while the environmental temperature for the natural convective cooling of the rear surface is the ambient temperature T_∞.

Two of the phenomena associated with the convective heat transfer to a fabric are the fabric pyrolysis and fabric porosity. These phenomena are discussed in the following paragraphs.

First, it is noted that decomposition gases emerging from the heated surface of cellulosic materials can be effective in protecting the surface from impinging gas flames (or from convective cooling during radiative heating). This effect has been cited as a major contributor to the error of predicted fabric ignition times based on film coefficients obtained from an inert body [22].

The second phenomenon occurs as the gas flames impinge on the fabric surface and flare out radially from the impingement point. A portion of the impinging flame gases bleed through the fabric to the unexposed side [7]. The rate at which these gases bleed through the fabric is proportional to the pressure differential exerted by the impinging flame gases, and the perfusion greatly augments the heat transfer.

A schematic presentation of the fabric-flame interaction and the coordinate system used in this analysis is shown in Figure 1. Three regions are considered in this analysis. Region (1) encompasses the premixed flame between the burner and the fabric, Region (2) is the porous fabric, and Region (3) is the environment above the rear fabric surface. Surface I is the interface between Regions (1) and

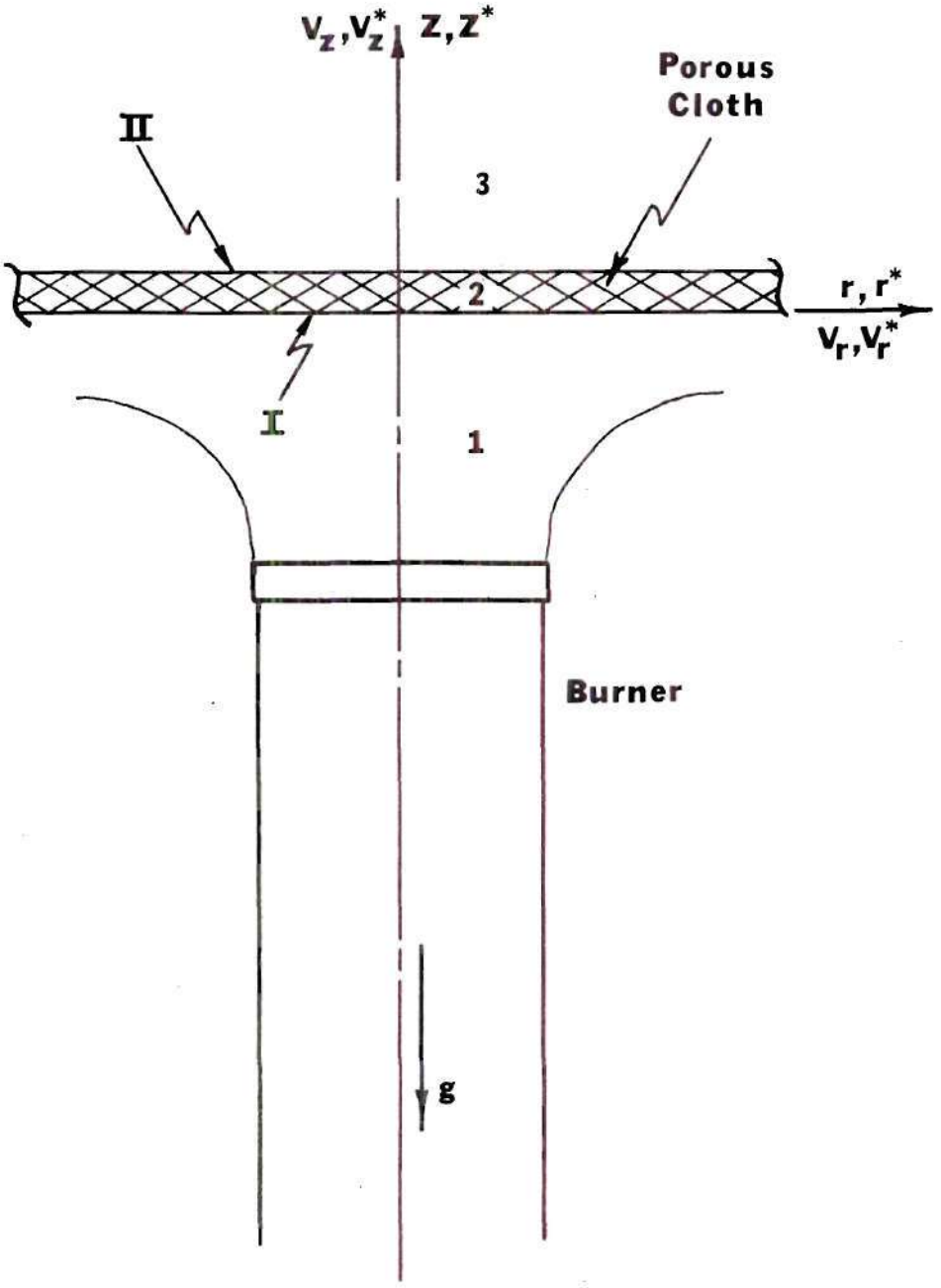

Figure 1. Model of Fabric-Flame Geometry for Heat Transfer Analysis

(2) and Surface II is the interface between Regions (2) and (3).

Governing Equations

The description of the convective heating of a porous cloth surface and the associated pyrolysis and flame penetration is presented in this section along with the derivation of the governing dimensionless groups. These dimensionless groups correlate the heat transfer data and provide criteria for similarity between the fabric ignition time measurements and the film coefficient determination tests.

The equations describing the convective heating of Surface I are first derived and the associated boundary conditions are specified. Specification of these boundary conditions requires the solution to the mass and momentum conservation equations for Region (2) and an analytical correlation which describes the convective cooling of the rear surface of the fabric. The governing equations and boundary conditions are normalized to form the similarity parameters which relate the film coefficient to the dimensionless groups accounting for flame dynamics, fabric pyrolysis, and flame penetration. The conservation of energy equation for the convective heating of a fabric is then presented, and a closed form solution which is used in the evaluation of fabric ignition time measurements is given.

Convective Heat Transfer Equations

The conservation equations for Region (1) shown in Figure 1 are first given in their general form and then specialized to the axisymmetric geometry of the flame-fabric system and to steady flow. For the range of parameters of interest in this study, the Mach number and the Eckert number are much less than one. Consequently, the flow is considered to be incompressible.

Momentum and Mass Conservation. The conservation of momentum equation is written as

$$\rho \frac{\partial \vec{V}}{\partial \tau} + \rho(\vec{V}\cdot\nabla)\vec{V} = -\nabla p - \nabla\cdot\bar{\bar{\tau}} + \rho\vec{g} \tag{3}$$

where ρ is the mass density, p is the pressure, $\bar{\bar{\tau}}$ is the stress tensor, $\vec{g}$ is the gravitational acceleration, and $\vec{V}$ is the velocity vector.

The cloth surface is perpendicular to the burner axis and hence the flow is axisymmetric and

$$\begin{aligned} V_\theta &= 0 \\ \partial/\partial_\theta &= 0 \end{aligned} \tag{4}$$

The momentum and mass conservation equation for steady, incompressible, axisymmetric flow is then written as

$$\rho(\vec{V}\cdot\nabla)\vec{V} = -\nabla p + \mu\nabla^2\vec{V} + \rho\vec{g} \tag{5}$$

where μ is the dynamic viscosity of the fluid.

Energy Conservation. The conservation of energy equation is written as

$$\frac{\partial}{\partial \tau}(\rho U+\frac{1}{2}\rho V^2)+\nabla\cdot(\rho U\vec{V}+\frac{1}{2}\rho\vec{V}V^2) = -\nabla\cdot[(p\vec{V}+\overline{\overline{\tau}}\cdot\vec{V})+\vec{q}]+\rho\vec{g}\cdot\vec{V} \quad (6)$$

where U represents the local specific internal energy of the gases, and $\vec{q}$ is the heat flux vector. There are no reactions with thermal effects taking place in Region (1) and therefore the thermal generation term has not been included. Neglecting the terms of mechanical energy with respect to the terms of thermal energy and neglecting the viscous dissipation, the conservation of energy equation is written for steady, incompressible axisymmetric flow as

$$\rho C_p(\vec{V}\cdot\nabla T) = k\nabla^2 T \quad (7)$$

in which $\vec{q}$ is expressed in terms of temperature gradients using the Fourier law and the specific heat at constant pressure C_p and thermal conductivity k of the gases are mean values.

Boundary Conditions. The boundary conditions for the conservation equations are, for the porous slab

$$
\left.
\begin{array}{ll}
\text{at } z = 0 & V_r = 0 \\
 & (\rho V_z) = (\rho V_z)\big|_{z=0} \\
 & -k \left.\frac{\partial T}{\partial z}\right|_{z=0} = \bar{h}_1 (T_f - T_s) \\
\text{at } z = \delta & -k \left.\frac{\partial T}{\partial z}\right|_{z=\delta} = \bar{h}_2 (T_\infty - T_s)
\end{array}
\right\} \qquad (8a)
$$

for the external flow

$$
\left.
\begin{array}{ll}
\text{at } \left\{ \begin{array}{l} z = -L \\ 0 \leq r \leq D/2 \end{array} \right. & V_r = 0 \\
 & V_z = V_b \\
 & T = T_f \\
\text{at } z = \infty & T = T_\infty
\end{array}
\right\} \qquad (8b)
$$

where $\bar{h}_1$ is the effective film coefficient for the front surface, $\bar{h}_2$ is the effective film coefficient for the rear cloth surface, r and z are the radial and axial coordinates, respectively, as defined in Figure 1, V_r is the radial component of the velocity vector, V_z is the axial component of the velocity vector, k is the thermal conductivity of the gases, T is the ambient temperature, and V_b is the burner exit velocity. For porous cloths which are heated in depth by the perfusion of gas flames, the axial temperature gradients are small [4] and are neglected. Hence, a single

cloth temperature T_s is used for both the front and rear surfaces of the fabric.

Two of these above boundary conditions will now be specified. First, the unknown mass flux at the porous boundary, $(\rho V_z)|_{z=0}$, is related to the known fabric porosity and decomposition rate through the momentum and mass conservation equations for Region (2). (The energy conservation equation for this region is given later in this chapter in conjunction with the fabric ignition time predictions.) Secondly, the natural convective heat transfer from the rear surface of the fabric, $h_2(T_s-T_\infty)$, is described using analytical and empirical correlations from the literature.

The mass and momentum conservation equations for Region (2) are simplified and then combined to form an expression for the mass flux at Surface I in terms of the porosity and decomposition of the fabric.

The first term of the mass conservation equation

$$\partial\rho/\partial\tau + \nabla\cdot\rho\vec{V} = 0 \qquad (9)$$

represents the rate of mass accumulation and is described here by an nth order Arrhenius decomposition law

$$\partial\rho/\partial\tau = -(\rho_o\delta)\varepsilon_g \dot{\lambda}_g/\delta \qquad (10)$$

where δ is the effective cloth thickness, $\rho_o\delta$ is the original mass per unit area of the fabric, ε_g is the fraction of original mass that participates in the gasification reaction and λ_g is the reacted mass fraction of the completed reaction and $\dot{\lambda}_g$ is the reaction rate given by

$$d\lambda_g/d\tau = k_g(1-\lambda_g)^{n_g} \exp(-E_g/RT_s) \tag{11}$$

where k_g is the frequency factor, n_g is the reaction order, and E_g is the activation energy. Substituting equation (10) into (9) and neglecting the mass flux within the cloth in the radial and angular directions, the mass conservation equation reduces to

$$\partial(\rho V_z)/\partial(z/\delta) = (\rho_o\delta)\varepsilon_g \dot{\lambda}_g \tag{12}$$

Integrating this expression from 0 to a position (z/δ) less than 1 gives the conservation of mass equation for a decomposing solid

$$\rho V_z = (\rho V_z)|_{z=0} + (\rho_o\delta)\varepsilon_g \dot{\lambda}_g(z/\delta) \tag{13}$$

The momentum conservation equation for the flow through a porous solid is [23]

$$\rho \frac{D\vec{V}}{D\tau} = -\nabla p - \rho\vec{g} - \vec{F}_D \tag{14}$$

where the viscous term is expressed by the frictional drag per unit volume $\vec{F}_D$. From Darcy's experiments, it is shown that for very slow flows dominated by viscous forces, the inertia terms are negligible

$$\rho \frac{D\vec{V}}{D\tau} = 0 \tag{15}$$

and the frictional drag is proportional to the velocity $\vec{V}$

$$\vec{F}_D = \frac{\mu}{K} \vec{V} \tag{16}$$

where K is the average permeability of the porous solid. Then, for one dimensional, steady, laminar flow, the conservation of momentum equation is

$$\rho V_z = -\rho K(\partial p/\partial z + \rho g)/\mu \tag{17}$$

and this equation is known as the Darcy law. The gravitational term is less than 2% of the total driving potential and is neglected. Equations (13) and (17) are combined and integrated over the cloth thickness δ to obtain the mass flux across Surface I

$$(\rho V_z)\big|_{z=0} = \rho K(p_o - p_s)/\mu\delta - (\rho_o \delta)\varepsilon_g \dot{\lambda}/2 \qquad (18)$$

where p_o is the absolute pressure at $z = 0$ and p_δ is the absolute pressure at $z = \delta$ (barometric pressure). Depending on the relative magnitudes of the two terms on the right hand side of the equation (18), the mass flux at surface $z = 0$ may be positive, negative, or zero.

The use of the simple form of Darcy's law is restricted to cases in which the inertia effects of the interstitial flow through the cloth are negligible with respect to the viscous effects. In general, this occurs when the Reynolds number based on the characteristic diameter

$$Re_d = \rho V d/\mu \qquad (19)$$

is less than 1 [24]. The best choice for the diameter d is the hydraulic diameter of the flow passage formed by the cloth threads or screen wires. Using this diameter d, $Re_d << 1$ so that the flow is laminar. Furthermore, the deviations from laminar behavior are negligible for $Re_d < 10$ for screens and less than 10% for the fabric porosities reported by Factory Mutual [8] for $Re_d < 1.2$. Consequently, the mass flux at the boundary $z = 0$ can be expressed by equation (18).

The natural convective heat transfer from the rear surface of the fabric, $\bar{h}_1(T_s - T_\infty)$, is described using

analytical and empirical correlations from the literature. These correlations are described and summarized in the following paragraphs. The domain of interest is Region (3) shown in Figure 1.

The fabric pyrolysis and gas flame perfusion produce a mass flux out of the rear surface of the fabric. This flow disrupts the natural convection currents and influences the convective cooling rate.

It is therefore desired to obtain a solution to the natural convection problem with mass transfer at the boundary, which, in the limit as the mass flux approaches zero, reduces to the solution of the problem describing a solid boundary.

The limiting case, that of no mass injection, is analyzed using the empirical correlations of Fishenden and Saunders [25]. The correlations for the case of free convective heat transfer with no mass transfer from horizontal and vertical surfaces are identical for a Prandtl number of .645 and differ by less than 1.6% over the entire Prandtl number range of interest in this study [25,26]. Assuming that there is a similarly close correlation between the heat transfer from horizontal and vertical plates with mass transfer, the analysis of Rohsenow and Hartnett [27] for vertical surfaces can be employed. This analysis treats the constant fluid property problem of free convection from an isothermal vertical plate with uniform mass injection. The

solution involves the approximation of local similarity, i.e. conditions at a given location are not severely influenced by conditions upstream. This assumption appears reasonable since the solution not only reduces to the correlation given by Fishenden and Saunders for zero mass injection, but also closely approximates the solutions for both small mass injection rates [28] and large mass injection rates [29].

The numerical solution obtained by Rohsenow and Hartnett is used in this thesis by fitting a polynomial through the numerical solution presented in Reference [27] to obtain a correlation of the form

$$Nu_{x,2}/Gr_x^{1/4} = f_n\{(\rho V_z)|_\delta x^{1/4}/4\mu C\} \tag{20}$$

where the convection parameter C is given by

$$C = [g\beta(T_s-T_\infty)/4\nu^2]^{1/4} \tag{21}$$

$$Gr_x = g\beta(T_s-T_\infty)x^3/\nu^2 \tag{22}$$

and

$$Nu_{x,2} = h_2 x/k \tag{23}$$

and where f_n represents a second order polynomial. This functional relation is then integrated over x to obtain the average Nusselt number

$$Nu_2/Gr^{1/4} = g_n[w] \tag{24}$$

where g_n is a second order polynomial and the injection parameter w is given by

$$w = [(\rho V_z)|_\delta R^{1/4}/4\mu C] \tag{25}$$

and

$$Nu_2 = \bar{h}_2 R/k \tag{26}$$

$$Gr = g\beta(T_s - T_\infty)R^3/\nu^2 \tag{27}$$

where R is the cloth radius and $(\rho V_z)|_\delta$ is the mass flux at the porous surface. These calculations and the resultant coefficients are given in Appendix E.

The effective film coefficient for the free convective cooling of the rear fabric surface is then given by

$$\bar{h}_2 = Gr^{1/4} g_n(w) k/R \tag{28}$$

where the thermodynamic and transport properties are evaluated at the mean film temperature

$$T_{mf} = (T_s + T_\infty)/2 \tag{29}$$

As in the previous section, the mass flux at the porous boundary $(\rho V_z)|_\delta$ is related to the known fabric porosity and decomposition rate. Equation (13) is evaluated at z equal to δ and combined with equation (18) to give

$$(\rho V_z)|_\delta = \rho K(p_o - p_s)/\mu\delta + (\rho_o \delta)\varepsilon_g \dot{\lambda}_g/2 \tag{30}$$

The heat transfer coefficient for the convective cooling of the rear fabric surface is then given as an explicit function of the Grashof number Gr and the injection parameter w

$$Nu_2 = f\{Gr, w\} \tag{31}$$

The Grashof number describes the magnitude of the natural convective currents, and w characterizes the fabric porosity and decomposition rate with respect to the rear surface of the fabric.

The boundary conditions, then, for the conservation equations describing the convective heating of a fabric are as summarized below.

For the porous slab

$$\left.\begin{array}{lll} \text{at } z = 0 & V_r = 0 & \\ & \rho V_z = \rho K(p_o - p_\delta)/\mu\delta - (\rho_o \delta)\varepsilon_g \dot{\lambda}/2 & \\ & -k \left.\frac{\partial T}{\partial z}\right|_{z=0} = \bar{h}_1 (T_f - T_s) & \\ \text{at } z = \delta & -k \left.\frac{\partial T}{\partial z}\right|_{z=0} = \bar{h}_2 (T_s - T_\infty) & \end{array}\right\} \quad (32a)$$

For the external flow

$$\left.\begin{array}{lll} \text{at } \left\{\begin{array}{l} z = -L \\ 0 \leq r \leq D/2 \end{array}\right. & V_r = 0 & \\ & V_z = V_b & \\ & T = T_f & \\ \text{at } z = \infty & T = T_\infty & \end{array}\right\} \quad (32b)$$

The surface temperature T_s is a time varying boundary condition, and, consequently, the governing equations for Region (1) are coupled with the energy conservation equation for Region (2). The degree of dependence will be determined experimentally.

Normalization of Conservation Equations and Boundary Conditions. The conservation equations and boundary conditions given in the preceding two sections are normalized using the following dimensionless quantities

$$
\left.
\begin{aligned}
r^* &= r/R \\
z^* &= z/R \\
V_r^* &= V_r/V_b \\
V_z^* &= V_z/V_b \\
T^* &= (T-T_\infty)/(T_f-T_\infty) \\
p^* &= (p-p_\infty)/\rho_f V_b^{\,2} \\
\rho^* &= \rho/\rho_f \\
\dot{\lambda}_g^* &= \dot{\lambda}_g/k_g \exp(-E/RT_i)
\end{aligned}
\right\} \quad (33)
$$

where R is the cloth radius, V_b is the velocity at the burner exit, T_∞ is the ambient temperature, ρ_f is the density evaluated at the flame temperature T_f, and T_i is the fabric ignition temperature. Substituting, then, equations (33) into the momentum conservation equation (5) and multiplying by $R/\rho_f V_b^{\,2}$ yields

$$
\rho^*(\vec{V}^* \cdot \nabla^*)\vec{V}^* = -\nabla^* p^* + \left[\frac{1}{\pi_1}\right]\nabla^{*2}\vec{V}^* + \left[\frac{1}{\pi_2}\right]\frac{\vec{g}}{g} \qquad (34)
$$

where

$$
\pi_1 = \rho_f V_b R/\mu \qquad (35)
$$

$$\pi_2 = V_b^2/gR \tag{36}$$

Similarily, using equations (33), the energy conservation equation (7), after multiplying by $R/C_p\rho_f V_b$, yields

$$\rho^*(V_r^*\nabla^*T) = [\frac{1}{\pi_1\pi_3}]\{\nabla^{*2}T\} \tag{37}$$

where

$$\pi_3 = C_p\mu/k \tag{38}$$

The nondimensional boundary conditions are,

for the porous slab

$$\left.\begin{aligned}
&\text{at } z^* = 0 \qquad V_r^* = 0 \\
&(\rho^*V_z^*) = \{\frac{\rho K(p_o - p_\delta)}{\mu\delta\rho_f V_b}\} - \{\frac{(\rho_o\delta)\varepsilon_g k_g \exp(-E/RT_i)}{2\rho_f V_b}\}\dot{\lambda}_g^* \\
&\qquad = \pi_4 - \pi_5\dot{\lambda}_g^* \\
&-\frac{\partial T^*}{\partial z^*} = \frac{\bar{h}_1 R}{k}(1-T_s^*) = \pi_6(1-T_s^*) \\
&\text{at } z = (\delta/R) \quad -\frac{\partial T^*}{\partial z^*} = \frac{\bar{h}_2 R}{k}T_s^* = \pi_7 T_s^*
\end{aligned}\right\} \tag{39a}$$

for the external flow

$$\left.\begin{array}{lll} \text{at} \begin{cases} z^* = -\pi_8 \\ 0 \le r^* \le \pi_9/2 \end{cases} & V_r^* = 0 \\ & V_z^* = 1 \\ & T^* = 1 \\ \text{at } z^* = \infty & T^* = 0 \end{array}\right\} \quad (39b)$$

where $$\pi_8 = L/R \quad (40)$$

$$\pi_9 = D/R \quad (41)$$

$$T_s^* = (T_s - T_\infty)/(T_f - T_\infty) \quad (42)$$

For the range of parameters encountered in this study, the square of the Froude number, π_2, is much greater than one so that this term may be readily neglected.

According to the Buckingham Pi theorem, the arrangement of the dimensional quantities in the above dimensionless groups is arbitrary; any one of the dimensionless groups may be replaced by the product of that one (raised to any power) by any of the others raised to any power. This allows the convenient rearrangement into the following scaling parameters:

$$L/D = \pi_8/\pi_9 \quad (43)$$

$$R/D = 1/\pi_9 \quad (44)$$

$$Re = \pi_1\pi_9 = \rho_f V_b D/\mu \quad (45)$$

$$Pr = \pi_3 = C_p \mu / k \tag{46}$$

$$Nu_1 = \pi_6 = \bar{h}_1 R / k \tag{47}$$

$$Nu_2 = \pi_7 = \bar{h}_2 R / k \tag{48}$$

$$T_s^* = (T_s - T_\infty)/(T_f - T_\infty) \tag{49}$$

$$(Re)_{o,p} = \pi_1 \pi_4 = \rho K (p_o - p\ ) R / \mu^2 \delta \tag{50}$$

$$(Re)_{o,g} = \pi_1 \pi_5 = (\rho_o \delta) \varepsilon_g k_g \exp(-E_g / RT_i) R / 2\mu \tag{51}$$

For a given decomposition rate $\dot{\lambda}_g^*$, the mass flux at the boundary is specified by the injection Reynolds number

$$(Re)_o = (Re)_{o,p} - (Re)_{o,g} \dot{\lambda}_g^* \tag{52}$$

The nine scaling groups, equation (43) through (51), are sufficient to describe the convective heat transfer to the fabric. The natural convective cooling of the rear surface of the fabric is expressed through the rear surface Nusselt number

$$Nu_2 = f\{Gr, w\} \tag{31}$$

and the forced convective heating of the front surface of the fabric is expressed through the front surface Nusselt number and is correlated by

$$Nu_1 = f\{L/D,\ R/D,\ Re,\ Pr,\ T_s^*,\ (Re)_o\} \tag{53}$$

The geometric ratio L/D is the burner-cloth spacing measured relative to the burner diameter, R/D is the ratio of the cloth radius to the burner diameter, Re describes the burner exit velocity, the Prandtl number describes the fluid properties, T_s^* represents the thermal response of the cloth to the convective heat source, and the injection Reynolds number $(Re)_o$ characterizes the fabric porosity and decomposition rate. This functional relationship expressed by equation (53) is as yet unknown and must be determined through experimental efforts.

Dynamic and thermal similarity is achieved when the scaling groups listed in the above equations (31) and (53) are identical for both the film coefficient determination tests and the fabric ignition time measurements, and these groups are employed in the reduction and correlation of data in the determination of the film coefficient $\bar{h}_1$.

Fabric Ignition Under Convective Heating

The third task of this chapter is to predict the ignition time of fabrics in terms of the material properties and convective heating conditions. To predict the fabric

ignition time, the conservation of energy equation for the convective heating of a fabric must be solved. This equation has been developed earlier [3,4], closed form solutions were presented [3,4] for idealized systems, i.e. convective or radiative heating of inert, thermally thin materials, and numerical solutions were obtained [3,4] for the complete equations describing the thermal decomposition of thermally thin media. A summary of the governing equations and the closed-form solutions is presented here.

The conservation of energy equation for the convective heating of a fabric is derived from equation (6), after including the energy generation term, and integrating over the slab thickness [3,4]

$$\rho\delta C_p \frac{dT}{d\tau} = h_1(T_f - T) - h_2(T - T_\infty) - 2\alpha\sigma F_{s\infty}(T^4 - T_\infty^4) + (\Delta i)_d[d(\rho\delta)/d\tau]_d + (\Delta i)_g[d(\rho\delta)/d\tau]_g \tag{54}$$

where

T_f = free flame gas temperature

T_∞ = ambient temperature

T = fabric temperature

$\bar{h}_1$ = effective film coefficient for forced convective heating of front surface

$\bar{h}_2$ = effective film coefficient for free convective cooling of rear surface

$\rho\delta$ = specific mass of fabric

C_p = specific heat of fabric

$F_{s\infty}$ = view factor of fabric with respect to the environment, averaged over front and back surfaces

α = absorptance

Δi = reaction enthalpy

The subscript d refers to the desorption of water and the subscript g refers to the gasification or pyrolysis of the fabric.

The mass which underwent reaction is expressed through the fraction λ of the total, decomposable mass as

$$(\rho\delta)_d = \varepsilon_d(\rho\delta)_o(1-\lambda_d) \tag{55}$$

$$(\rho\delta)_g = \varepsilon_g(\rho\delta)_o(1-\lambda_g) \tag{56}$$

where ε is the fraction of original mass per unit area that participates in the reaction. The rate of reaction is described by Arrhenius type laws

$$\frac{d\lambda_d}{d\tau} = k_d(1-\lambda_d)^{n_d}\exp[-E_d/RT] \tag{57}$$

$$\frac{d\lambda_g}{d\tau} = k_g(1-\lambda_g)^{n_g}\exp[-E_g/RT] \tag{58}$$

The convective heating and cooling terms are combined

by an overall convective film coefficient $2\bar{h}$ averaged over front and back surfaces and based on the flame temperature.

$$2\bar{h} = \frac{\bar{h}_1(T_f - T) - \bar{h}_2(T - T_\infty)}{(T_f - T)} \tag{59}$$

Normalization of equation (54) yields [3]

$$\frac{d\theta}{d\tau} = \theta_f - \theta - \pi_{12}\{[1+\pi_{11}(\theta-1)]^4 - (1-\pi_{11})^4\} - \pi_{13}\left(\frac{d\lambda_d}{d\bar{\tau}}\right) - \pi_{14}\left(\frac{d\lambda_g}{d\bar{\tau}}\right) \tag{60}$$

where

$$\bar{\tau} = \frac{2\bar{h}\tau}{\rho\delta C_p} \tag{61}$$

$$\theta = \frac{T - T_\infty}{\bar{T}_i - \bar{T}_\infty} \tag{62}$$

$$\pi_{11} = 1 - (T_\infty / T_i) \tag{63}$$

$$\pi_{12} = \frac{\alpha\sigma F_{s\infty} T_i^{\,4}}{\bar{h}(T_i - T_\infty)} \tag{64}$$

$$\pi_{13} = \frac{\varepsilon_d (\Delta i)_d}{C_p (T_i - T_\infty)} \tag{65}$$

$$\pi_{14} = \frac{E_g (\Delta i)_g}{C_p (T_i - T_\infty)} \tag{66}$$

T_i is the fabric ignition temperature and T_∞ is the ambient temperature or initial fabric temperature. The normalized desorption and gasification terms are then given by

$$\frac{d\lambda_d}{d\bar{\tau}} = \pi_{15}(1-\lambda_d)^{n_d}\exp\{-\pi_{16}/[1+\pi_{11}(\theta-1)]\} \tag{67}$$

and

$$\frac{d\lambda_g}{d\bar{\tau}} = \pi_{17}(1-\lambda_g)^{n_g}\exp\{-\pi_{18}/[1+\pi_{11}(\theta-1)]\} \tag{68}$$

where

$$\pi_{15} = (\rho\delta)_o C_p k_d/2\bar{h} \tag{69}$$

$$\pi_{16} = E_d/RT_i \tag{70}$$

$$\pi_{17} = (\rho\delta)_o C_p k_g/2\bar{h} \tag{71}$$

$$\pi_{18} = E_g/RT_i \tag{72}$$

An order of magnitude analysis reveals that the π_{12} term, which represents the ratio of radiative exchange to convective heating, can be neglected for cloth temperatures below 300°C.

Similarily, since the fabrics of Reference [4] were desiccated in a 5-7% relative humidity environment before the ignition tests, the energy required for the desorption of water is neglected.

The energy required for gasification is neglected with respect to the larger convective heating fluxes since several of the GIRCFF fabrics have small π_{14} values. The significance of the gasification term will be reviewed later in the evaluation of ignition time predictions. Although the energy required for gasification is neglected, the effect of gasification on the convective heat transfer coefficient is not neglected, but is introduced in the evaluation of the convective film coefficient.

The conservation of energy equation is then reduced to the ordinary first order differential equation

$$\frac{d\theta}{d\bar{\tau}} = \theta_f - \theta \tag{73}$$

for which the solution is [3,6]

$$\theta = (1-e^{-\bar{\tau}})\theta_f \tag{74}$$

The nondimensional flame temperature θ_f is given by

$$\theta_f = \frac{(T_f - T_\infty)}{(T_i - T_\infty)} \tag{75}$$

At $\theta = 1.0$, the dimensionless time becomes the ideal or predicted ignition time $\bar{\tau}_i^{\,o}$

$$\bar{\tau}_i^{\,o} = \ell n[\theta_f/(\theta_f - 1)] \tag{76}$$

The actual ignition times of several different fabrics, measured at various heating intensities, are presented using the nondimensional fabric destruction time given by the Fourier number [4]

$$Fo = \frac{\tau_i (k/\delta)}{C_p (\rho\delta)} \tag{77}$$

where τ_i is the actual ignition time, (k/δ) is the fabric thermal conductance, C_p is the fabric specific heat, and $(\rho\delta)$ is the mass per unit area of the fabric. The convective heating intensity is also nondimensionalized to form q*, where

$$q^* = \left(\frac{2\bar{h}}{k/\delta}\right)(\theta_f - \bar{\theta}) \tag{78}$$

The nondimensional heating intensity q* is the product of the Biot number, the ratio of conductive resistance to convective resistance, and the nondimensional average excess flame temperature above the fabric temperature. The average, nondimensional fabric temperature $\bar{\theta}$ is defined [3,6] by

$$\bar{\theta} = \frac{1}{\bar{\tau}_i^{\,o}} \int_o^{\bar{\tau}_i^{\,o}} \theta d\bar{\tau} \tag{79}$$

which is evaluated using equation (76) to give

$$\bar{\theta} = \theta_f + 1/\ell n(1-1/\theta_f) \tag{80}$$

Using this definition, equation (74), the solution to the inert heating equation, is written as

$$Fo = \frac{\bar{\tau}_i^{\,o}(k/\delta)}{C_p(\rho\delta)} = (q^*)^{-1} \tag{81}$$

These nondimensional groups and the above equation are used in the presentation of actual and predicted ignition times of fabrics.

The dimensionless heat flux q^*, which is required by equation (81) for the prediction of fabric ignition times, depends on the overall convective film coefficient $2\bar{h}$. The overall convective film coefficient, in turn, depends on both the fabric front surface film coefficient $\bar{h}_1$ and the fabric rear surface film coefficient $\bar{h}_2$. Consequently, explicit functional relationships in terms of known parameters are required for both $\bar{h}_1$ and $\bar{h}_2$. The fabric rear surface film coefficient $\bar{h}_2$ is given explicitly in dimensionless form in equation (24) and in dimensional form in equation

(28). However, the functional relationship expressed by equation (53) for the fabric front surface film coefficient h_1 is as yet unknown. It is therefore necessary to conduct experiments which will determine the functional relationship which correlates the seven parameters listed in equation (53). The experimental simulation and determination of the fabric-flame interaction is discussed in the following chapter.

CHAPTER III

EXPERIMENTAL SIMULATION OF FABRIC-FLAME INTERACTION

Fabrics which are exposed to a methane-air flame undergo water desorption, pyrolysis, and eventually melt or ignite. Because of the reactive nature of fabrics, the convective film coefficients which describe the fabric-flame interaction must be determined from inert wire cloths which simulate the fabric geometry.

The experimental simulation of the convective heat transfer to a fabric requires the geometric, dynamic, and thermal similarity established by the dimensionless groups in equations (31) and (53). In this section, the methods of experimental simulation are discussed and each of the similarity parameters are considered.

The first requirement of the experimental apparatus is to maintain geometric similarity between the fabric ignition time measurements and the convective film coefficient determination tests. A fine mesh wire cloth is used to simulate the fabric weave and is mounted in a geometrically similar holder. Geometric similarity of the cloth surface exposed to the burner is then insured by using the same blast type burner for the convective heat flux and the same Convective Ignition Time Apparatus [4]. With the above configuration,

the R/D parameter remains constant and the burner-to-cloth spacing is characterized by the ratio L/D.

Simulation of the fabric porosity and pyrolysis is achieved through the duplication of the injection Reynolds number $(Re)_o$. This requires the controlled mass flux at the surface of the porous cloth. It is accomplished by providing an air injection/suction chamber behind the wire cloth which will regulate the pressure behind the cloth and thereby control the mass flux through the screen.

Depending on the relative magnitudes of fabric porosity, stagnation pressure on the flame side of the fabric, and the fabric decomposition rate, the net mass flow rate through the fabric may be greater than, less than, or equal to the flameward flow rate induced by the decomposed mass.

The experimental tests, accordingly, can be divided into three categories: Measurements with injection, no injection, and suction. The physical cases which are simulated by each of these categories are considered separately.

(i) Film coefficient measurements in which there is no air injection simulate two cases. The first occurs when there is negligible fabric decomposition and when the fabric is very dense. The second case occurs when the rate of pyrolysate evolved toward the burner is exactly equal to the mass flux through the fabric, determined by the external pressure differential.

(ii) Film coefficient measurements in which the air

is injected through the screen toward the burner simulate the case where the fabric is decomposing at a sufficient rate to force some of the pyrolysates to escape from the front surface of the fabric.

(iii) Film coefficient measurements in which there is air suction simulate the third case in which the fabric does not decompose at a sufficient rate to keep the free stream gas flames from passing through the fabric.

The external flow is characterized, in part, by the burner Reynolds number Re. This is duplicated by maintaining equal stoichiometric equivalence ratios and the same mixture mass flow rates of the air and methane.

The Prandtl number Pr relates the temperature distribution to the velocity distribution and must be the same in both the fabric ignition time measurements and the film coefficient determination tests. Since the flame temperature is dictated by process parameters which are duplicated in these studies (stoichiometric equivalence ratio, mixture mass flow rate, and spacing), and since the Prandtl number does not vary appreciably either between various gases or with temperature, it is expected that this parameter will remain constant for both studies.

The effect of the excess temperature ratio (T_s^*) is determined by maintaining the same flame temperature T_f and varying the surface temperature T_s. This is accomplished by heating the air being injected through the screen into the

boundary layer.

The two parameters which characterize the convective cooling of the rear fabric surface are the Grashof number Gr and the injection parameter w. Neither of these parameters is simulated in the determination of the convective film coefficient. However, the heat transfer from the rear surface of the screen is negligible with respect to the convective heat flux to the front surface of the screen. Before the screen is exposed to the burner, the air being injected through the screen is at approximately the same temperature as the screen, and the air therefore has no cooling effect on the screen. When the screen is then exposed to the burner, there is a step change in the front free stream temperature. As shown in Figure 2, there is a large temperature difference between the cloth and the front free stream temperature at time $\tau = 0+$, but only a small temperature difference ΔT between the cloth and the rear environmental temperature. Consequently, the film coefficient, evaluated at time $\tau = 0+$ (where $\Delta T \approx 0$), is not reduced by any convective cooling of the cloth and describes the effective heat transfer to the front surface only. The coupled heat transfers of convective cooling and convective heating of the fabric are decoupled in the determination of the film coefficient. The convective cooling of the cloth's rear surface is described by the analytical correlation given by equation (31) and the convective heating of the cloth's

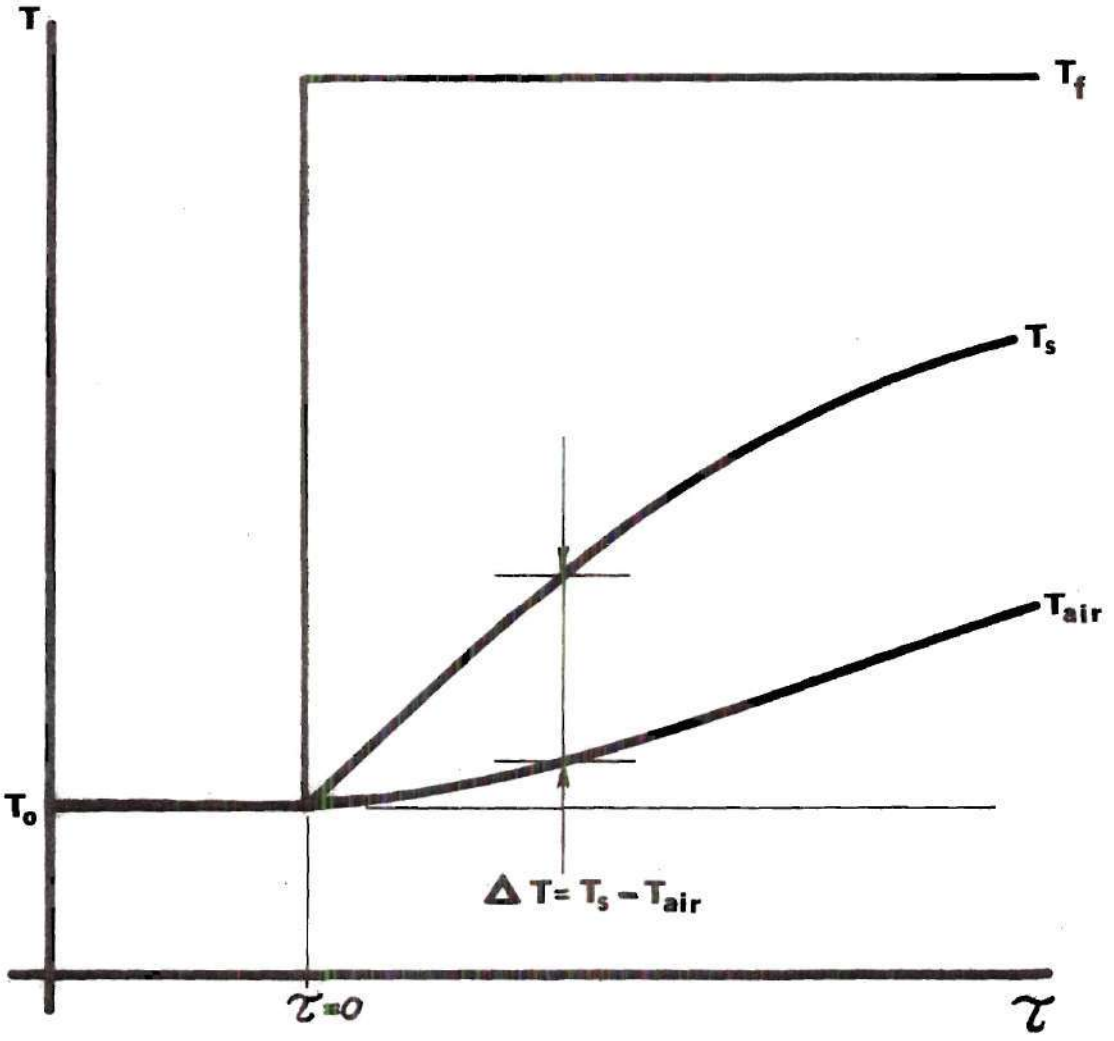

Figure 2. Chamber Temperature and Screen Temperature Versus Time

front surface is described through the film coefficient determination tests.

The results of the film coefficient determination tests are therefore correlated in terms of the parameters listed in equation (53) which describe the convective heating of the cloth's front surface.

The conservation of energy equation for the convective heating of a fabric is specialized for the convective heating of a screen to provide a method of determination of the convective film coefficients. The screen does not undergo desorption or gasification, nor does it experience any convective cooling, as discussed previously. The energy balance for the screen then gives the following expression for the convective heat transfer coefficient $\bar{h}_1$:

$$h_1 = \frac{(\rho\delta)_s \, C_{p,s} (dT_s/d\tau)}{(T_f - T_s)} \tag{82}$$

where $(\rho\delta)_s$ is the specific mass of the screen, $C_{p,s}$ is the specific heat of the screen, T_s is the screen temperature and T_f is the flame temperature. A radiation term does not appear in this expression since the film coefficient is evaluated at the initial screen temperature where the net losses are balanced to be zero.

CHAPTER IV

EQUIPMENT AND INSTRUMENTATION

In this chapter, the equipment and instrumentation which is required for the determination of the film coefficient is presented first, and then the equipment and instrumentation which was used to determine the stagnation pressure of the gas flame is described.

Introduction and Operating Principle

The primary task of determining the convective film coefficients is accomplished experimentally by using a stainless steel screen thermocouple. The screen was exposed to the same convective heat flux source (blast type burner) as used in the fabric ignition time tests. This, in conjunction with a similar holder design and the same burner-cloth spacing, insure geometric similarity of the cloth surface exposed to the burner. Using the screen as one of the two dissimilar metal components of a thermocouple junction allows the direct measurement of the thermal response of the screen to the ignition source.

The convective heat transfer coefficient, $\bar{h}_1$, is derived from an energy balance for the screen, and given previously by equation (82).

$$\bar{h}_1 = \frac{(\rho\delta)_s \, C_{p,s} (dT_s/d\tau)}{(T_f - T_s)} \tag{82}$$

where $(\rho\delta)_s$ is the specific mass of the screen, $C_{p,s}$ is the specific heat of the screen, T_s is the screen temperature, and T_f is the flame temperature. The determination of the convective heat transfer, then, requires the measurement of T_f, T_s, and $(dT_s/d\tau)$.

The convective heat source is described in terms of its stoichiometric equivalence ratio (0.86), the total mass flow rate of air and methane, the burner diameter, and the resultant flame temperature.

The action of air injection or suction over the range of -3 to +3 cm/s simulates the evolution of pyrolysates during fabric decomposition and the mass flux through the fabric due to its porosity, respectively. The entire range of fabric porosities as well as decomposition rates are covered by this variation of injected mass flow rate.

The use of wire cloth insures geometric similarity with the fabrics and the effect of fabric weave is determined by testing screens of varied mesh. The range of thread count for the 20 fabrics selected by GIRCFF is 26 (GIRCFF fabric No. 7, Jersey Tube Knit) to 130 (GIRCFF fabric No. 2, Textured Woven Blouse). The corresponding range of thread diameters, as indicated by the fabric thickness, is .00144-inch (GIRCFF fabric No. 14, Taffeta) to .0273-inch (GIRCFF

fabric No. 9, Terry Cloth). Two wire cloths were used to determine the heat transfer coefficients. The first was a 200 mesh, .0021-inch wire diameter screen. The second was a 150 mesh, .0026-inch wire diameter screen.

The Convective Film Coefficient Apparatus (CFCA) was designed to be used with the Convective Ignition Time Apparatus (CITA) to determine the film coefficients describing the cloth-flame interaction. CITA was designed to expose a fabric sample to a premixed methane-air flame. The action of two solenoid valves retract water cooled shutters which initially shield the fabric from the burner flames. The shutter system, the gas burner, and the related instrumentation are the major components of CITA which are used in determining the film coefficients. The operating procedures and the design details of CITA, CFCA, and the instrumentation used for the tests are described in the following sections.

Convective Ignition Time Apparatus

The design of CITA centers around a six-inch diameter opening in a one-inch thick aluminum base plate. A superstructure is mounted directly over this opening and a support cradle and vertical adjusting rod are used to position and support the CFCA. An overall view of the CFCA and CITA superstructure is given in Figure 3. A burner support base is provided directly below the opening to allow accurate positioning of the gas burner during testing. A water-cooled,

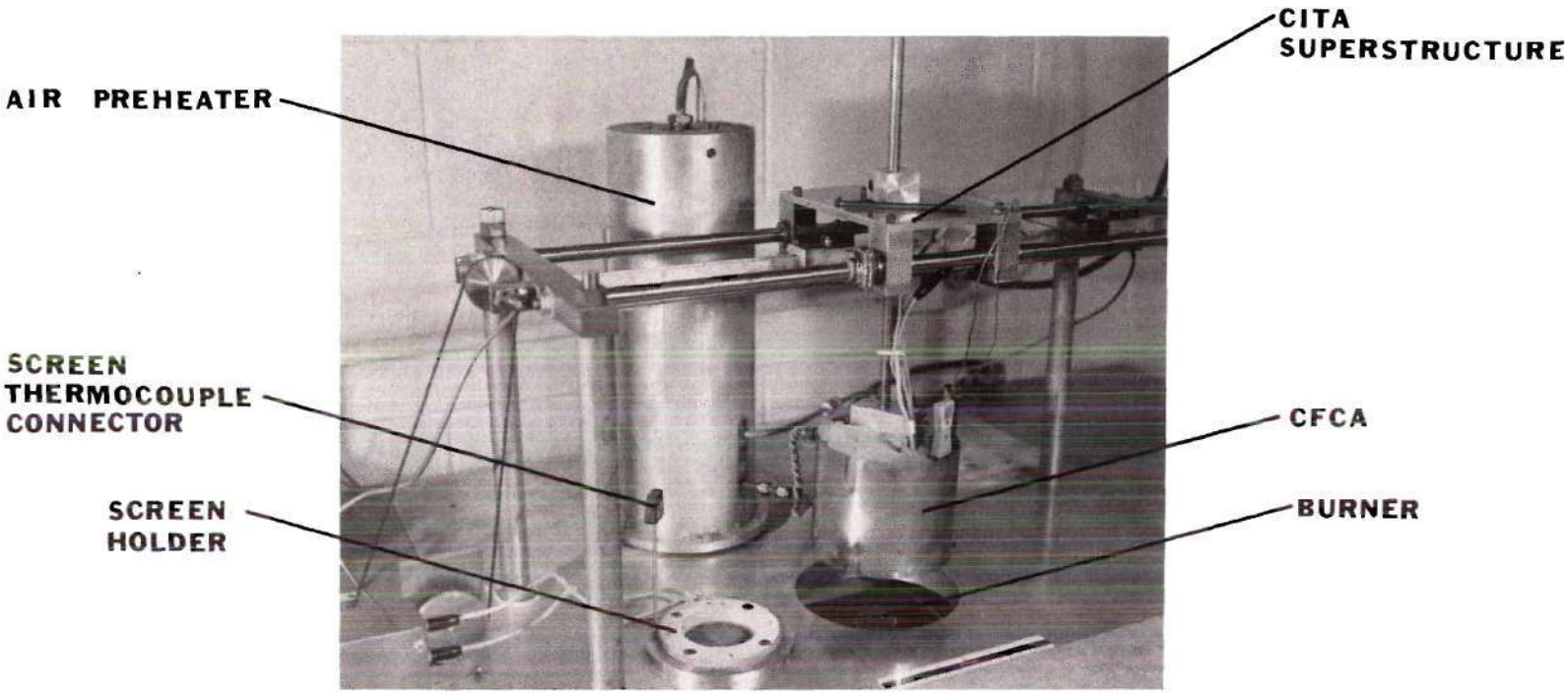

Figure 3. Overall View of the CFCA and CITA Superstructure.

pneumatically controlled shutter system is mounted just below the opening and protects the CFCA from the convective heating of the burner before the test takes place. The burner and shutter system are shown in Figure 4, and the related instrumentation is shown in Figure 5. The burner, which was used in both the fabric ignition tests and the film coefficient determination tests, is a Blast Type burner, Fisher Scientific Co., No. 3-910-5. This burner was modified by totally blocking the air ports and providing the air to the burner from the compressed air supply in the laboratory. The burner exit nozzle was fitted with a course screen and has an exit diameter of 37 mm. This burner provides a premixed air-methane flame with a useable methane flow rate range of 10-200 g/hr. The results of the burner characterization tests are given in Reference [3] and the relevant results reproduced in Appendix H.

A schematic of CITA is given in Figure 6. Specific design details of CITA are given in Appendix B.3 of Reference [3] and in Reference [6].

Convective Film Coefficient Apparatus

The Convective Film Coefficient Apparatus (CFCA) consists of three primary sections: (i) an aluminum clevis and its support rod, (ii) a transite inlet chamber and porous bronze assembly, and (iii) an inert wire cloth and screen holder assembly. A cross-sectional view of the CFCA

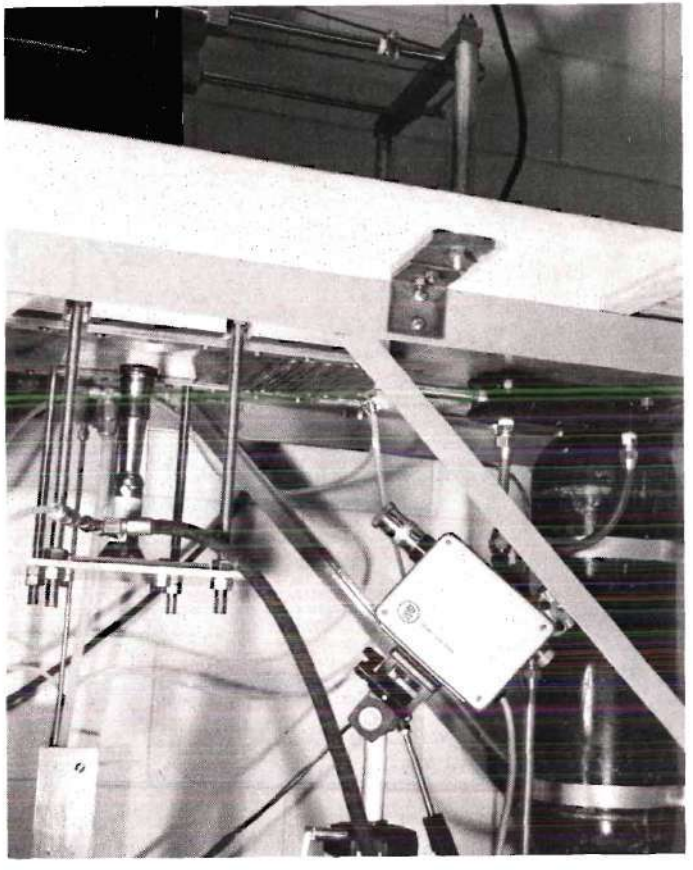

Figure 4. Lower Structure of CITA with Burner in Position.

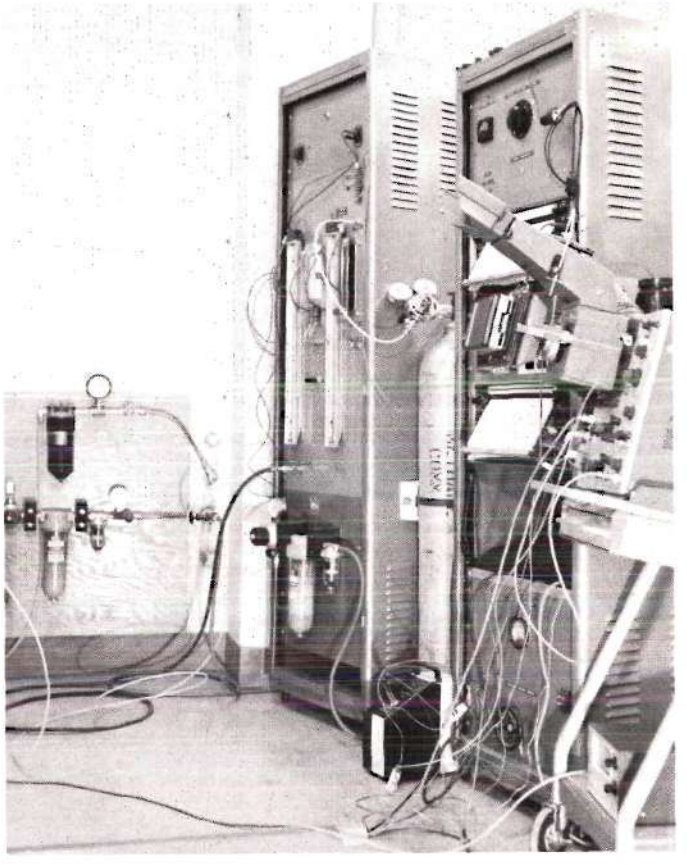

Figure 5. Recording Instrumentation, Flow Control and Flow Measuring Devices.

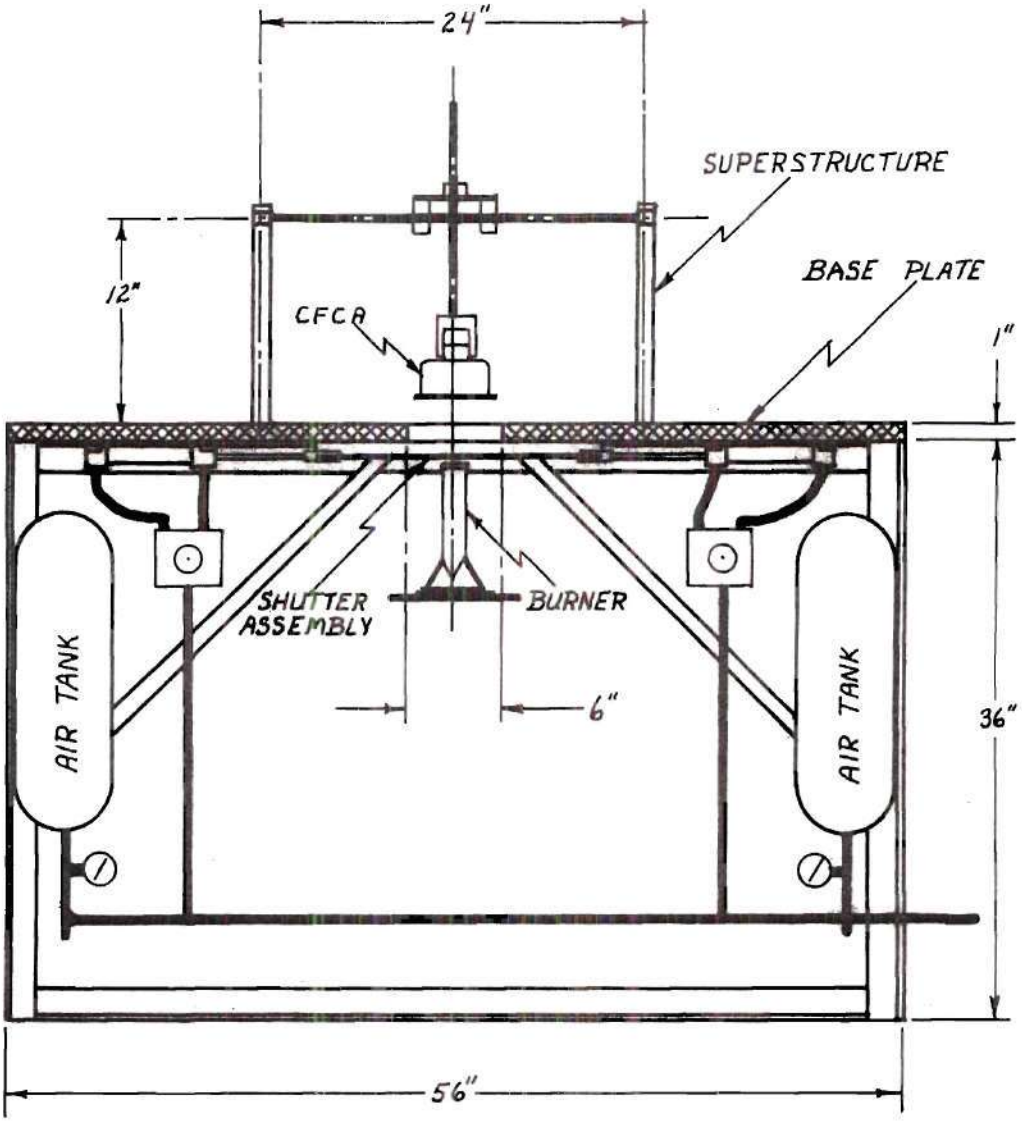

Figure 6. Cross-Sectional View of CITA

is given in Figure 7 and the three primary sections are discussed below.

(i) The clevis and support rod have been designed to allow vertical to horizontal positioning of the wire cloth for testing at various angles between the wire cloth and the burner axis.

(ii) The transite inlet chamber and porous bronze assembly have been designed to produce uniform temperature and velocity profiles of the injected air. The inlet chamber and the porous bronze holder were constructed from transite. Its low thermal conductivity helps insulate the heated air and minimize the heat losses. A porous bronze filter was used to produce a uniform velocity profile across the wire cloth. It was inserted between the inlet chamber and the filter holder and the two parts tightened securely. A chromel-alumel thermocouple was then positioned behind the bronze plate through a 1/8-inch diameter opening in the inlet chamber. Provision was made for thermocouple probes to check the temperature profiles for uniformity both upstream and downstream of the bronze filter and for continuous monitoring during testing.

(iii) The screen holder assembly was designed primarily for structural support of the test screen. The holder tops were made of transite for insulation and the holder bases were made of stainless steel for protection from the burner flame and for the structural support. The stainless steel

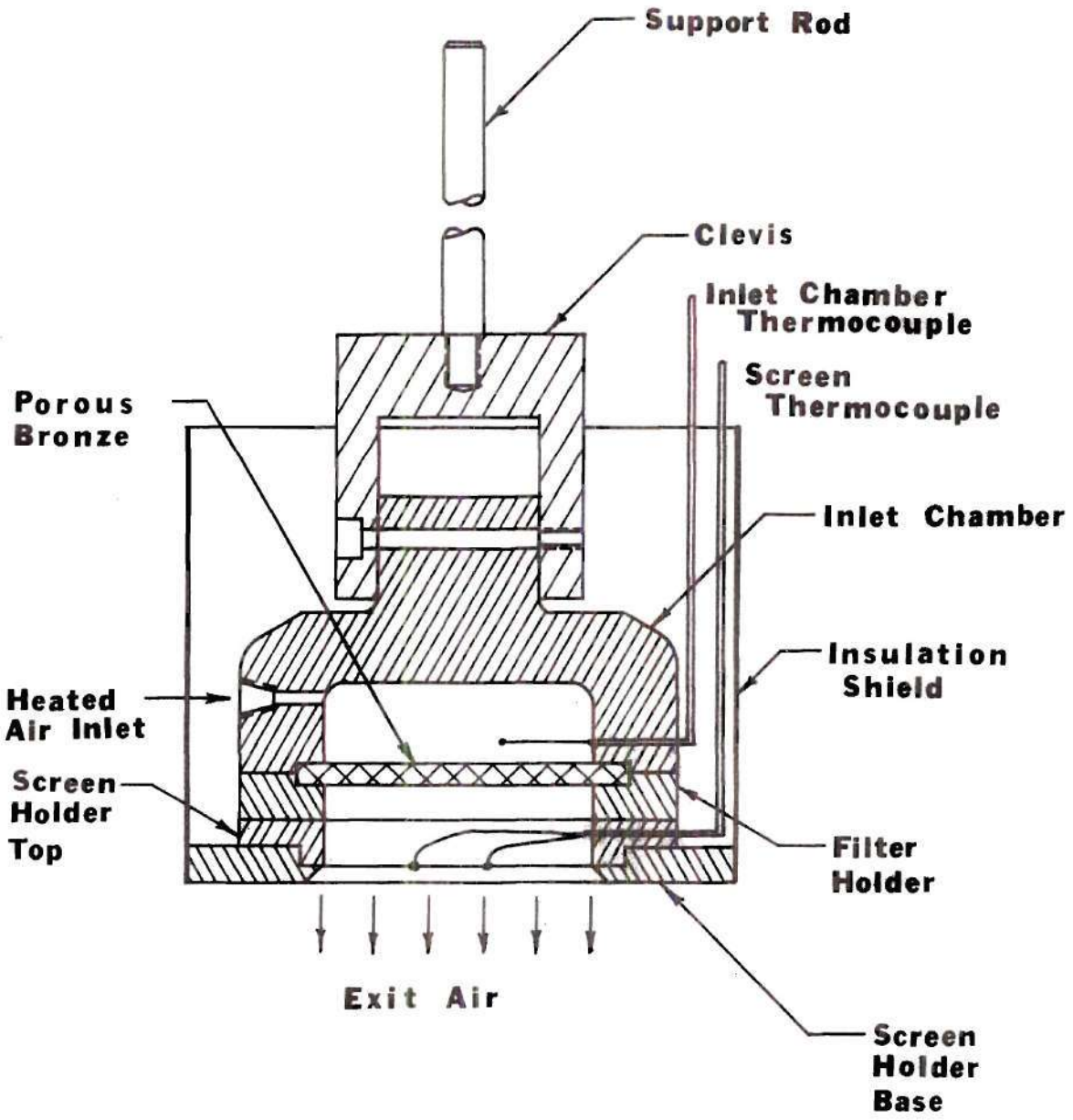

Figure 7. CFCA Assembly Drawing

screens were cut to 3-inch diameter circles, the diameters measured (±1/64-inch), and the screens weighed on a Christian Beckers Analytical Balance (±0.0006 g). From these measurements, a specific mass (g/cm^2) was determined for each screen (±3%). The results are given in Appendix A along with other relevant test screen data. A 0.006-inch diameter 316 stainless steel wire and a 0.005-inch diameter constantan wire were welded to each screen using a Baldwin Lima Hamilton Corporation Model VTW 34 Welder so that the screen-constantan weld formed the thermocouple junction. The wire leads were routed through ceramic insulators in 1/8-inch diameter stainless steel tubing through holes provided in the screen holder.

The screens were mounted between the stainless steel holder base and the transite holder top, being insulated from the base by a 0.020-inch thick 1/4-inch wide asbestos ring.

The diameter of the portion of the 3-inch screen which was exposed to the gas flame burner was 2.5-inches (6.35 cm). A bottom view of the CFCA is given in Figure 8 along with a stainless steel screen mounted in one of the screen holders.

Air Preheater

An electric preheater was used to heat the air before it entered the injection chamber, thereby requiring only guard heating for the chamber. The air preheater is shown

Figure 8. View of Bottom of the CFCA, 63 mm Diameter Stainless Steel Screen.

in Figure 9. The air flows first through the outer annulus, reverses itself and passes through the 1.3 mm wide inner annulus along the 300 mm long, 16 mm diameter Watlow heater element of 1 kW heating capacity (Type L12A21). The outer-flow passage is insulated with fiberglass.

The preheater power was controlled by a Superior Electric Co. Type 5649 Powerstat variable transformer. The Watlow heater element had a resistance of 14 ohms which was constant with temperature. A voltage measurement was used to indicate the power output.

Guard Heating and Apparatus Assembly

Three separate guard heaters were used to eliminate heat loss from the CFCA and from the preheater-to-inlet chamber air line. The inlet chamber was first wrapped with a single layer of Scotch glass cloth electrical tape (No. 20), and approximately 13.2 feet of Driver-Harris Nichrome resistance tape (1/8-inch x .005-inch, 1.010 ohms per foot) was then wrapped around the assembly taking special care to avoid any shorts. This, in turn, was covered with two more layers of the glass cloth tape.

A 3 foot, 7.3 ohm shielded resistance wire (.006-inch diameter) was wrapped around the air inlet line and 4.2 foot 10 ohm resistance wires (.006-inch diameter) were wrapped around the transite screen holder top of each screen assembly. The estimated heat losses from each part of the

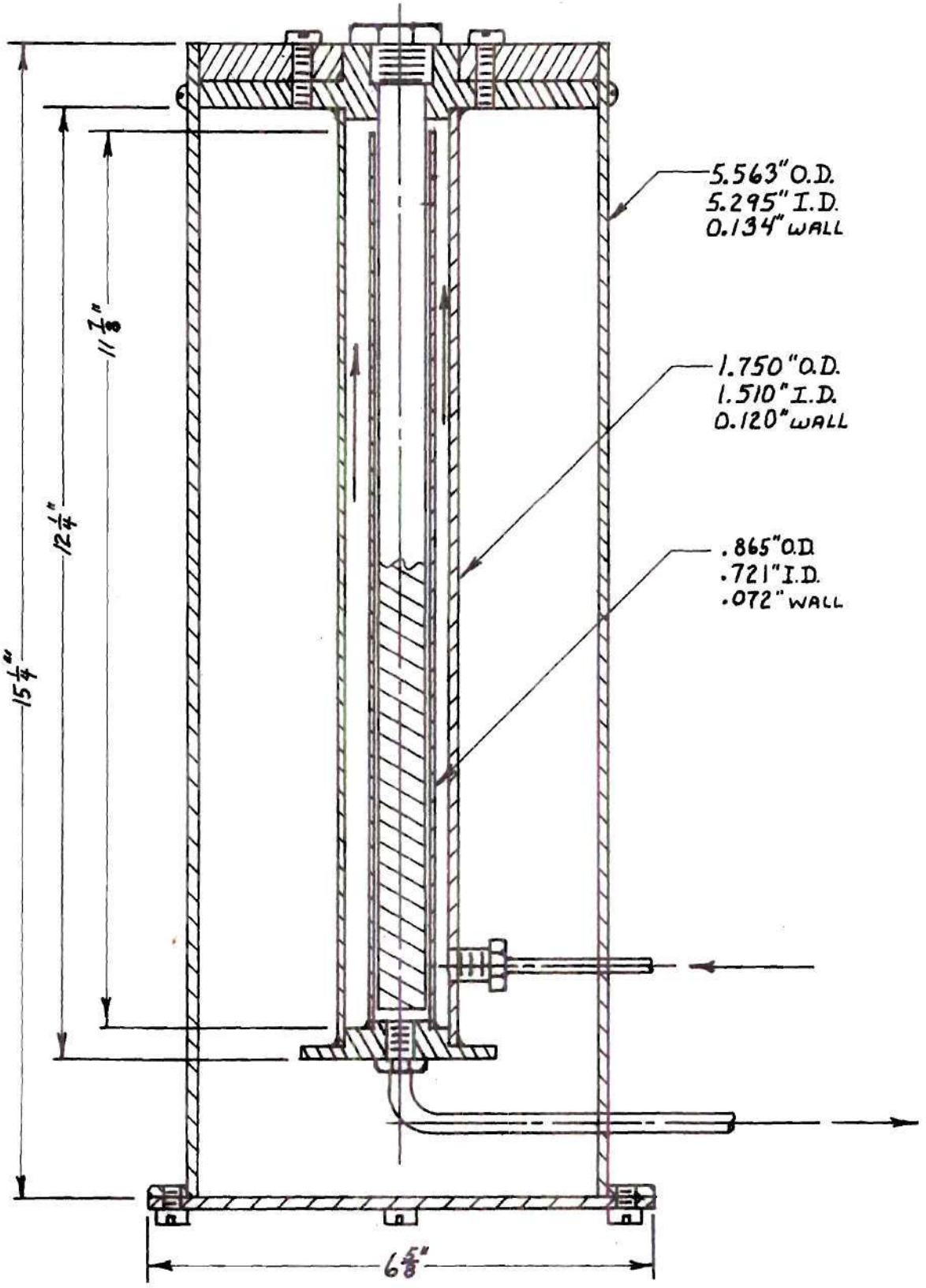

Figure 9. Cross-Sectional View of Air Preheater

CFCA were approximately equal, and so all of the guard heaters were wired in series, a total resistance of 30 ohms. The entire assembly was then checked for electrical shorts.

The power input to these heaters was controlled by a separate Superior Electric Co. Type 5649 Powerstat variable transformer. A voltage measurement was used to indicate the power output.

An inconel insulation shield was mounted to the stainless steel holder base, separated by an asbestos paper ring. Fiber glass insulation was packed around the chamber behind the insulation shield.

The apparatus was positioned over the shutters of CITA at the desired height above the burner. The guard heater wires were connected and routed to the powerstat and the thermocouple leads connected to the recording equipment via an Omega Model TRC ice point reference chamber.

Since AC guard heating was used, it was necessary to provide special grounding wires to the apparatus to eliminate interference on the thermocouple.

Instrumentation

Instrumentation was required to monitor and control the air and methane flow rates to the burner and the air flow rate to the injection chamber. Metering systems were also required to supply air to the pneumatic shutters and water to cool these shutters. Schematics of the

instrumentation are shown in Figures 10 and 11. Instrumentation and operation of the burner and shutter systems remained the same as those for CITA (Reference [6]).

The mass flow rate through the heater and the film coefficient assembly was determined by means of flow rate, pressure, and temperature measurements.

An iron-constantan thermocouple was used to measure the air temperature at the flow meter and its output was recorded on a Leeds and Northrup Model Speedomax W strip chart recorder. The air flow rate was measured using a calibrated Brooks Type 1357-01F1AAA Sho-Rate flow meter R-2-25-B tube with tantalum and glass floats. This provided a volumetric air flow rate range of 1 to 15 SCFH. The air pressure at the flow meter was measured using a Meriam Instrument Company 24-inch u-tube manometer. Water was used in the manometer for the injection tests and mercury was used in the manometer for the suction tests. The pressure in the laboratory air lines was used for air injection tests and a water aspirator was used to produce a vacuum for the air suction tests.

The air temperature in the inlet chamber was monitored continuously on a Hewlett-Packard Moseley Autograf model 7100MB strip chart two pen recorder.

For the film coefficient determination, a 6-volt DC voltage source and a microswitch, which was activated by one of the moving shutters, were used to detect the instant

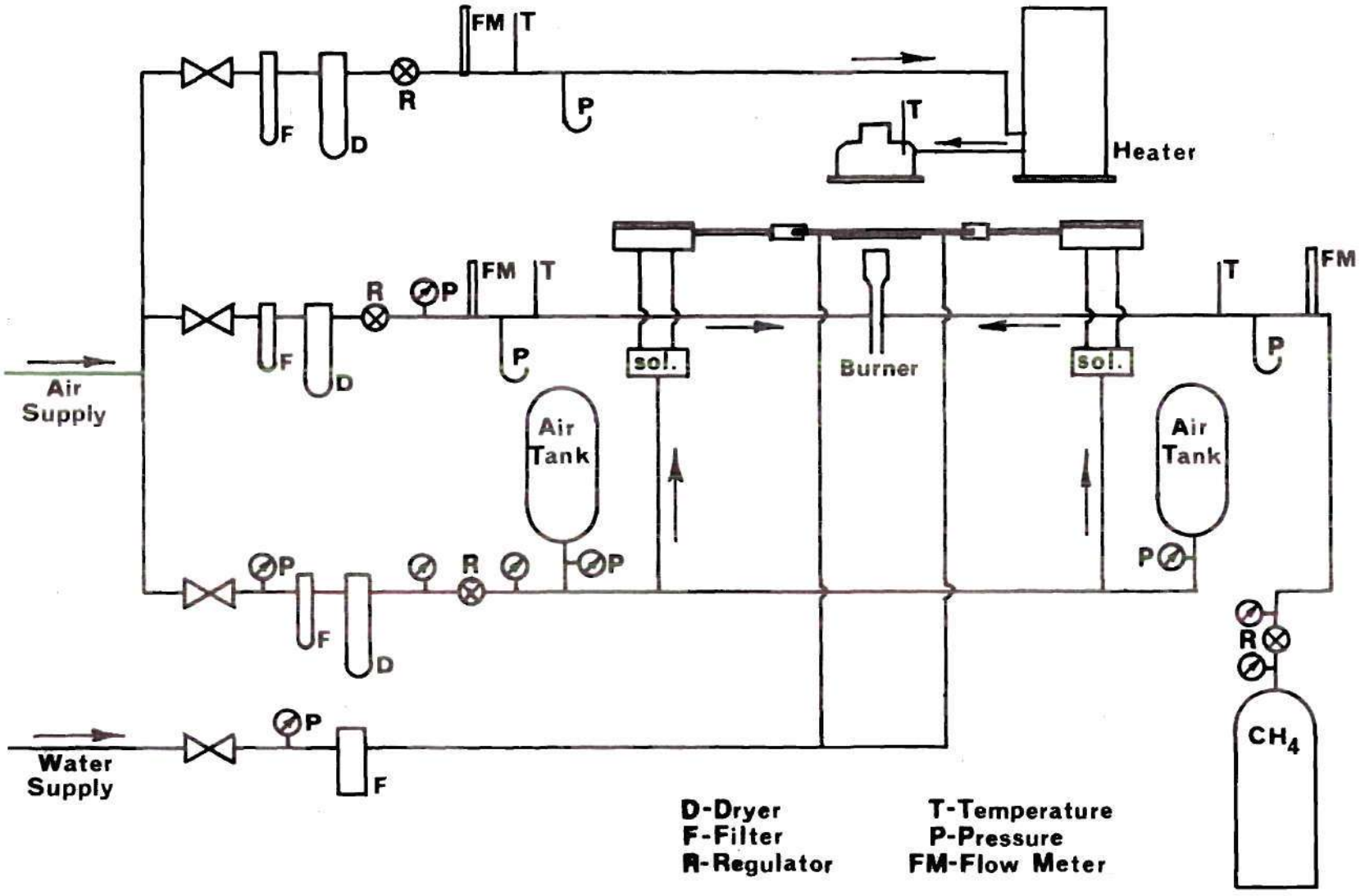

Figure 10. Flow Diagram for CFCA Measurement with Air Injection

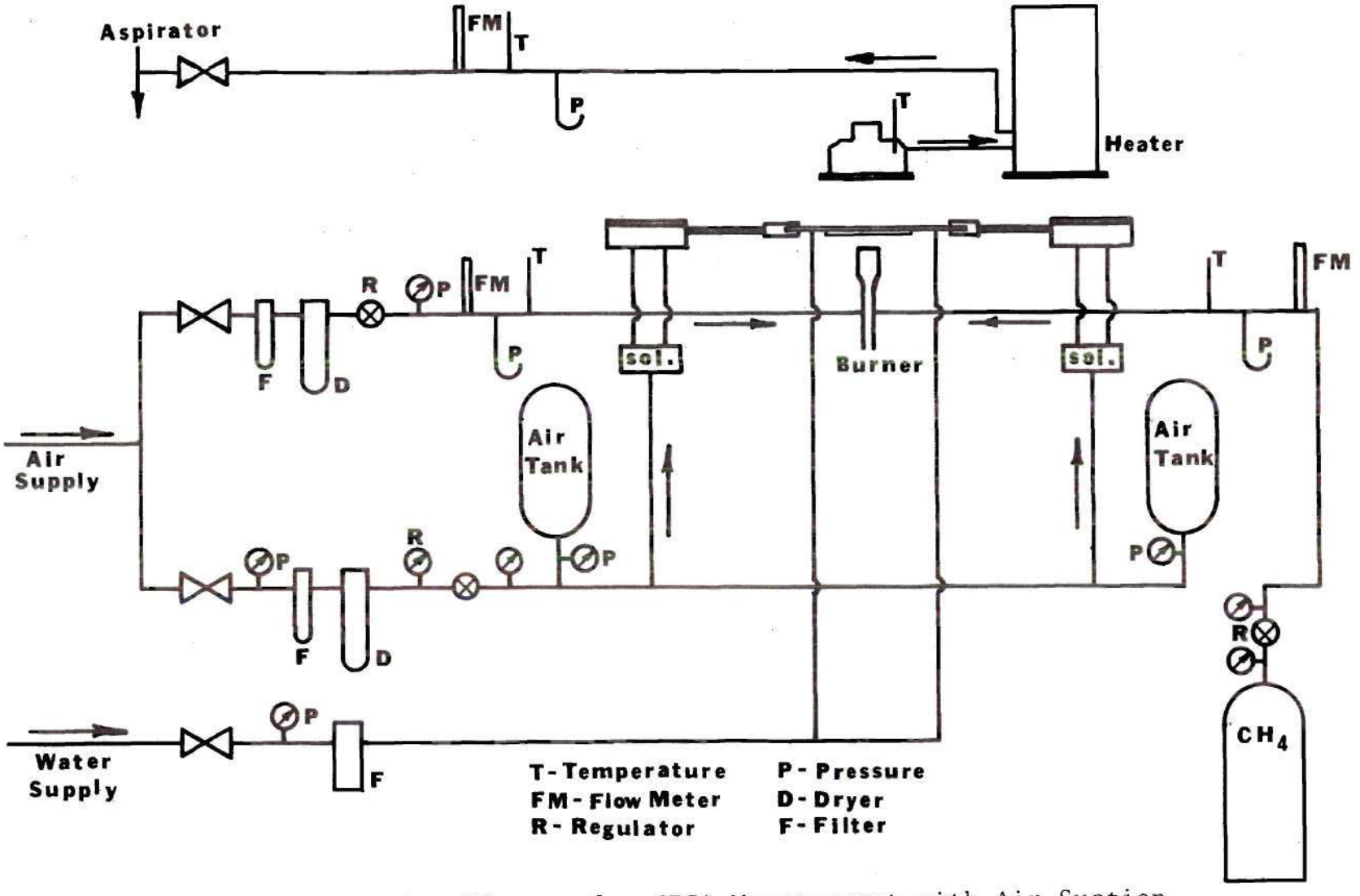

Figure 11. Flow Diagram for CFCA Measurement with Air Suction

of shutter separation and wire cloth exposure to the burner flame. A schematic of this instrumentation is shown in Figure 12. This signal triggered a dual beam Type 502A Tektronix Oscilloscope which recorded the wire cloth thermocouple mV output on Polaroid film (oscillogram).

The signal from the microswitch was also used to produce a spike in one of the traces of the two-channel Hewlett Packard Moseley Autograf model 7100MB strip chart recorder at the instant of exposure. The other trace recorded the output of the thermocouple probe upstream of the bronze filter. This record was used to determine the temperature of the incoming gas, and helped to select the minimum amount of guard heating required to keep the injected air temperature within 10°C of the screen temperature.

Flame Stagnation Pressure

Numerical evaluation of the injection Reynolds number given by equation (52) for decomposing porous fabrics requires the stagnation pressure of the combustion gases in the flame which impinges on the front surface of the cloth.

In general, it is not difficult to predict the pressure drop for a given velocity or to accurately determine the total pressure. The problem, however, arises in that firstly, the velocity profiles can not be accurately predicted because of the many interacting effects previously discussed. Secondly, the total or stagnation pressure is extremely

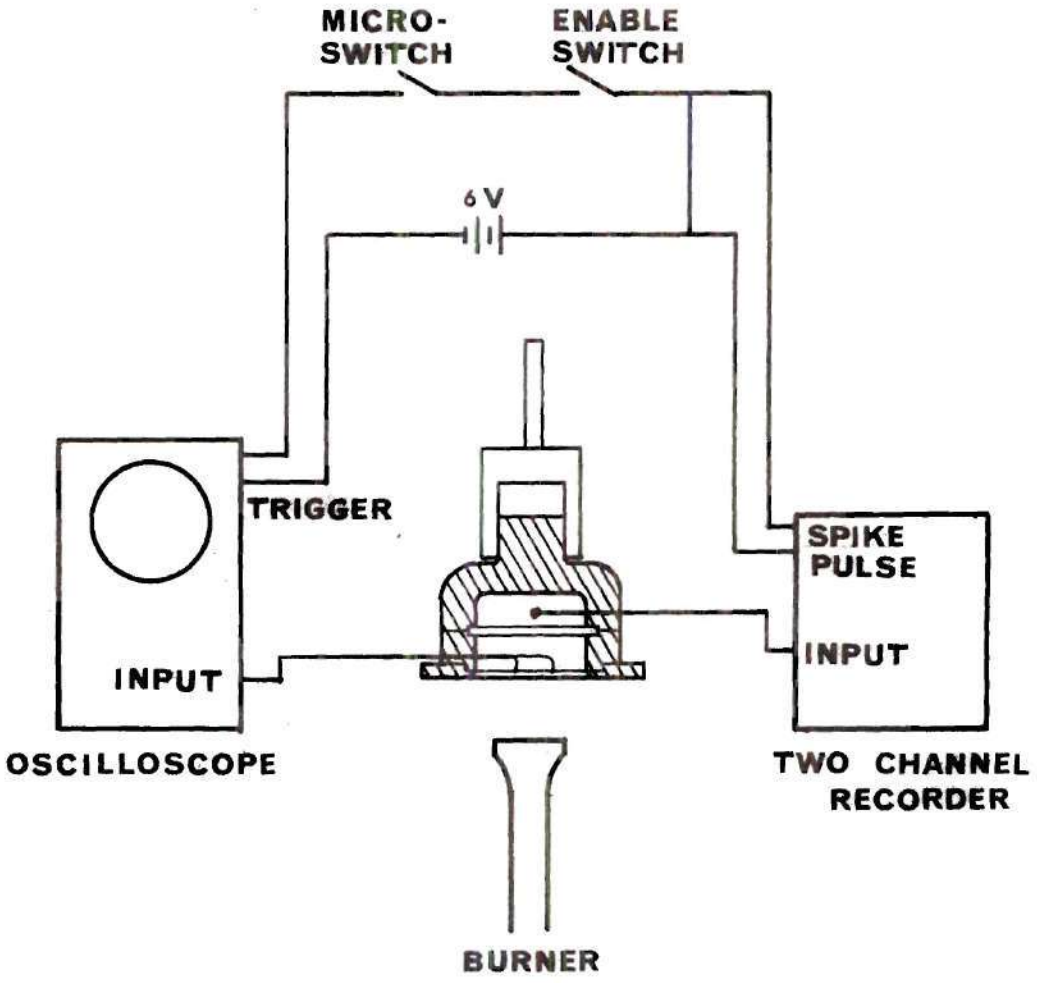

Figure 12. Schematic of Instrumentation for Temperature Measurement in the CFCA

small, i.e. of the order of 10^{-4} psig, and can not be accurately measured by ordinary water manometers. For this reason, two of the methods and techniques of micro-manometry were investigated.

For the first method, a Meriam micro-manometer, Model 34FB2 was used. The reported accuracy is $\pm$0.001-inch of water ($\pm .36 \times 10^{-4}$ psi) when corrected for temperature variations from the calibrated conditions. A simple quartz pitot tube shown in Figure 13 was used to obtain the stagnation pressures.

For the second method, a Datametrics Electronic Manometer, Type 1014A was used with a Barocel pressure sensor, Type 511-10 (Range: 10 mm Hg). The full scale linearity was calibrated and deviations found to be less than 0.35%. The x0.001 full scale reduction was used and afforded an accuracy of better than $\pm 2.0 \times 10^{-6}$ psi.

For both of the instruments used above, the pressure line from the quartz pitot tube to the measuring device was a four foot long 1/4-inch diameter Tygon tube.

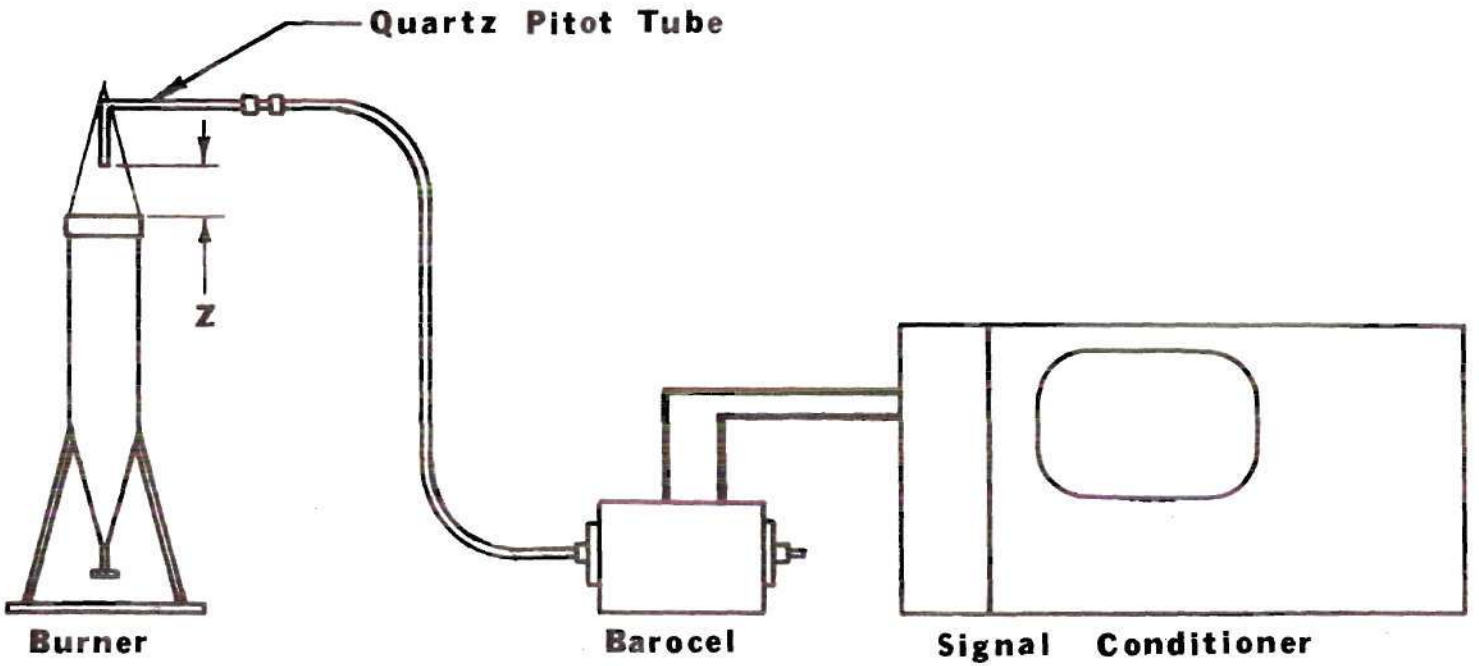

Figure 13. Quartz Pitot Tube

CHAPTER V

EXPERIMENTAL PROCEDURE

The previous chapter presented the equipment and instrumentation required for the determination of the convective film coefficients. This chapter lists the experimental procedures which were followed in obtaining the required data. First, a detailed outline of the film coefficient testing procedure is given. This includes not only the screen calibration and operating procedures, but also the ranges of process parameters. Secondly, the procedures followed in obtaining the gas flame stagnation pressure profiles are reviewed. Finally, the methods used to determine the rear surface free stream temperature are given.

Film Coefficient Testing Procedure

Since the temperature-time response of the stainless steel screens is required for the determination of the convective film coefficient, it was first necessary to calibrate the screen thermocouples. Small samples of the test screens selected to simulate the fabric geometry were made to form a thermocouple junction and their mV-temperature response was calibrated.

The wire cloth samples were first cut to approximately

11/16-inch diameter circles. A 0.0065-inch diameter 316 stainless steel wire was then welded to each screen using a Baldwin Lima Hamilton Corporation Model VTW 34 welder. Similarly, a 0.005-inch constantan wire was welded to the screens approximately 1/4-inch from the first weld. These second welds then formed the dissimilar thermocouple junctions. The three screens were placed inside radiation shielding along with an iron-constantan thermocouple. The entire assembly was placed in a Thermodyne Type 1400 furnace. The furnace temperature was raised in approximately 34°C increments to 540°C, each time allowing the furnace to reach a steady state, isothermal temperature. The mV output of each screen and the thermocouple were recorded at each step increment. The thermocouple output was converted to temperature readings, and the screen mV thermocouple temperature data was used to determine the fifth degree polynomial coefficients for a least square fit. Only one set of coefficients was determined from all the data of the screens since there was no significant difference in mV response among the three screens tested (150, 200, 250 mesh). The coefficients and a T-mV plot are given in Appendix G.

The following is a detailed outline of the testing procedure used in the determination of the convective film coefficients.

All recording equipment was turned on and sufficient

time allowed for it to warm up. The ventilation hood fan was turned on, the shutter solenoid power connected, and the 6V trigger battery switched on. Next, the cooling water to the shutters was turned on, and the primary valve for the injection air was opened, and both the room temperature and the barometric pressure were recorded.

The screen support assembly was mounted on the CFCA and positioned as required with respect to its height and orientation above the burner nozzle. The inlet line was connected to the air preheater. The oscilloscope triggering level, time base, and beam sensitivities were adjusted to the appropriate values and checked for triggering and response. The shutters of CITA were closed and the air tanks pressurized. The temperature of the injected air was slowly increased to the desired value, avoiding significant differential thermal expansions within the CFCA chamber while maintaining the required injection air flow rate. For the suction tests, there was no preheating and so the flow was simply set at the desired rate.

After the methane was ignited with the burner placed outside of CITA, the flame was stabilized at the desired heating intensity through air and fuel rate selection. The thermocouple output, manometer readings and flow meter readings were recorded for both the burner gases and the injection air.

The temperature behind the porous bronze plate in the

CFCA was monitored continuously on a Hewlett-Packard Moseley 7100MB strip chart recorder. The initial screen temperature (emf) was read from a Leeds and Northrup potentiometer.

The burner was placed below the water-cooled shutters, the shutter on the camera was opened, and the CITA shutter solenoid quickly released. The activation of the solenoid valves pressurized the air cylinders, retracted the shutters, and exposed the screen to the gas flame. One of the moving shutters closed a microswitch which connected a 6V DC voltage source and triggered the oscilloscope. One of the beams of the dual channel oscilloscope traced the temperature-time response of the wire cloth. The traces were recorded on Polaroid film (oscillogram).

After the oscilloscope trace was completed, the burner was removed from under the screen to avoid extensive heating of the chamber. The chamber thermocouple output, the oscilloscope time base and sensitivity, and the voltages which were required for the guard heater and air preheater were then noted.

Testing was done at three heights above the burner: 1.9 cm (3/4-inch), 7.9 cm (3-inches), and 10.5 cm (4-1/8-inches). At each height, three air-methane flow rate combinations were used: $\dot{m}_{air}$ = 1197.2 g/hr, $\dot{m}_{fuel}$ = 60.8 g/hr (low flow rate); $\dot{m}_{air}$ = 2072.0 g/hr, $\dot{m}_{fuel}$ = 104.6 g/hr (medium flow rate); $\dot{m}_{air}$ = 2814.3 g/hr, $\dot{m}_{fuel}$ = 140.7 g/hr (high flow rate). The above approximate flow rates produced

a stoichiometric equivalence ratio ϕ of 0.86 $\pm$ .01 (lean mixture, excess oxygen).

At each height, the injection mass flow rate was varied from 0 to approximately 300 g/hr. At the spacing of 1.9 cm, the suction mass flow rate was also varied from 0 to approximately -400 g/hr.

The temperature of the injected air was varied from room temperature to 300°C at each of the spacings as required for correlation.

The above tests were performed on the 200 mesh screen. For the 150 mesh screen, the air was injected at room temperature and the mass flow rate was varied from 0 to approximately 300 g/hr for each of the three air-fuel flow rate combinations at a spacing of 1.9 cm.

Rear Surface Reference Temperature

Since there are hot flame gases which flow through the cloth surface, it was suggested that the free stream reference temperature for the cloth's rear surface be the plateau temperature of the temperature-position profile. This plateau is shown in Figure 14. To determine whether or not such a plateau exists, the following test was made. An inert, 200 mesh stainless steel screen was mounted in a sample holder and suspended from the CITA support cradle with a sample holder support, as shown in Figure 15. A chromel-alumel thermocouple was suspended over the screen

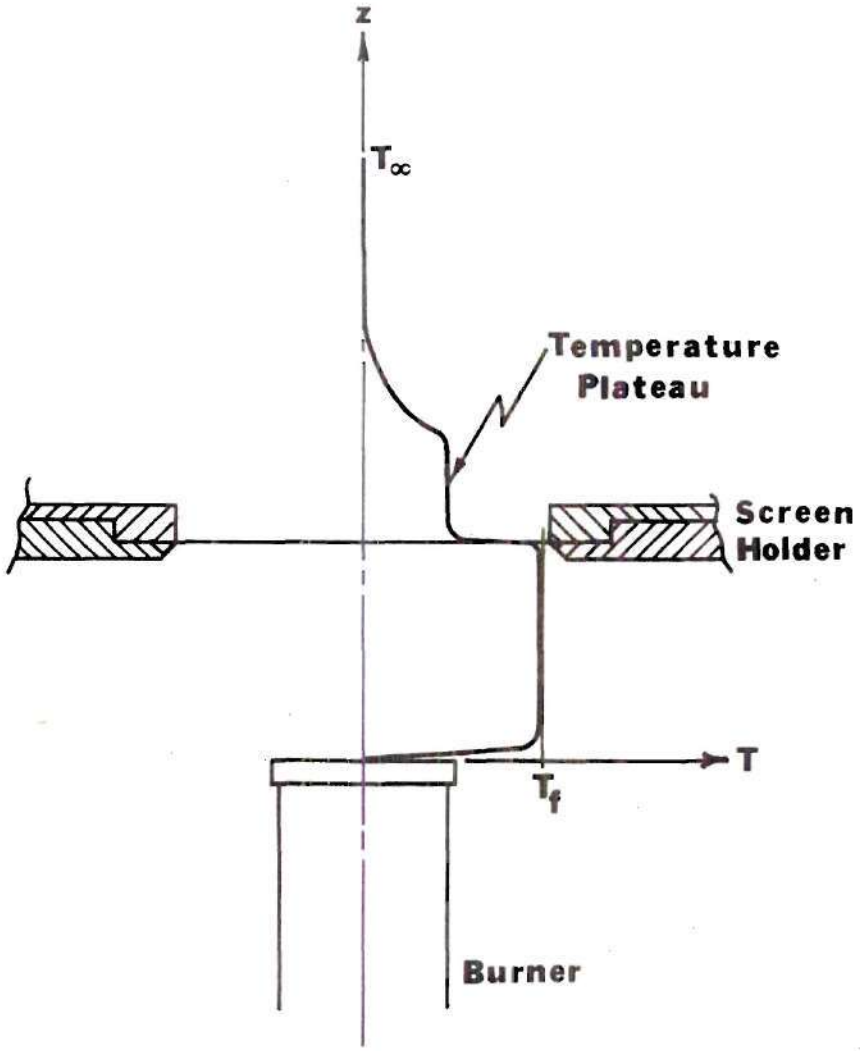

Figure 14. Free Stream Temperature-Position Profile

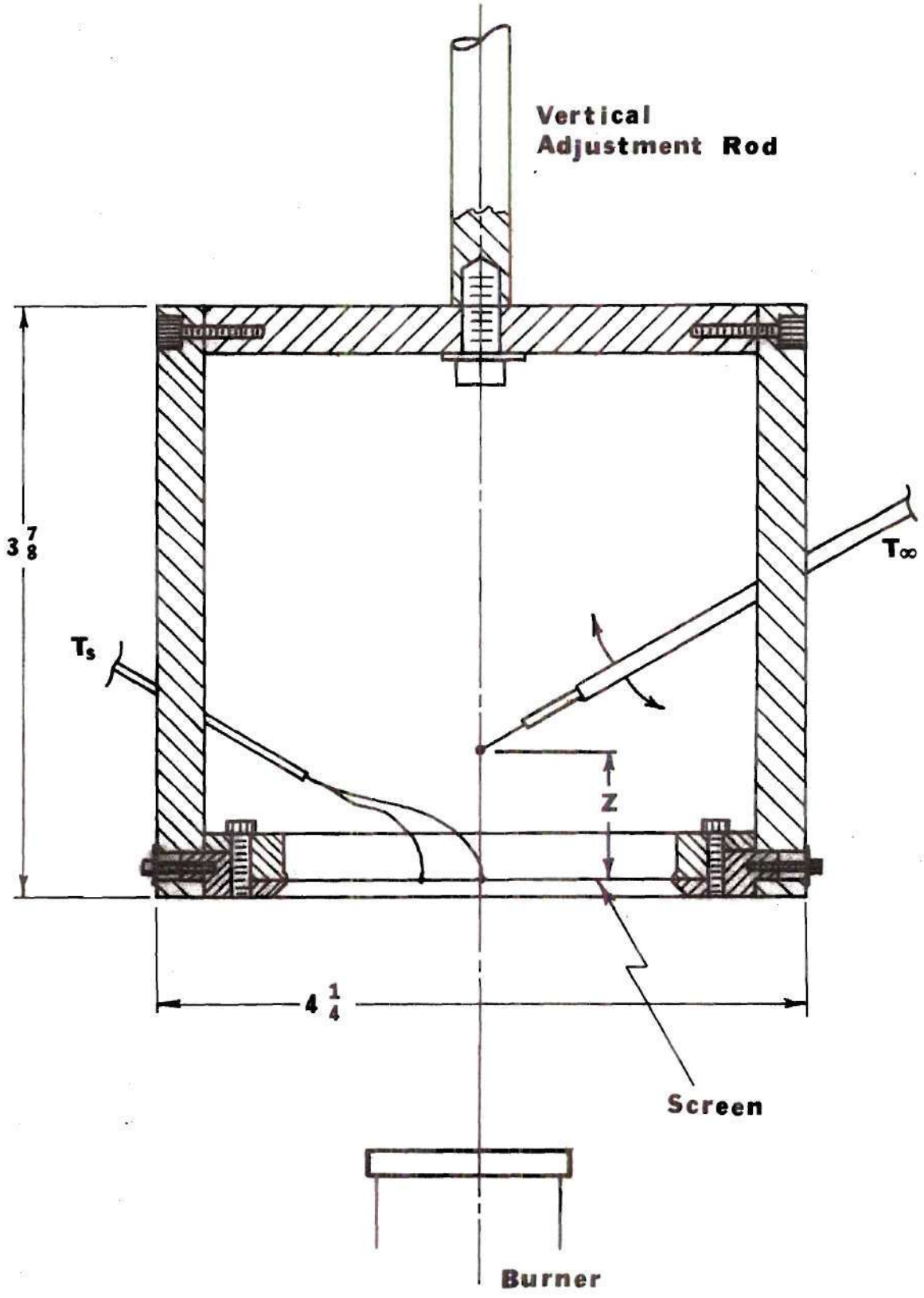

Figure 15. Screen Holder and Support in Position for Temperature Plateau Measurements

so that the T. C. bead could be positioned at various heights. Both a constantan wire and a stainless steel wire were welded to the screen and the screen was calibrated with a procedure similar to that used for the test screen.

The screen was suspended 3/4-inch above the burner and exposed to the high intensity convective heat flux. For these exposure conditions, the pressure differential which was exerted across the screen produced a mass flux through the screen. The free stream temperature position profile was recorded as the thermocouple bead was moved from a zero spacing to approximately 2.5 inches above the screen. This profile is shown in Figure 16.

The temperature initially decreased rapidly with spacing, and then decreased linearly at a lesser slope. The linear decay may be due to a mixing plume. However, there is neither an apparent temperature-position plateau nor an exponential temperature decay and the results must be viewed as inconclusive. For the special case of convective cooling of a plane horizontal solid surface, the driving potential for the heat transfer is the temperature difference between the plate and the ambient air. Due to the lack of conclusive evidence, this difference was used in this study.

Flame Stagnation Pressure Profiles

In order to determine a numerical value for the

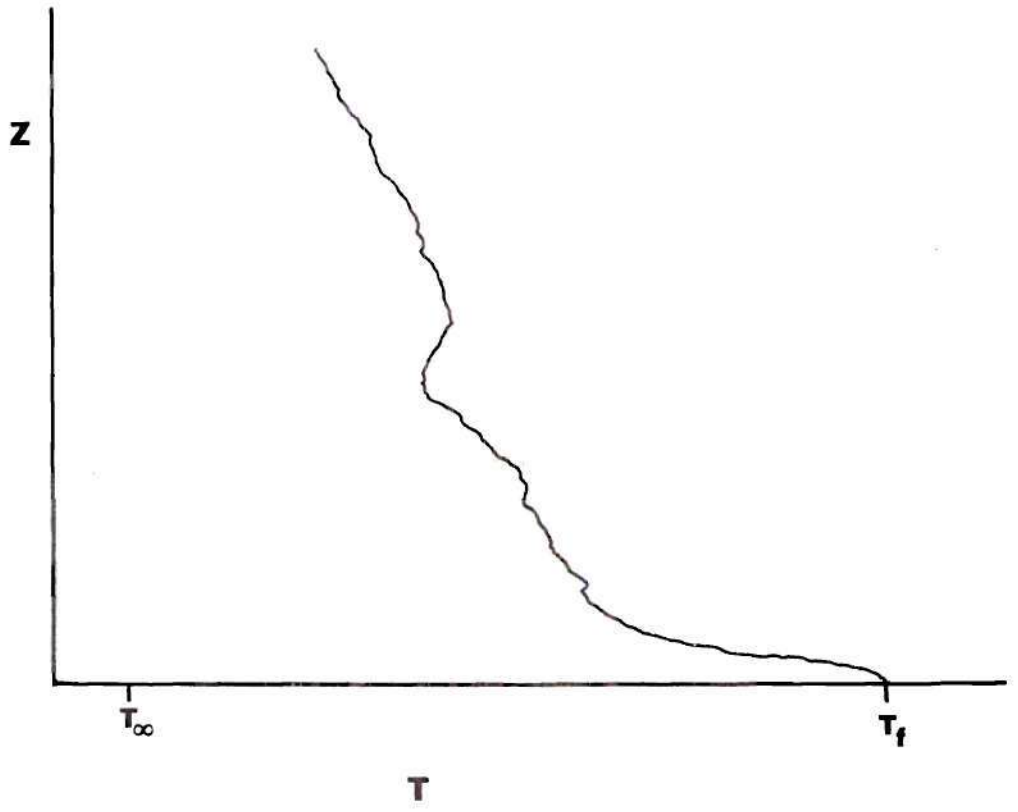

Figure 16. Free Stream Temperature Profile Test

injection Reynolds number $(Re)_o$ for decomposing, porous fabrics, it is necessary to know the stagnation pressure of the flame impinging on the fabric. This was determined experimentally.

The stagnation pressure profiles were first obtained using the simple quartz pitot tube shown in Figure 13 and the Meriam micromanometer described in the previous section. The maximum stagnation pressure was measured at five positions above the burner (0, 3/4, 1-3/4, 3, and 4-1/8 inches) for each of three burner mass flow rates (1265, 2158, and 2951 g/hr).

These measurements were then repeated using the Datametrics Electronic manometer in place of the micromanometer. The maximum stagnation pressures were measured at ten positions ranging from 0 to 12 cm above the burner. Again, these measurements were made for each of the three burner mass flow rates. There was considerable variation between the minimum and maximum stagnation pressures at less than 6 cm above the burner for the large burner mass flow rates. Consequently, both the maximum and minimum stagnation pressures were recorded at these positions.

At the larger spacings (greater than eight centimeters), there were considerable convective lateral fluctuations of the flame, particularly at the lowest burner flow rate. To minimize these fluctuations in order that representative pressure measurements could be made, two 12-inch x 20-inch

boards were placed vertically on each side of the burner and spaced 12-inches apart. This did not restrict the flow of air in the vicinity of the burner, but reduced the influence of the convective air currents in the laboratory.

CHAPTER VI

DATA REDUCTION AND RESULTS

In the previous two chapters, the equipment and instrumentation required for the determination of the convective film coefficients was discussed in detail and the experimental procedures were reviewed. In this chapter, the specific details of property evaluation are given and the results and correlations of the convective film coefficient determination tests are presented. The stagnation pressure profiles of the gas flame are then given and these experimental results and correlations are used in the prediction of fabric ignition times.

Determination of Property Data

The overall formulation of the problem was presented in the analysis and here are given the subsidiary details required for the determination and evaluation of thermophysical and material properties appearing in the dimensionless groups.

The problem of evaluating the gas properties is twofold. Firstly, the flow field consists of both the injected air and the combustion products of methane-air mixture from the burner. The properties of different gases, in general, behave differently with temperature. Secondly,

the temperature variations encountered in the flow field are very large.

It was first noted, however, that for a stoichiometric equivalence ratio of 0.86, the properties of the combustion products of methane in air are very closely approximated by those of air alone. Hence, the transport properties of the gases are taken to be that of air. Polynomial coefficients were determined for the least-square-fit of the property data of air and used in the evaluation and reduction of data. The property evaluations are given in Appendix D.

To account for property variation with temperature, the reference temperature method was employed. For this method, the transport properties appearing in the dimensionless groups are evaluated at a mean temperature between the cloth temperature and the flame temperature. The selection of the reference temperature was based on a least-square-fit criterion in correlating the data from the film coefficient determination tests. The gas properties within the cloth instirstices and below the cloth surface were evaluated at this reference temperature. Above the cloth surface, the gas properties were evaluated at the mean film temperature defined by equation (29).

The thermophysical properties of the twenty GIRCFF fabrics were determined at Georgia Tech and presented in the Second Final Report on the Fabric Flammability Research [3]. Those properties relevant to this study are summarized

in Appendix F.

One of the material properties which must be specified in order to compute the numerical values of the dimensionless groups is the fabric permeability K. The ratio of permeability to viscosity μ and effective cloth thickness δ is commonly given as the porosity P.

$$P = \frac{K}{\mu\delta} \tag{83}$$

Factory Mutual measured the room temperature porosities [8] of the twenty GIRCFF fabrics and these measurements are used to determine the ratio of the room temperature permeability to the effective cloth thickness

$$\frac{K}{\delta} = P\mu_a \tag{84}$$

The porosity measurements, as reported by Factory Mutual, are given in Appendix B. The range of room temperature porosities for the twenty GIRCFF fabrics is 0.072 to 7.4 ft^3/lb_f.

The porosity values for fine mesh wire cloths are available from the literature, Appendix C, and are given by

$$P = \frac{0.02}{\mu M}\left(\frac{\alpha^{3/2}}{1-\alpha^2}\right) \tag{85}$$

where α is the fraction of open area and M is the mesh number. Typical fine mesh screens have a porosity range of 0.80 to 8.9 ft^3/lb_f. A "zero porosity" screen can be simulated by a metal foil or the heat transfer can be inferred by interpolation of injection and suction data to zero mass flux at the screen surface.

Determination of Convective Film Coefficients

The equipment and instrumentation used in the determination of the convective film coefficients were described in Chapter III and the associated procedures were outlined in Chapter IV. The scaling parameters which describe the heat transfer process and correlate the experimental data were presented in Chapter II. Here the results of these tests are presented and the data are correlated in terms of the derived scaling parameters.

A total of 128 tests were made in which the following five process parameters were varied over the ranges described in the previous chapter: the screen temperature T_s, the injection mass flow rate $\dot{m}_o$, the burner mixture mass flow rate $\dot{m}_b$, the cloth-burner spacing L, and the screen mesh M.

The description of the external flow required the stoichiometric equivalence ratio, the total mass flow rate to the burner, and the free flame temperature at the selected screen position. The stoichiometric equivalence ratio ϕ was held at 0.86 $\pm$ 0.01 (lean mixture, excess

oxygen). Both the air and methane flow meters had been calibrated and each measured flow rate was corrected for both temperature and pressure variations from the air calibration conditions [30] using

$$q_1 = q_c \sqrt{\frac{T_\ell \; P_c}{T_c \; P_\ell}} \tag{86}$$

where the subscript 1 refers to the laboratory or actual conditions, the subscript c refers to the calibration conditions, and q is the volumetric flow rate. The gas flame temperatures T_f used in this study are the results of averages taken over several fabric ignition time tests [3]. The steady state flame temperature was measured during these ignition time measurements in the plane of the fabric holder after the fabric had burned or melted away. Each of these temperatures were experimentally confirmed by repeating the flame temperature measurements and additional data taken where needed. A summary of these temperatures is given in Appendix H.

The mass flux through the screen was measured as outlined in Chapter IV using a calibrated variable area flow meter. The volumetric flow rate reading was corrected for both temperature and pressure using equation (86).

The film coefficient was evaluated directly from equation (82)

$$\bar{h}_1 = \frac{(\rho\delta)_s (dT_s/d\tau) C_{p,s}}{(T_f - T_s)} \tag{82}$$

in which the specific heat $C_{p,s}$ was evaluated at the initial screen temperature. The specific mass of the screen $(\rho\delta)_s$ was determined as outlined in Chapter IV and is given in Appendix A. The thermal response of the screen to the gas flame was characterized by its temperature-time profile as recorded on the oscillograms. From each emf-time oscillogram, 30 to 40 points were read and the emf values converted to temperatures using the calibration polynomial given in Appenidx G. The temperature-time values were then plotted and the curves found to be very nearly linear. The screen response was therefore characterized by the linear slope $(dT/d\tau)$ obtained by passing a straight line through the points. In cases where the entire temperature-time profile was not linear, the initial slope was used to characterize the response. A sample data sheet and its reduction are shown in Figures 17 and 18.

The film coefficient $\bar{h}_1$ is presented in terms of the Nusselt number based on the screen radius as given by equation (47). This equation is repeated here for convenience

$$Nu_1 = \frac{\bar{h}_1 R}{k} \tag{47}$$

GEORGIA INSTITUTE OF TECHNOLOGY
SCHOOL OF MECHANICAL ENGINEERING
FABRIC FLAMMABILITY PROJECT
CONVECTIVE HEAT TRANSFER COEFFICIENT

DATE: 12-4-73 TEST NO. 14
DATA: G.L.W. HOLDER NO. 1
MESH 200

SCREEN TEMP. 1.744 mV 37.9 °C
SCREEN HEIGHT ABOVE BURNER 3/4 inches.
SCREEN INCLINATION ANGLE 0 degrees.
ROOM TEMPERATURE 67 °F
BAROMETRIC PRESSURE 28.985
INJECTION AIR PRESSURE 5.85 inches, water.
INJECTION AIR I-C THERMOCOUPLE 1.020 mV, 20 °C.
INJECTION AIR FLOW RATE 6.125 tant. cm, 5.479 CFH.

	P, REG DEL, PSI	P("Hg)	T(mV)	T(°F)	R(cm)	R(CFH)
METHANE	6	12.6	1.040	68.7	9.45	3.50
AIR	20	13.8	1.008	67.6	6.85	51.2

A/F: 19.95 Ø: 0.8582

PREHEATER AC VOLTAGE 11 V.
GUARD HEATER AC VOLTAGE 0 V.
INLET CHAMBER C-A T.C. 1.360 mV, 33.9 °C.

COLD JUNCTION 0 °C.

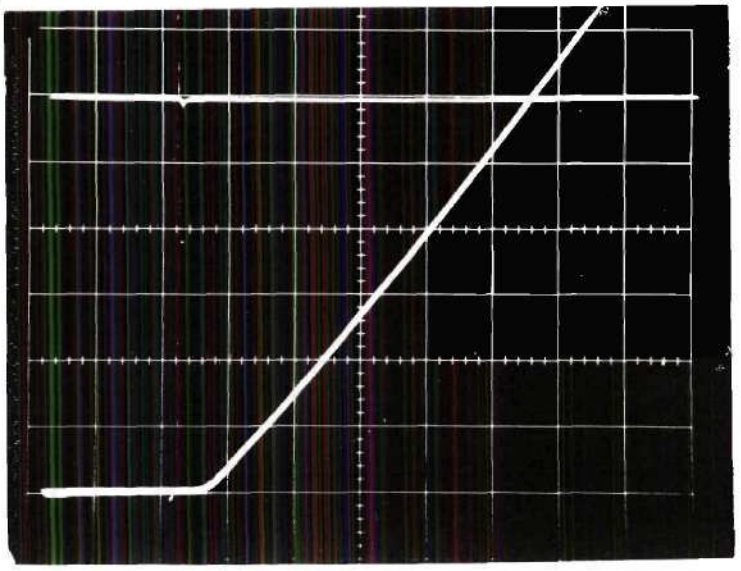

--OSCILLOSCOPE--

TIME BASE 50 m sec/cm

UPPER BEAM 2. V/cm

LOWER BEAM 1. mV/cm

Figure 17. Sample Data Sheet (Oscillogram).

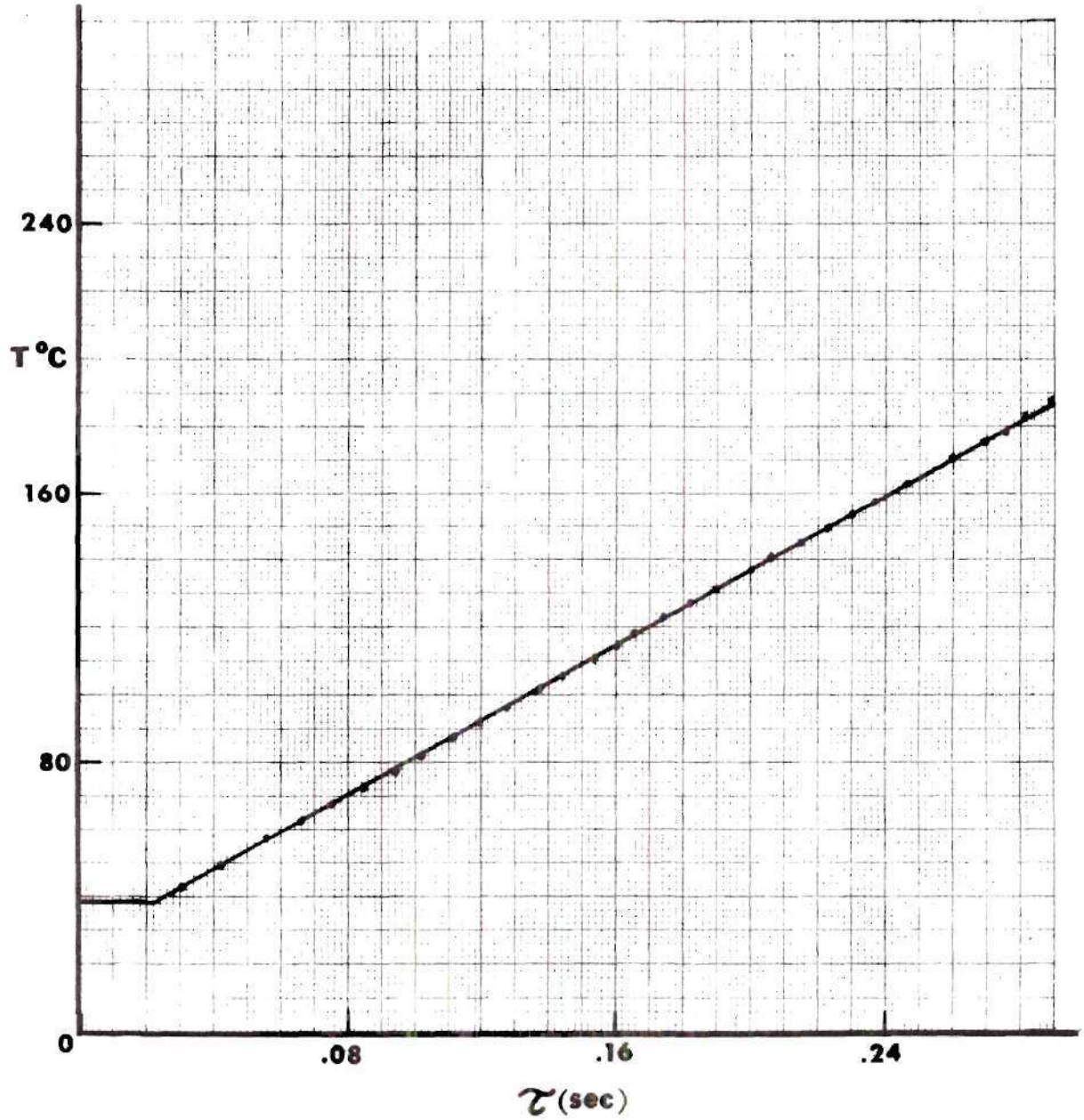

Figure 18. Temperature-Time Plot of Screen Response

The heat transfer data was then correlated using the burner Reynolds number Re and the injection Reynolds number $(Re)_o$ given by equations (45) and (52), respectively.

The mass flux at the fabric suface is simulated by the controlled mass injection or suction. The injection Reynolds number $(Re)_o$ is based on this mass flux $\dot{m}_o$ and is given as

$$(Re)_o = \frac{(\dot{m}_o/A_s)R}{\mu} \tag{87}$$

where A_s is the area of the screen, 31.67 cm^2, and R is the screen radius. The Nusselt number was found to vary linearly with this parameter as seen in Figures 19 to 23. Further, there were no systematic departures from this linear dependency with the 25 tests with elevated initial cloth temperatures.

The burner Reynolds number is based on the burner mass flow rate $\dot{m}_b$ and is given as

$$Re = \frac{(\dot{m}_b/A_b)D}{\mu} \tag{88}$$

in which A_b is the burner exit area, 10.75 cm^2.

The selection of the reference temperature was based on a least-square-fit criterion in which the reference temperature, Reynolds number exponent ex, and constant

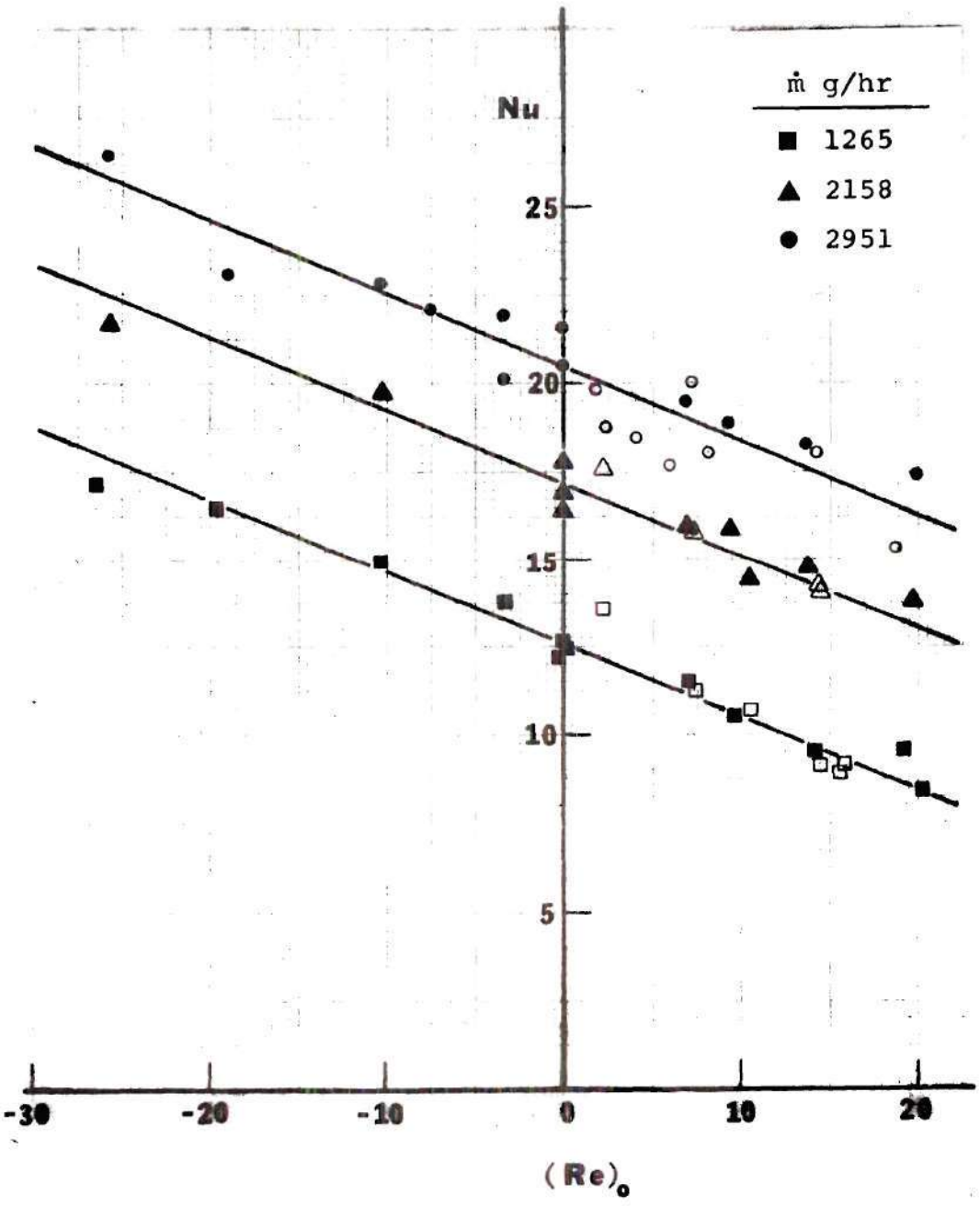

Figure 19. Nusselt Number vs Injection Reynolds Number with Free Stream Reynolds Number as Parameter at L/D = 0.515 (Open symbols designate elevated temperature)

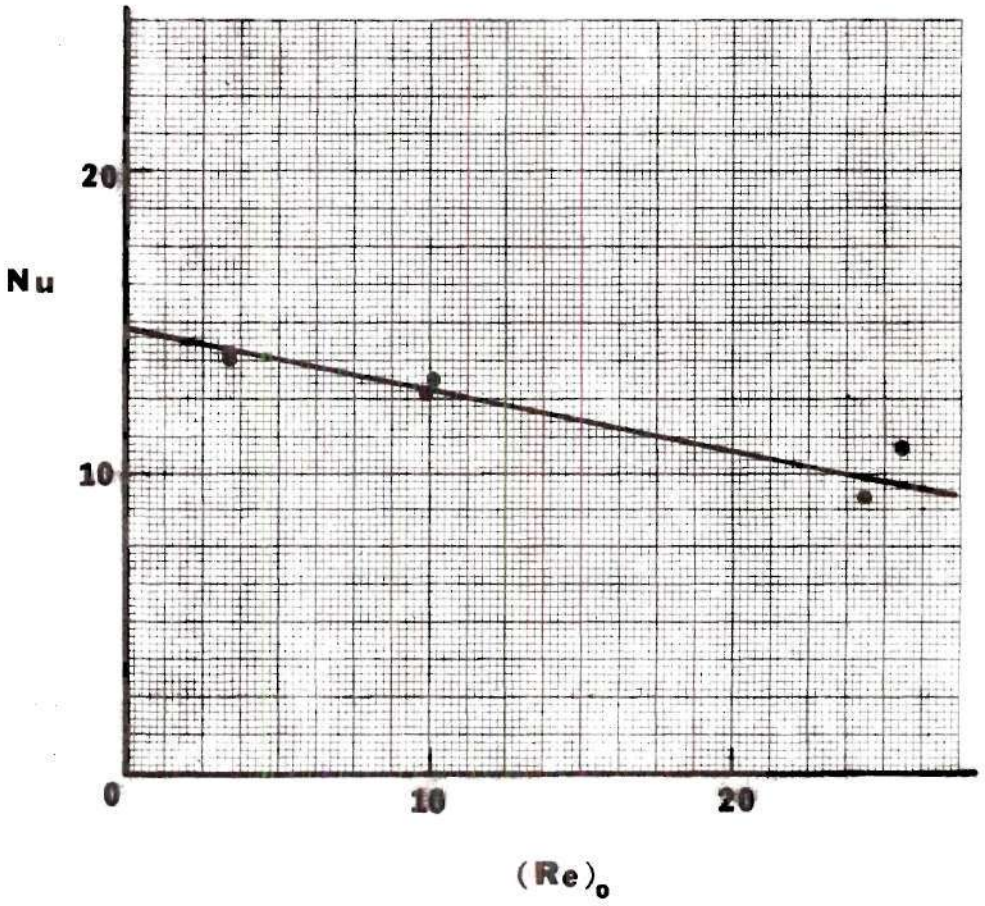

Figure 20. Nusselt Number vs Injection Reynolds Number at L/D = 1.20

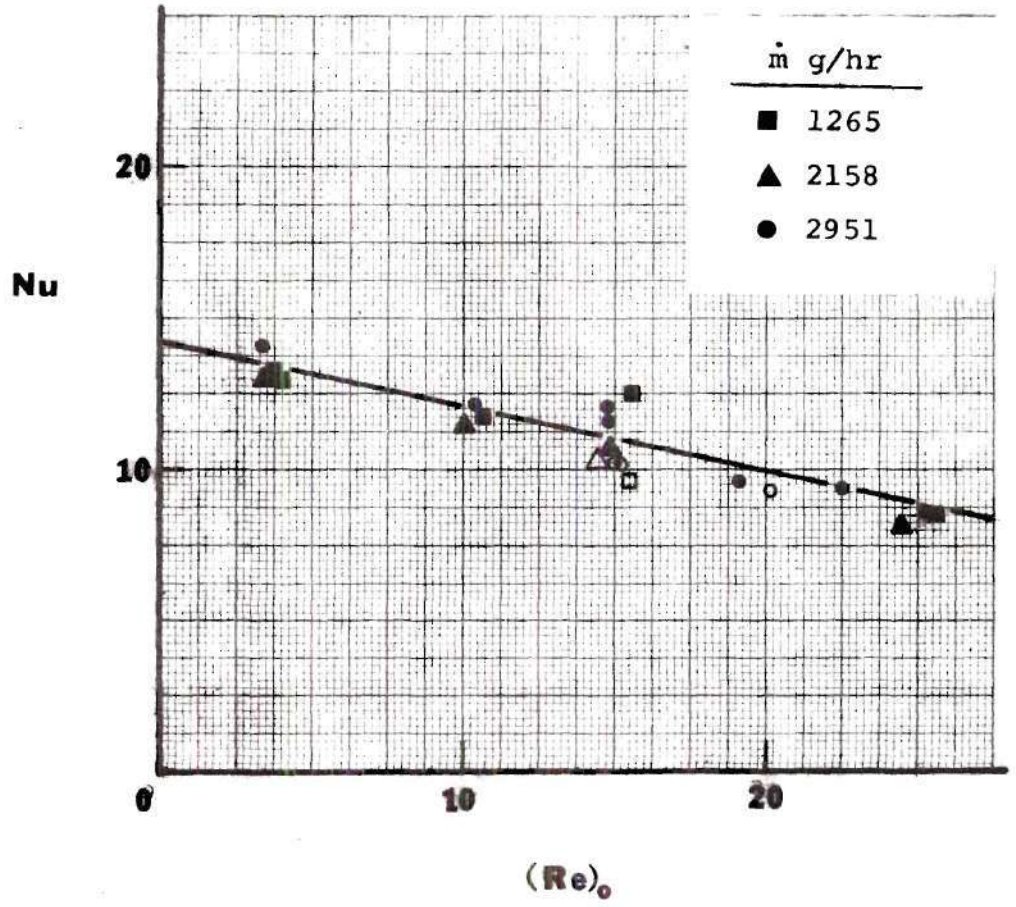

Figure 21. Nusselt Number vs Injection Reynolds Number at L/D = 2.06 (Open symbols designate elevated temperatures)

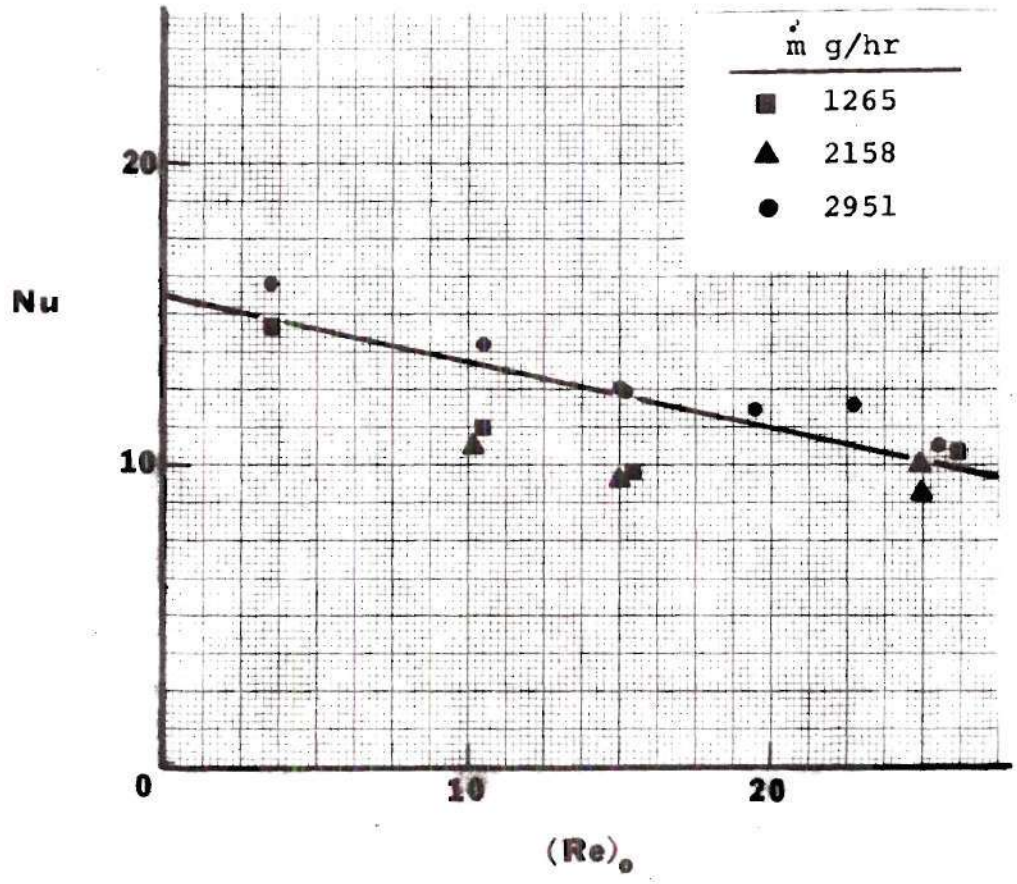

Figure 22. Nusselt Number vs Injection Reynolds Number at L/D = 2.83

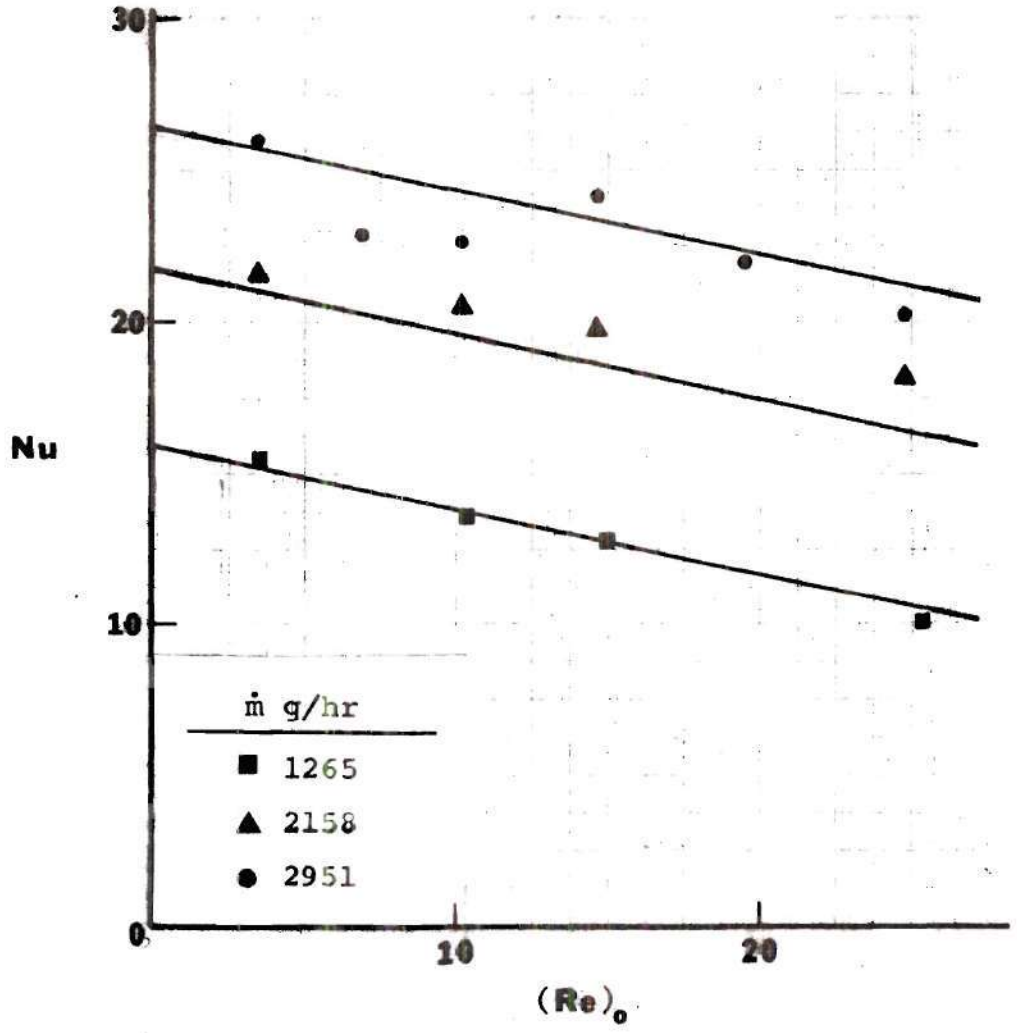

Figure 23. Nusselt Number vs Injection Reynolds Number with Free Stream Reynolds Number as Parameter at L/D = 0.515 for a 150 Mesh Screen

coefficients C_1 and C_2 were simultaneously optimized for the form

$$Nu = C_1(Re)_o + C_2Re^{ex} \tag{89}$$

Using this optimization for the data at L/D = 0.515, the minimum standard deviation was obtained when the thermodynamic and transport properties are evaluated at the free flame temperature T_f and the Reynolds number exponent was found to be 0.59. For this spacing, the numerical coefficient C_1 is -0.19829. (Positive injection Reynolds number indicates injection. Negative injection Reynolds number indicates suction.)

The least-square-fit criterion was also used to correlate the data at the other spacings. Again, the free flame temperature gave the best correlation. For each spacing, the numerical coefficient of the injection Reynolds $(Re)_o$ was found to agree very well with that obtained at L/D = 0.515. There also was no discernable mesh number effect or burner Reynolds number effect on this coefficient. Since more data values were obtained at this spacing than at the other spacings, a greater confidence is placed on that coefficient and that value of C_1 was chosen to be a constant for all the tests.

Six heat transfer coefficients were obtained at a spacing of L/D = 1.20 (1.75-inch spacing) to confirm the

linearity of the Nusselt number dependence on the injection Reynolds number. Since all six tests at this spacing were at the high burner flow rate, the free stream Reynolds number exponent could not be determined, and was arbitrarily set equal to zero.

At the two largest spacings (L/D = 2.06 and L/D = 2.83), the heat transfer was found to be independent of the burner flow conditions, within the range of this study as defined in the previous chapter. That is, the least-square-fit criterion gave a zero exponent for the burner Reynolds number.

The coefficient of the burner Reynolds number was found to vary with both spacing and mesh, so that this coefficient must be given as a function of L/D and mesh number. Without additional data, small differences in the exponent of the burner Reynolds number for different screen meshes are not distinguishable, and the exponent is listed as 0.59 for both the 200 mesh screen and the 150 mesh screen.

The resultant correlation equations are given below. For the 200 mesh screen:

$$Nu = -0.19829\ (Re)_o + 0.5159\ Re^{.59} \quad \text{for } L/D = .515 \qquad (90)$$

$$Nu = -0.19829\ (Re)_o + 14.829\ Re^{0*} \quad \text{for} \begin{cases} L/D = 1.20 \\ Re \approx 515 \end{cases} \qquad (91)$$

$$Nu = -0.19829\ (Re)_o + 14.085\ Re^0 \text{ for } L/D = 2.06 \qquad (92)$$

$$Nu = -0.19829\ (Re)_o + 15.066\ Re^0 \text{ for } L/D = 2.83 \qquad (93)$$

For the 150 mesh screen at a spacing of L/D = 0.515:

$$Nu = -0.19829\ (Re)_o + .65501\ Re^{.59} \qquad (94)$$

The values of the Nusselt number predicted by the above equations $(Nu)_{pr}$ are plotted versus those measured experimentally Nu in Figure 24. The standard deviation is 0.835. A sample listing of the experimental results is given in Table 1. A complete listing is given in Appendix I.

Two of the parameters listed in equation (53) which may effect the heat transfer were not varied. The first of these is the geometric scaling parameter R/D. Neither the burner diameter D nor the screen radius R were varied in these tests. The second parameter was the Prandtl number Pr which was found to remain constant over the entire range of testing. The influence of the Prandtl number on the heat transfer could not be determined, but since the free flame temperature was used to evaluate the properties, the same Prandtl number would also occur in the fabric ignition

---

*As was noted previously, the exponent on the Reynolds number could not be determined and was arbitrarily set equal to zero.

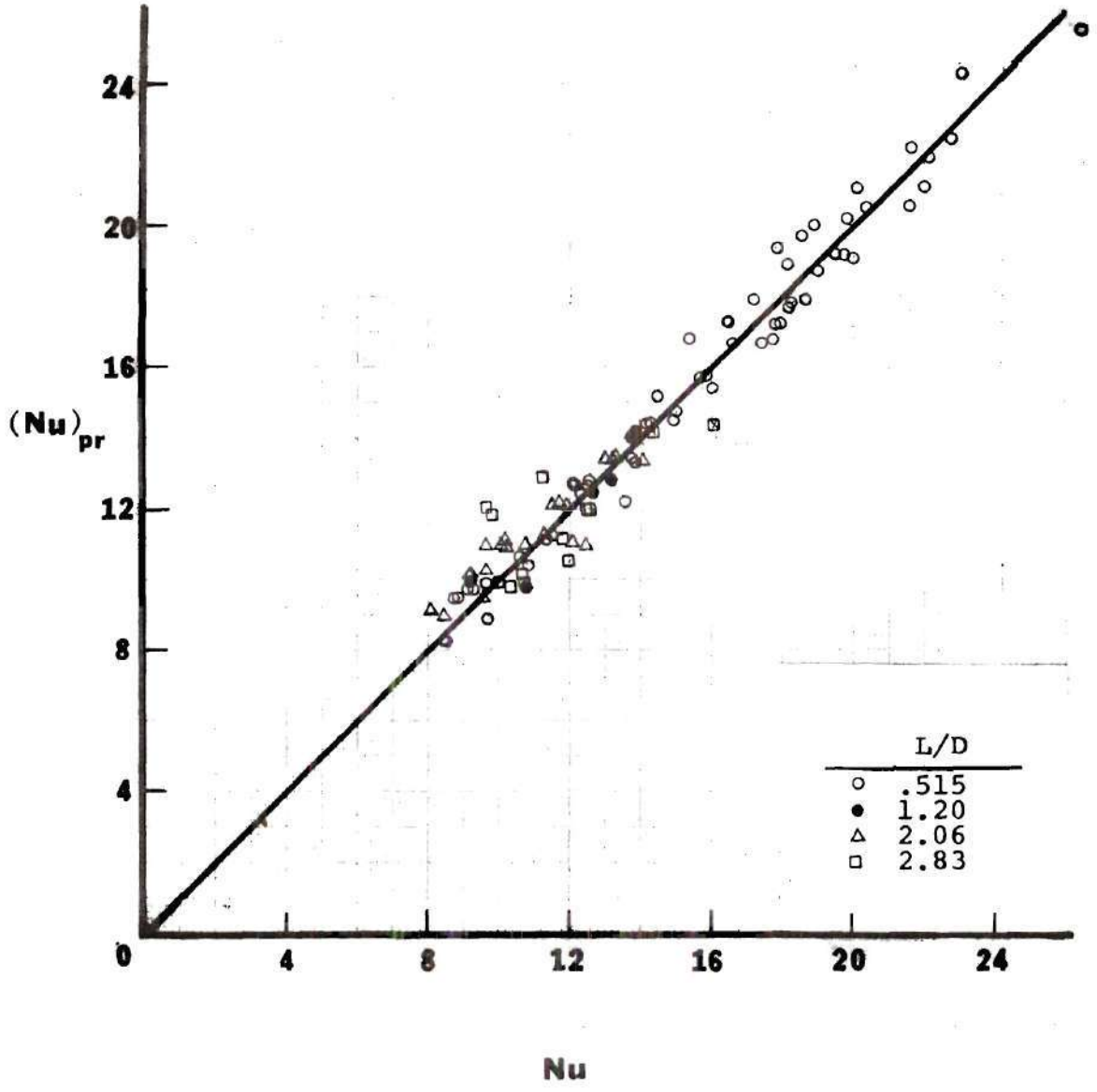

Figure 24. Correlation of Experimental Results

Table 1. Convective Heat Transfer - Similarity Parameters

Exp.	T_s(°C)	T_f(°C)	h(W/cm^2°C)	Nu	$(Re)_o$	Re	Pr	L/D	M	V_o(cm/s)
1	38.2	1290	.0029852	9.68	19.32	227.6	.683	.514	200	2.950
2 *	40.3	1290	.0029682	9.63	19.17	228.1	.683	.514	200	2.947
3 *	38.2	1352	.0060385	18.94	19.80	517.1	.681	.514	200	3.088
4 *	38.6	1352	.0058241	18.26	19.80	518.0	.681	.514	200	3.092
5	38.5	1352	.0055423	17.38	19.80	516.8	.681	.514	200	3.089
6 *	40.1	1347	.0046522	14.63	19.40	380.3	.681	.514	200	3.038
7 *	38.6	1347	.0043764	13.76	19.89	382.3	.681	.514	200	3.101
8	38.9	1347	.0043943	13.82	19.87	385.3	.681	.514	200	3.101
9 *	38.2	1347	.0046955	14.76	19.87	382.4	.681	.514	200	3.094
10 *	38.9	1290	.0027881	9.04	19.82	228.1	.683	.514	200	3.032
11	38.7	1290	.0026114	8.47	20.27	227.3	.683	.514	200	3.099
12 *	38.1	1290	.0030990	10.05	9.65	226.5	.683	.514	200	1.489
13	38.7	1290	.0032607	10.58	9.67	227.2	.683	.514	200	1.478
14	37.9	1347	.0050836	15.99	9.47	381.2	.681	.514	200	1.488
15	38.4	1352	.0060540	18.99	9.44	517.8	.681	.514	200	1.489
16 *	38.0	1290	.0036537	11.85	.00	225.9	.683	.514	200	.000

tests and so thermal similarity is maintained.

In addition to the parameters used in the above correlations, the injected air velocity was computed to allow possible comparison to experimental investigations in which the results are correlated in terms of a velocity. To calculate this velocity, the injected air temperature is required. The screen and initial injected air temperatures were taken as being equal since the chamber temperature was found to be within 10°C of the screen temperature. The mass flow rates were used directly for both the free stream and injection Reynolds numbers and therefore these parameters are not affected by this assumption and represent area averaged rates.

Flame Stagnation Pressure Profiles

The equipment and instrumentation used to measure the stagnation pressure of the burner gas flames were described in Chapter III and the associated procedures outlined in Chapter IV. The results of these measurements are presented in this section.

Two sets of stagnation pressure measurements were obtained using the Meriam Micro-manometer and the quartz pitot tube. The maximum variation between pressures measured in the consecutive tests was as much as 40%. The results of the two sets of pressure measurements were averaged and these averages are given in Table 2. Despite the considerable

Table 2. Pressure Profile Measurements

$P \times 10^4$ psi

Test 1 = Meriam Micromanometer
Test 2 = Electronic Manometer

L		Burner Mass Flow Rate, g/hr					
cm	in	1265		2158		2951	
0	0	4.695	3.868	5.5025	-----	8.216	-----
1	-	-----	0.5995	-----	1.643	-----	2.166/.6382
1.905	3/4	0.900	0.7253	1.569	1.296	2.057	1.895/.735
3	-	-----	0.8703	-----	1.431	-----	1.934/1.354
4.445	1 3/4	1.165	1.064	1.972	1.644	2.422	2.031/1.683
6	-	-----	1.296	-----	1.837	-----	2.03
7.62	3	1.499	1.451	2.395	2.031	2.740	2.166
9	-	-----	1.354	-----	2.263	-----	2.263
10.775	4 1/8	1.330	1.354	2.495	2.418	2.981	2.398
12	-	-----	1.354	-----	2.514	-----	2.514
		Test 1	Test 2	Test 1	Test 2	Test 1	Test 2

error, these readings indicate the trend, if not the magnitudes, of the pressure profiles.

A third set of stagnation pressure measurements was obtained using the Datametrics Electronic Manometer in place of the Meriam micro-manometer. The accuracy and resolution of the Electronic Manometer was recognized to be much better than the Meriam manometer and, consequently, this set of measurements was used to characterize the stagnation pressure. These results are also given in Table 2 and plotted in Figure 25. Several stagnation pressure profiles were also obtained as the quartz pitot tube traversed horizontally through the flame. These profiles were obtained at several heights above the burner. A representative profile is shown in Figure 26.

It may be noted from both Table 2 and Figure 26 that there were large global pressure variations in addition to the local fluctuations for the burner flow rate of 2951 g/hr. The global variations remained relatively fixed in location with respect to the burner exit nozzle. However, these variations rapidly decreased in about one burner diameter, and so the global maximum and minimum pressure readings (within the projected area of the burner face) are recorded for the lower spacings only.

It may be noted from Figure 25 that the stagnation pressure dropped sharply to a minimum and then began to gradually increase. Each of these phenomena are discussed

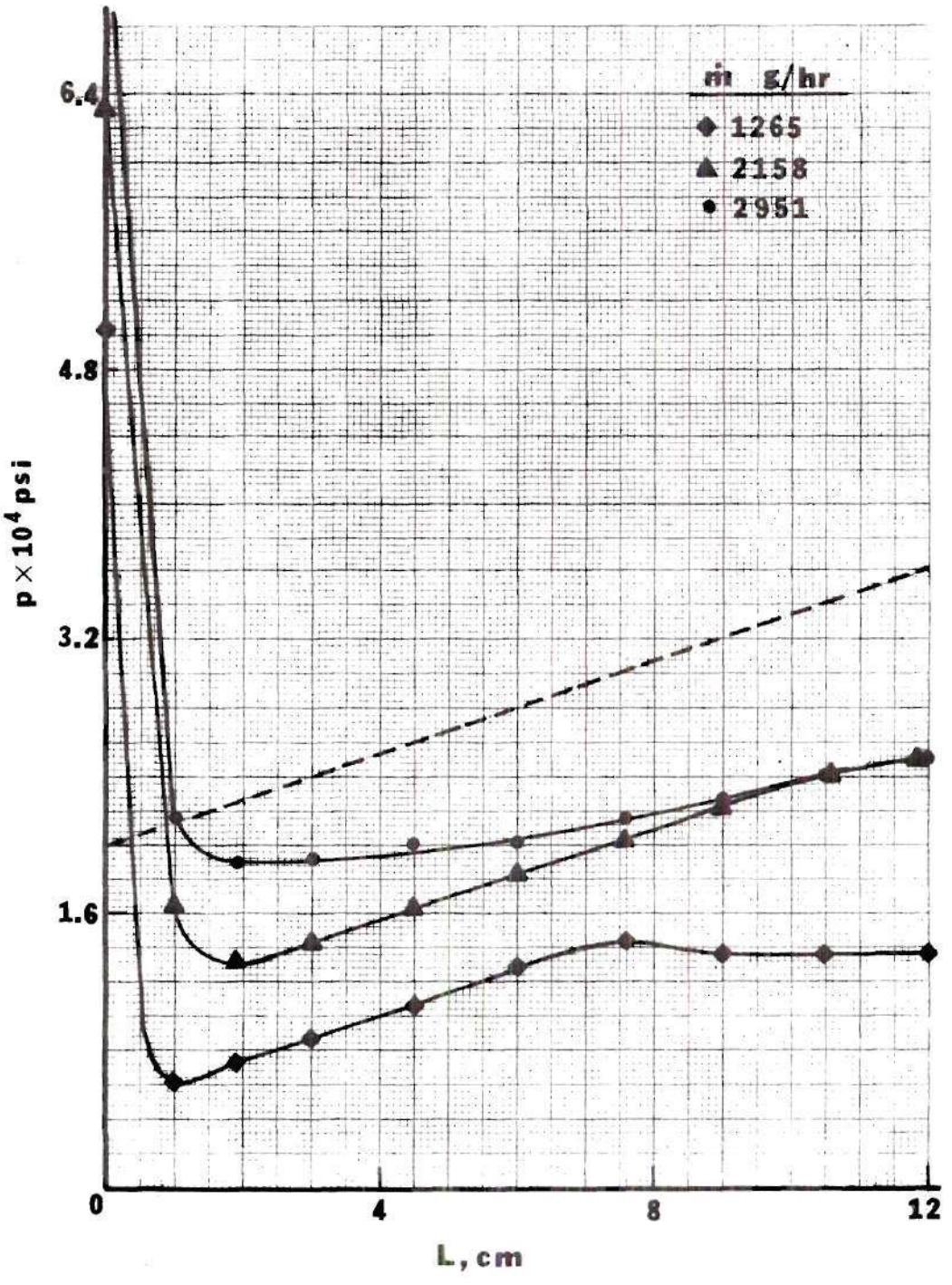

Figure 25. Flame Stagnation Pressure Profiles (Dashed line represents the pressure profile predicted by using equation (66) for the large burner mass flow rate)

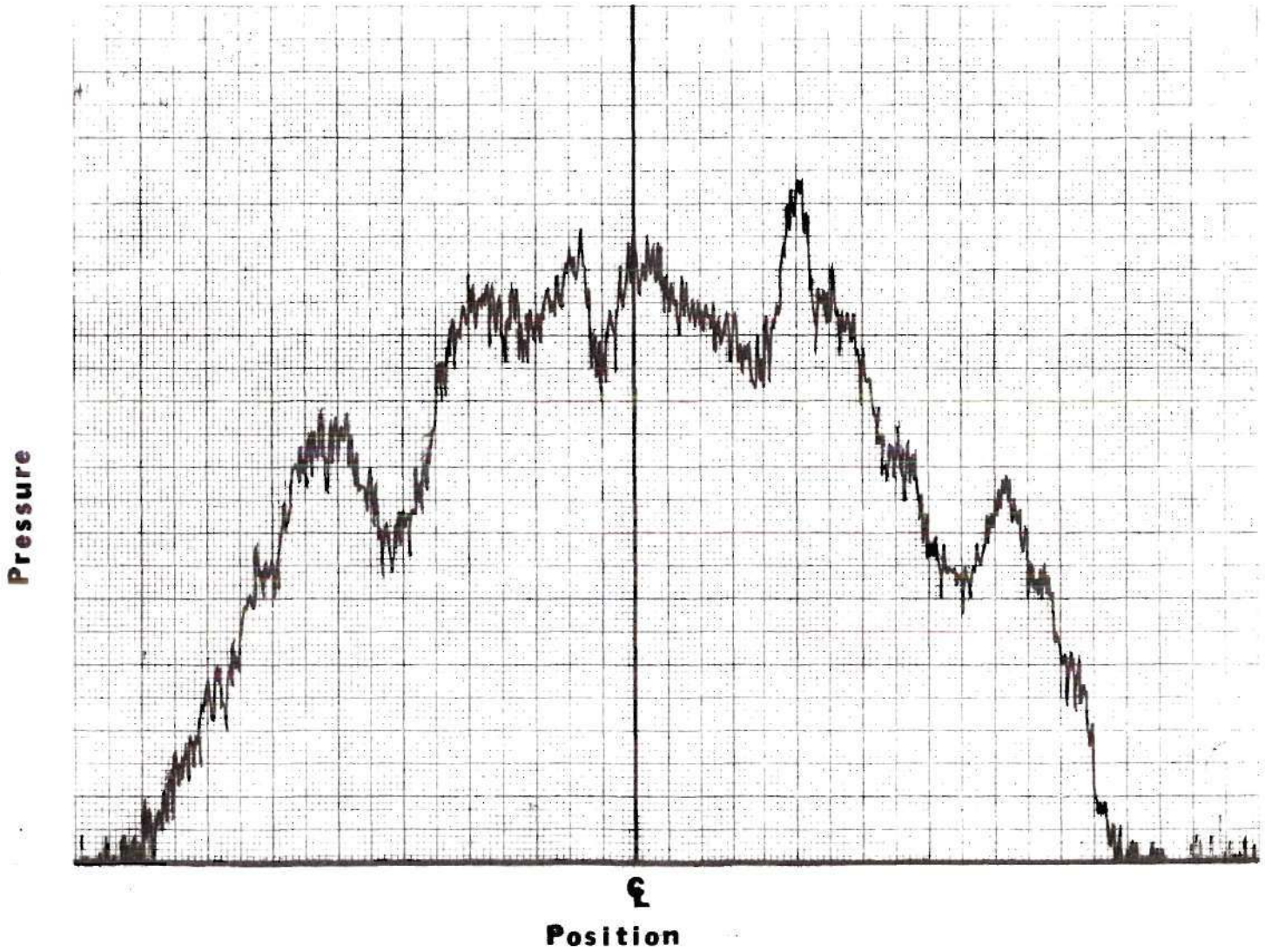

Figure 26. Horizontal Plane Pressure Profile at L/D = 0.515

below.

The sharp increase in stagnation pressure found at very small burner-pitot tube spacing is accounted for by noting that a very course grid at the face of the burner reduces the effective cross-sectional area by approximately 38%. Thus, the velocity or mass flux through the 2mm square grid openings is considerably larger than that a short distance downstream.

The gradual increase in stagnation pressure (and hence velocity) is largely attributable to the buoyancy forces associated with the temperature difference between the flame gases and the ambient air. The extent to which these buoyancy forces influence the velocity profile is determined by applying the Bernoulli equation for inviscid flow between the burner and a point within the flame potential core at some distance L above the burner. Combining this with the static ambient pressure drop

$$V_L = \sqrt{\frac{2gL(\rho_\infty - \rho_f)}{\rho_f} + V_b^2} \tag{95}$$

in which V_L is the velocity at location L. This equation is readily nondimensionalized by introducing the Reynolds number Re as defined in equation (45) to form the expression

$$Re_L = Re\sqrt{1+\left(\frac{Gr}{Re^2}\right)\left(\frac{D}{L}\right)^2} \tag{96}$$

in which the ratio of buoyancy forces to inertia forces is expressed by the familiar term Gr/Re^2. The modified Reynolds number at spacing L in the above expression is defined as

$$Re_L = \frac{\rho_f V_L D}{\mu} \tag{97}$$

Since the burner gases form a free jet, the stagnation pressure is equivalent to the dynamic pressure so that the velocity V_L predicted by equation (95) is used to predict the shape of the stagnation pressure profile

$$\Delta P = \frac{1}{2} \rho_f V_L^2 \tag{98}$$

It was found, however, that this simple model can be used only to predict the shape of the stagnation pressure profile for the high burner mass flow rate. This predicted curve is shown in Figure 25 as a dotted line. The pressure profiles for the other flow rates can not be as accurately predicted, especially for the low flow rate at larger spacings. Both the drag and heat loss, which were implicitly neglected in using the Bernoulli equation, would tend to lower the velocity and hence the measured stagnation pressure. Since the Bernoulli equation predicted a higher pressure drop than what was experienced, the drag and heat loss are considered to be significant.

Exposure Time Delay

There is a time delay between the instant the CITA shutters separate to the time when the flame gases reach the fabric surface. This time was considered [6] to be negligible with respect to the much longer fabric ignition times. The interval of time from the instant the two shutters separate to full exposure of a 63.5 mm diameter cloth was reported [6] to be about 15 milliseconds. This time, combined with the effective time required for the flame to reach the cloth surface, comprise the exposure time delay. A convenient byproduct of the film coefficient tests is the determination of this cloth exposure time lag.

At the instant of shutter separation, a spike was placed in the oscilloscope trace which recorded the thermal response of the screen. The time that is effectively required for the shutters to open and the flame to reach the screen can then be determined from the known sweep rate and the distance between the spike and the sudden rise in the screen temperature. This time depends on both the spacing and the burner mass flow rate. Averages were taken over all of the film coefficient tests and the results are given in Table 3. Since the ignition time of the fabrics in Reference [6] was taken to be the time between the oscilloscope spike and the fabric ignition, these time lags can be used to correct the ignition times to reflect only that time which the fabric was actually exposed to the convective heating

Table 3. Exposure Delay Times

L		τ, seconds		
		Burner Mass Flow Rate, g/h		
cm	inches	1265	2158	2951
1.906	3/4	.0316	.0171	.0147
4.445	1-3/4	--	--	.06025
7.62	3	.15408	.0987	.0948
10.48	4-1/8	.1740	.1334	.1254

of the burner. The error associated with neglecting this time lag is generally less than 5%. These corrections become significant only for extremely short ignition times. Nevertheless, all of the fabric ignition times used in the following section were corrected for the exposure delay.

Fabric Ignition Times

The experimentally determined ignition times of several fabrics were compared to those predicted by the inert heating model and the film coefficients determined in this investigation. Each of the ignition times was corrected for the exposure time delay. The normalized heat flux q* is given as

$$q^* = \frac{2\bar{h}(\theta_f - \bar{\theta})}{(k/\delta)} \tag{69}$$

and the normalized ignition time is represented by the Fourier number

$$Fo = \frac{\tau_i (k/\delta)}{(\rho\delta)C_p} \tag{77}$$

The solution of the inert heating equation (without radiative and convective losses) is represented by the straight line shown in Figures 27, 28 and 29. The closer the points are to the inert heating line, the better the inert model predicts the heat transfer process.

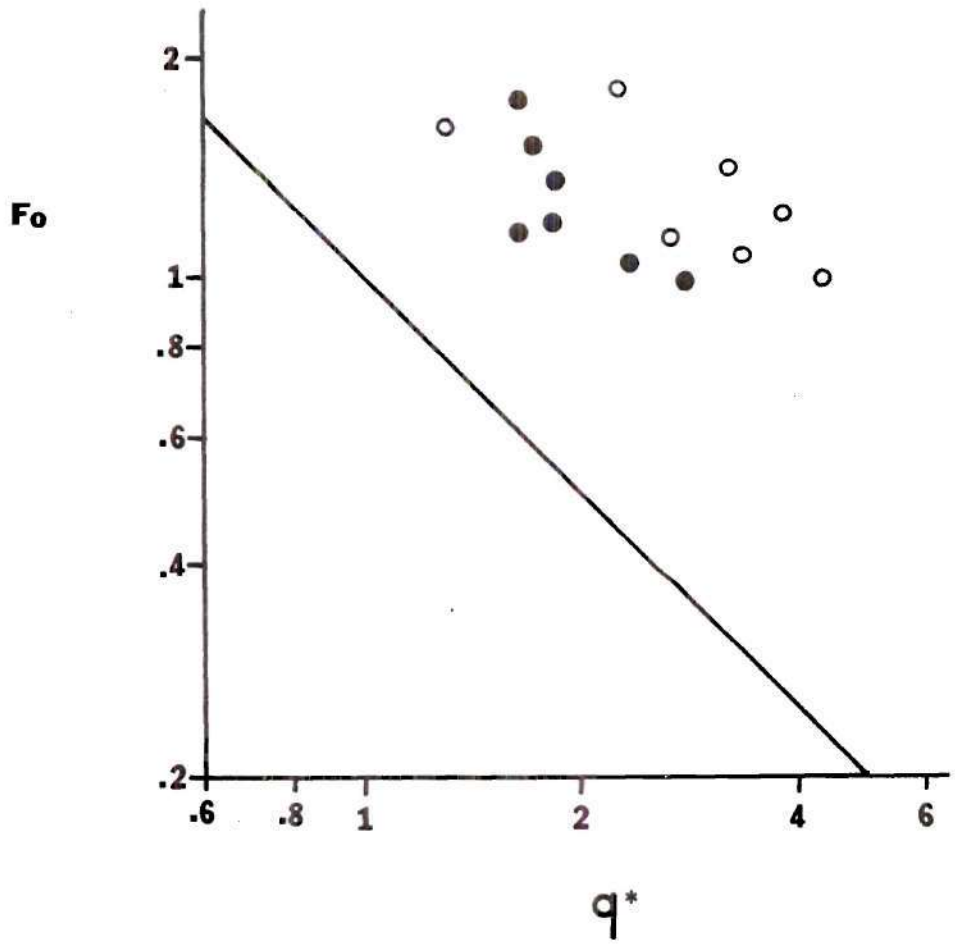

Figure 27. Normalized Ignition Times vs Normalized Convective Heat Flux for the GIRCFF Fabric No. 5, 100% Cotton (Open symbols designate previous film coefficients in reduction of data)

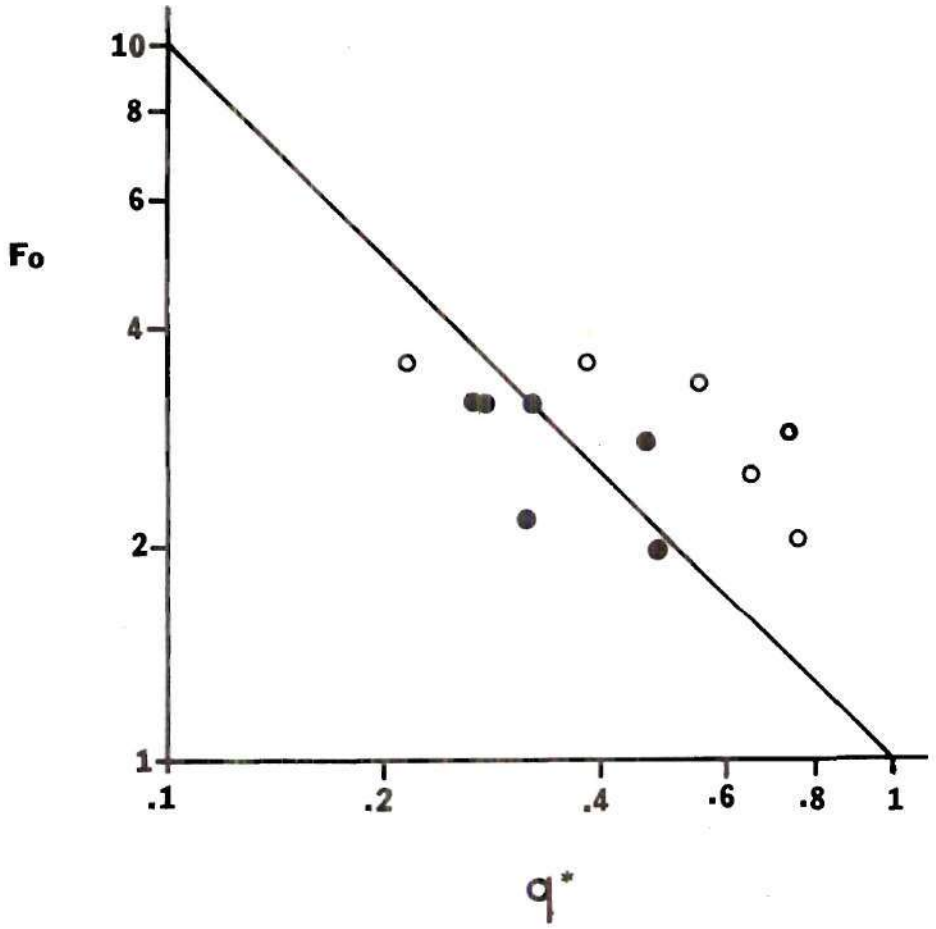

Figure 28. Normalized Ignition Times vs Normalized Convective Heat Flux for the GIRCFF Fabric No. 10, 100% Cotton (Open symbols designate previous film coefficients in reduction of data)

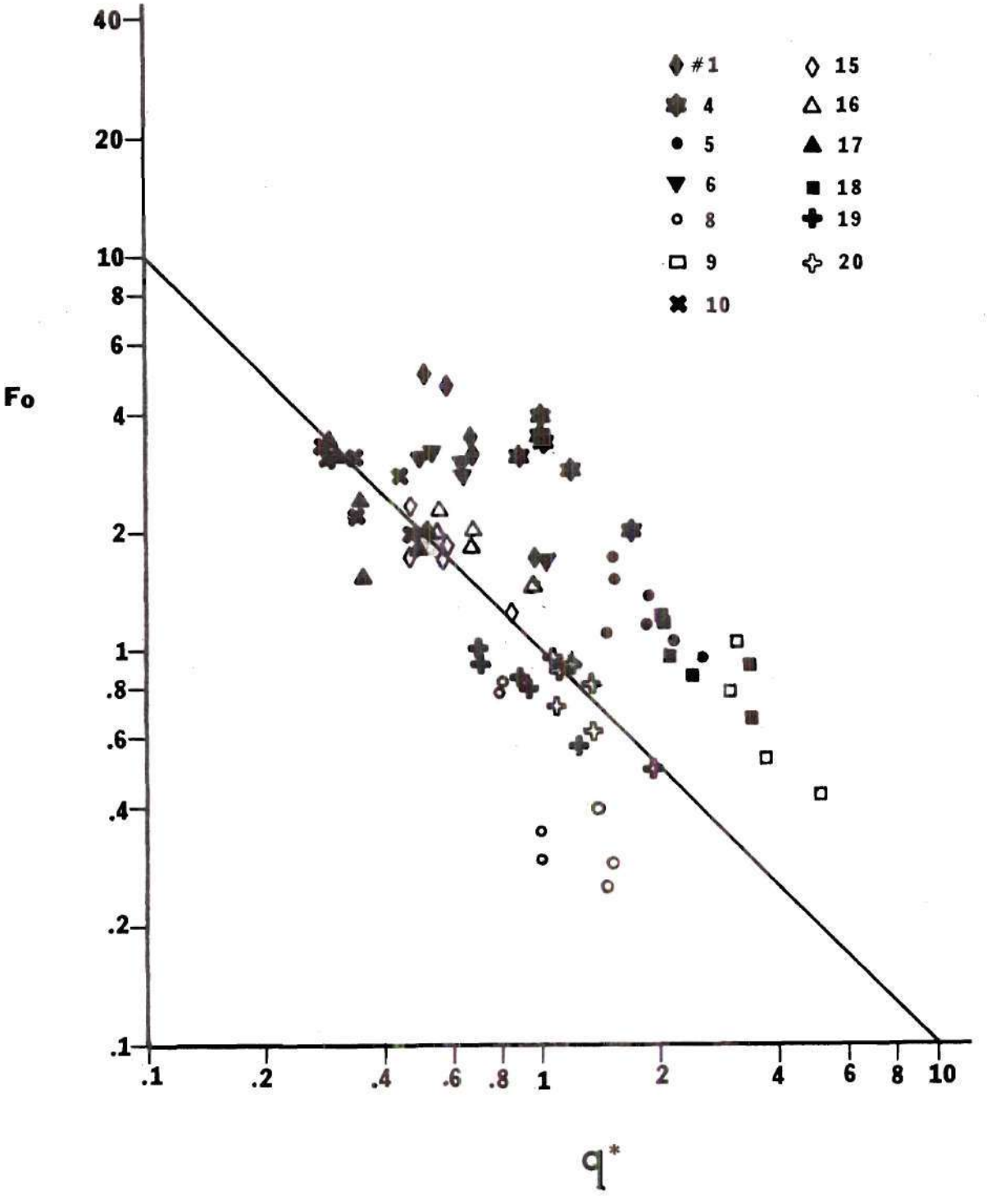

Figure 29. Normalized Ignition Times vs Normalized Convective Heat Flux for the GIRCFF Primary and Secondary Igniting Fabrics

Figures 27 and 28 show the experimentally determined ignition times of GIRCFF fabrics 5 and 10, respectively, plotted against the normalized heat flux. (A complete list of the GIRCFF fabrics identifying their composition is given in Appendix B.1.) These are shown using both the present heat transfer coefficients and those used previously. The increase in correlation is apparent. Figure 29 shows the same results for all of the primary and secondary igniting GIRCFF fabrics.

A sample of the results of ignition time tests are listed in Table 4. A complete listing is given in Appendix J. The standard deviation of these points from the line of inert heating is less than .717. This may be compared to the standard deviation of .935 when using the film coefficients previously employed. The standard deviations of particular fabrics were reduced by as much as 72%.

Table 4. Summary of Fabric Destruction Times with CITA, GIRCFF Fabric No. 1

GIRCFF FABRIC NO. 1 (Polyester Cotton)

k/δ = .017300 W/cm^2K

C_p = 1.494 Ws/gK

$\rho\delta$ = .023490 g/cm^2

T_i = 416.00 °C

Exp. No.	L cm	$\dot{m}_{mix}$ g/h	T_o °C	T_f °C	θ_f	τ s	$\bar{\tau}^{\circ}_i$	$\bar{\tau}_i$	θ_m	$\bar{2h}$ W/cm^2	Fo	q*
25	10.50	2929	22.2	1255	3.130	6.985	.384	0.908	.531	.004563	3.443	0.685
28	10.50	1262	22.7	1082	2.693	9.826	.464	1.210	.538	.004324	4.843	0.538
32	7.60	2176	22.2	1310	3.270	6.401	.364	0.805	.530	.004415	3.155	0.699
33	7.60	1265	22.2	1220	3.041	9.066	.398	1.069	.533	.004139	4.469	0.600
39	1.90	2948	23.0	1352	3.381	3.315	.350	0.618	.529	.006550	1.634	1.080

CHAPTER VII

DISCUSSION

It was established that the convective film coefficients can be measured as presented in this thesis and that the results can be applied, through modeling techniques, to the prediction of ignition times of fabrics. The modeling rule can be expressed by

$$Nu = f\{(Re)_o, Re, Pr, L/D, R/D, T_s^*, GR, w\} \qquad (99)$$

where the overall heat transfer coefficient is expressed through the Nusselt number Nu as a function of 8 parameters. The Reynolds number Re and the geometric ratio L/D characterize the external flow, the injection Reynolds number $(Re)_o$ characterizes the fabric porosity and decomposition rate with respect to the front cloth surface, the Prandtl number Pr relates the thermal and momentum boundary layers, R/D is a constant geometric parameter, T_s^* represents the thermal response of the cloth to the convective heat source, and the Grashof number Gr and injection parameter w characterize the convective cooling of the rear surface of the fabric.

The simulation of the fabric flame interaction produced the heat transfer coefficient which describes the

convective heating of the cloth's front surface. These heat transfer coefficients were than correlated by expressing the Nusselt number as a function of the two Reynolds numbers and geometric parameters. The theoretical analysis of Eckert and Drake [31] on transpiration cooling in plane stagnation flow predicts the same form of the heat transfer correlation if the numerical solution is linearized about the zero injection case. The coefficients are comparable, however, the Nusselt number dependence on the Reynolds number in that study is 0.5 since the flow was considered laminar.

The Nusselt number was consistently found to vary linearly with injection Reynolds number over the range $-30<(Re)_o<30$. Extrapolation beyond the range of this study requires further experimental justification. This range, however, was sufficient for all fabrics encountered in this study.

The heat transfer coefficients previously obtained using a freely suspended screen were predicted using the methods of this study. The general trend could be predicted, but the magnitude was somewhat lower. This is partly attributed to the porosity which was computed for this screen. Accurate predictions of heat transfer to screens requires experimental determination of the screen porosity using procedures similar to those used by Factory Mutual in the determination of fabric porosities.

The corrections for the exposure time delay did not

greatly change any of the ignition times since most of these times were of the order of one to ten seconds.

In the predictions of fabric ignition times, the convective film coefficients were first evaluated for the fabrics at room temperature, then evaluated for the fabrics at the ignition temperature allowing for pyrolysis, and finally evaluated for the fabrics at the ignition temperature, but neglecting pyrolysis.

In the first case, there is no convective cooling of the rear surface of the fabric and the fabric has not yet begun to decompose. Assuming that the permeability of the fabric does not change with time or temperature, then the overall convective film coefficients evaluated for this case are the largest expected for this particular fabric. These heat transfer rates were used in the last chapter in the prediction of fabric ignition times and produced a 23% reduction in the standard deviation of the actual ignition times to the predicted ignition times.

In the second case, convective cooling of the rear surface of the fabric is at its maximum and the fabric is decomposing at the largest conceivable rate. Again, assuming that the permeability of the fabric has not changed, then the overall convective film coefficients for this case are the smallest expected for this particular fabric. There was a 10 to 20% reduction in the film coefficients and these produced a further reduction in the standard deviation, but

only a 3.6%.

In the third case, convective cooling of the rear surface of the fabric is again at its maximum; however, there is no fabric decomposition. The reduction in the overall convective film coefficients from those of the first case (fabric at the ambient temperature) is due entirely to free convection. Comparison with the case in which decomposition is considered shows that approximately 40% of the 10 to 20% reduction in heat transfer coefficients is due to pyrolysis for GIRCFF fabrics 1, 4, 5, 6, 8, and 9. The others showed the effect of pyrolysis is negligible.

The following is a brief discussion of the external flow conditions encountered in this investigation.

At a spacing of L/D equal to .515, the Nusselt number dependence on the Reynolds number was found to be to the 0.59 power. McNaughton and Sinclair [32] report fully laminar jets for a Reynolds number less than 1000. The 0.59 exponent, however, indicates that the flow was somewhat turbulent, even though the Reynolds number was always less than about 600. This is expected for three reasons. The first is that the burner tube was fitted with fine mesh and coarse mesh screens and also with a coarse grid. These act as turbulence promoters [17]. Secondly, a further increase in the level of turbulence is caused by the combustion process itself. Thirdly, the cloth surface roughness or screen mesh produce an effect similar to that occuring in

flows in circular pipes in which an increase in roughness causes an early transition from laminar to turbulent flow.

The stagnation pressure profile for the low burner flow rate (Re ≈ 220) did not increase with L as did the two other flow rates (Re ≈ 380, Re ≈ 515). It was noted by McNaughton and Sinclair [32], however, that a dissipated laminar jet occurs at a Reynolds number less than 300. In this case, the viscous forces are large compared to the inertia forces and the jet diffuses rapidly into the surrounding fluid.

Buoyancy forces predominate for the other two burner flow rates at only a few burner diameters. This was anticipated in view of the similar pressure (hence velocity) profiles obtained at spacings greater than two burner diameters.

CHAPTER VIII

CONCLUSIONS AND RECOMMENDATIONS

The first objective of this thesis was to describe the fabric-flame interaction through the determination and evaluation of film coefficients which would account for the effects of fabric decomposition and fabric porosity. This objective has been met and the results of the film coefficient determination tests were presented and discussed in the previous chapter.

The second objective of this thesis was the prediction of fabric ignition times using the results of the film coefficient determination tests. This was done using the model of inert heating in which the overall heat transfer coefficient accounted for fabric porosity and gasification.

As was pointed out in the presentation of the ignition time data, more accurate predictions of fabric ignition times are made using the film coefficients of this study. Nevertheless, there is still considerable deviation which must be considered.

It may first be noted that the fabric ignition times varied by more than 30% for a given fabric under the same exposure conditions. Consequently, only gross and systematic deviations may be meaningfully considered without a

statistical representation of the scatter.

The most outstanding of these deviations occured for GIRCFF fabrics 1, 4, 5, 9 and 18, as seen in Figure 29. These fabrics have consistently longer ignition times than those predicted by the inert heating model. It has been theorized that these fabrics require a significant amount of energy to decompose, and hence the inert model is not totally applicable [3]. The gasification terms in the conservation of energy equation can not be neglected for these fabrics.

The only other systematic departure from the predictions of the inert model occurs with fabric number 8. This fabric ignites much sooner than would be predicted. The explanation offered here is that this polyester cotton blend exhibits an early collapse of the polyester fibers (at approximately the melting temperature of the polyester alone). This collapse causes an increase in the fabric porosity and the associated increase in heat transfer. In using the fabric porosities, it was an implicit assumption that the permeability did not vary with temperature. This assumption would be violated if either the collapse of the polyester fibers or the rate of decomposition is significant.

The prediction of fabric ignition time was also noted to be highly dependent on ignition temperature. Both fabrics 5 and 10 are 100% cotton, and yet a 122°C difference in the ignition temperatures was reported. If it is assumed that

the ignition temperature is dependent only on the fiber chemistry, then this difference should be nominal. For this reason, the ignition temperature of fabric number 5 was taken to be equal to that of number 10 (443°C) and the correlation was seen to be much better. Careful checks on the fabric ignition temperature are therefore recommended.

The only available porosity measurements were made at room temperature necessitating the assumption that there was no permeability dependence on temperature. The validity of this assumption should be verified if the film coefficients of this study are to be further refined.

The heat transfer coefficient may decrease by up to 20% for a particular fabric as its temperature is increased from room temperature, where there is no convective cooling, to its ignition temperature, where the maximum rates of decomposition and convective cooling are encountered. Consequently, the use of time varying heat transfer coefficients, as well as the inclusion of the gasification term in the energy equation, would be expected to produce a more accurate description of the convective heating of a fabric.

Much of the experimental scatter encountered in this study resulted from the convective fluctuations of the burner flame. A disproportionately large number of free flame temperature measurements were found in error in the fabric ignition time tests at larger spacings. For this reason, the lower spacing ignition time tests and film coefficient tests are considered with a higher degree of certainty.

APPENDICES

APPENDIX A

TEST SCREEN DATA

The relevant data on the two screens used in the film coefficient determination tests is given in Table A.1. The first two screens listed are the ones investigated in this study. The others, which were considered for future investigations, are included for completeness.

Table A.1. Test Screen Data

Screen Mesh (inches)	Wire Diam. (inches)	Material	Supplier	$\rho\delta$ (g/cm^2)	P_f ($ft^3/lb_f\ sec$)	α %
150	.0026	St.St.316	Multi-Metal	.032964	7.66	37.4
200	.0021	"	"	.025541	4.74	33.6
250	.0016	"	"	.020645	4.29	36.0
325	.0014	"	Cambridge	.0188475	2.40	30.0
400	.0010	"	"	.0149574	2.68	36.0
200	.0021	"	-----	.02742	4.74	33.6

APPENDIX B

FABRIC POROSITY VALUES

The twenty primary fabrics designated by the Government-Industry Research Committee on Fabric Flammability (GIRCFF) are listed in Table B.1. The corresponding porosity measurements, as reported by Factory Mutual [8], are given in Table B.2.

Table B.1. Fabric Identifications [33]

GIRCFF NO.	Classification	Fiber Composition	Color	Finish
1	Durable Press Slack	65/35%Pe./C.	White	DP Treated
2*	Textured Woven Blouse	100% Polyester	Yellow	-
3	Double Knit	100% Polyester	White	-
4	Denim	100% Cotton	Navy Bl.	-
5*	T-Shirt Jersey	100% Cotton	White	-
6	Untreated Slack	65/35%Pe./C.	White	-
7	Jersey Tube Knit	100% Acrylic	Gold	-
8*	T-Shirt Jersey	65/35%Pe./C.	White	-
9	Terry Cloth	100% Cotton	White	-
10*	Batiste	100% Cotton	Purple	-

Table B.1. Fabric Identifications (continued)

GIRCFF NO.	Classification	Fiber Composition	Color	Finish
11*	Tricot	80/20%Acet./Nyl.	White	-
12*	Tricot	100% Nylon	White	-
13*	Tricot	100% Acetate	White	-
14	Taffeta	100% Nylon	White	-
15	Durable Press Slack	65/35%Pe./Ray.	Brown	DP Treated
16	Shirting	50/50%Pe./C.	White	-
17*	Batiste	65/35%Pe./C.	White	-
18*	Flannel	100% Cotton	White	-
19*	Flannel	100% Cotton	White	Fire Retard
20	Flannel	100% Wool	Navy Bl.	-

*Ten Primary GIRCFF Fabrics

Table B.2. Results of Porosity Measurements at Ambient Conditions (Approx. 30% R.H. and 77 °F) [8]

Porosity: $(ft/sec)/(lb/ft^2)$

GIRCFF NO.	Face Exposure	Back Exposure
1	0.181	0.139
2	0.70	ND
3	5.1	4.9
4	0.072	0.074
5	1.18	1.14
6	0.182	0.180
7	2.6	2.5
8	1.03	1.19
9	1.20	NA
10	3.4	NA
11	0.40	0.40
12	7.4	ND
13	6.8	ND
14	0.58	NA
15	1.71	NA
16	0.92	NA
17	1.89	NA
18	1.19	0.99
19	0.90	0.70
20	0.92	ND

NA = not applicable (face and back nominally identical)
ND = not done

APPENDIX C

SCREEN POROSITY VALUES

The technical data on screen porosities given in Reference [34] is reproduced in Figure C.1 where

$r = b/\sqrt{a}$

$a = .00674A$

$b = 7740B$

$A = (1-\alpha^2)/\alpha$

$B = D_o/\alpha$, inches

α = fraction of open area

$D_o = (\frac{1}{M}-D_w)$ = size of each projected hole, inches

D_w = wire diameter, inches

M = mesh number, wires per inch

ΔP = pressure differential, psi

V = velocity, ft/sec

μ = viscosity, centipoise

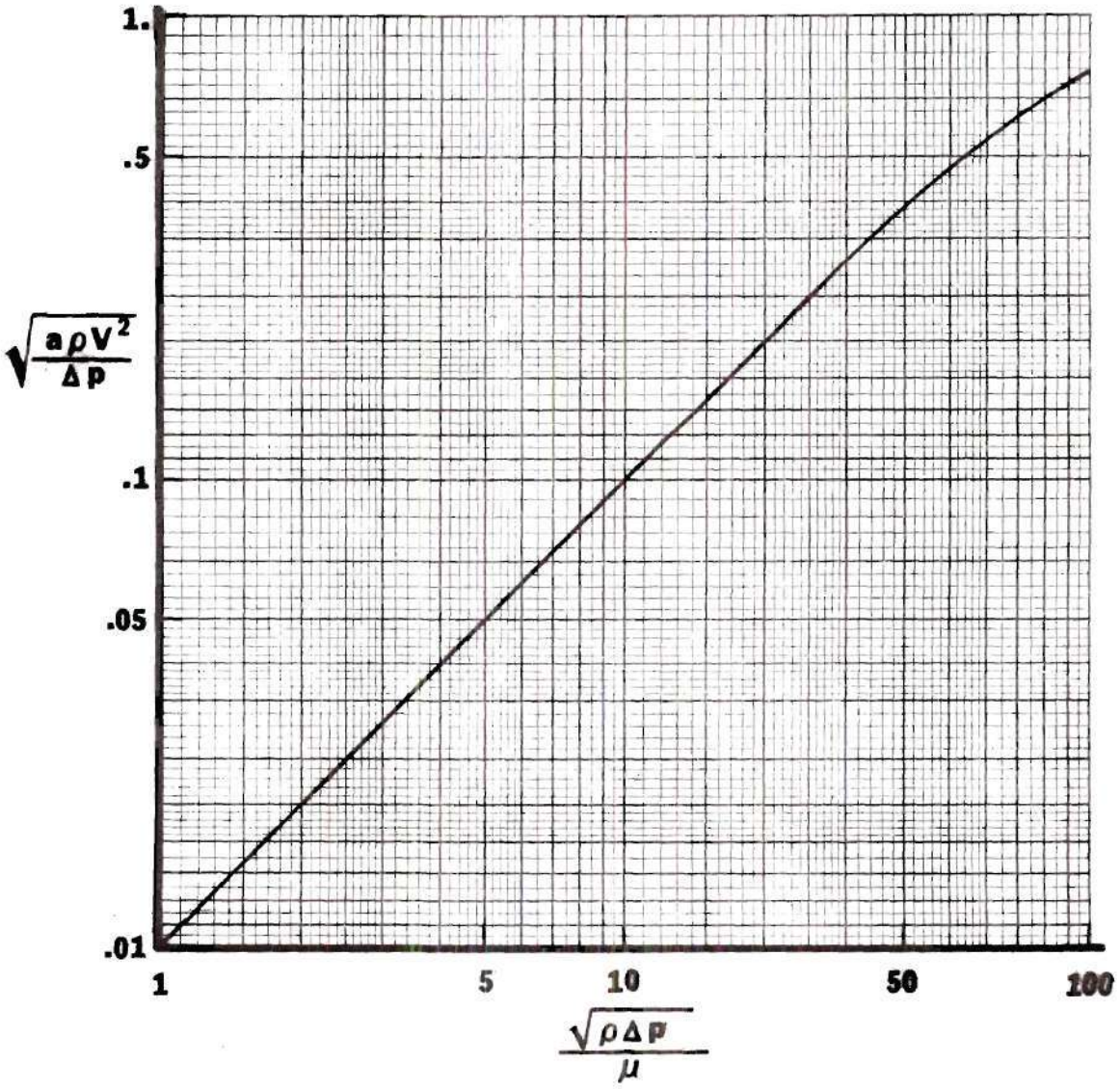

Figure C.1. Flow Rate-Pressure Drop Relation for Metallic Cloths [34]

The equation for the screen porosity was obtained as follows: The linear portion of Figure C.1, $\frac{r\sqrt{\rho\Delta p}}{\mu} < 40$, can be represented by the equation

$$\log\left(\frac{a\rho v^2}{\Delta p}\right) = d \log\left(\frac{r\sqrt{\rho\Delta p}}{\mu}\right) + \log e$$

where

$$d = 1.0$$

From Figure C.1

$$e = 0.01$$

This equation is then rearranged as follows:

$$\left(\frac{a\rho v^2}{\Delta p}\right)^{1/2} = \frac{r\sqrt{\rho\Delta p}}{\mu}\ 0.01$$

$$V = 0.01\ r\Delta p/\mu\sqrt{a}$$

$$V = \frac{0.01(b/\sqrt{a})}{\mu\sqrt{a}}\ \Delta P$$

$$V = \frac{0.01(7740B)}{\mu(.00674A)}\ \Delta P$$

$$V = \frac{11483.7(D_o/\alpha)}{\mu(1-\alpha^2)/\alpha^2}\ \Delta P$$

$$V = \frac{11483.7\ \sqrt{\alpha}/M}{\mu(1-\alpha^2)/\alpha}\ \Delta P$$

$$V = \frac{11483.7\ \alpha^{3/2}}{\mu M(1-\alpha^2)}\ \Delta P$$

Recognizing the term in brackets as an expression for the porosity, then the form of the screen porosity equation is the same as that of the fabric porosity equation, i.e. $V \alpha \Delta P$. Hence,

$$P = \frac{V}{\Delta P} = \frac{11483.7\ \alpha^{3/2}}{\mu(1-\alpha^2)M}\ \left[\frac{ft/sec}{lb_f/in^2}\right]$$

$$P = \frac{79.748\ \alpha^{3/2}}{\mu M(1-\alpha^2)}\ \left[\frac{ft/sec}{lb_f/ft^2}\right]$$

where μ is expressed in g/cms and M in mesh number per inch. This equation can be made to be independent of property dimensions to give

$$P = \frac{.02}{\mu M}\ \left(\frac{\alpha^{3/2}}{1-\alpha^2}\right)$$

APPENDIX D

THERMODYNAMIC AND TRANSPORT PROPERTIES

The dimensionless property data for k, c_p, and μ of air was obtained from References [35,36] at one atmosphere over the temperature range shown in Figures D.1, D.2 and D.3, respectively. The corresponding polynomial coefficients are given in Table D.1.

The polynomial coefficients for the specific heat of the screen $c_{p,s}$ are the result of a least square fit over the data given for 316 stainless steel in References [37, 38,39,40]. The results are shown in Figure D.4 and Table D.1.

Table D.1. Polynomial Coefficients for Property Data

	k/k_o	C_p/R	μ/μ_o	$C_{p,s}$ (cal/g°C)
b_0	.185890286300 ex-1	.371861259452 ex+1	-.236068199600 ex-1	.394695550590 ex-1
b_1	.361946702360 ex-2	-.186161061660 ex-2	.477489753837 ex-2	.358010348962 ex-3
b_2	.101434163520 ex-5	.490115530370 ex-5	-.465988336552 ex-5	-.469174397802 ex-6
b_3	-.566424575090 ex-8	-.407680617060 ex-8	.354942007466 ex-8	.217933235101 ex-9
b_4	.610446806220 ex-11	.148863491912 ex-11	-.146516791303 ex-12	0
b_5	-.273249831464 ex-14	-.189988653180 ex-15	.243464237004 ex-15	0
b_6	.451608274299 ex-18	0	0	0

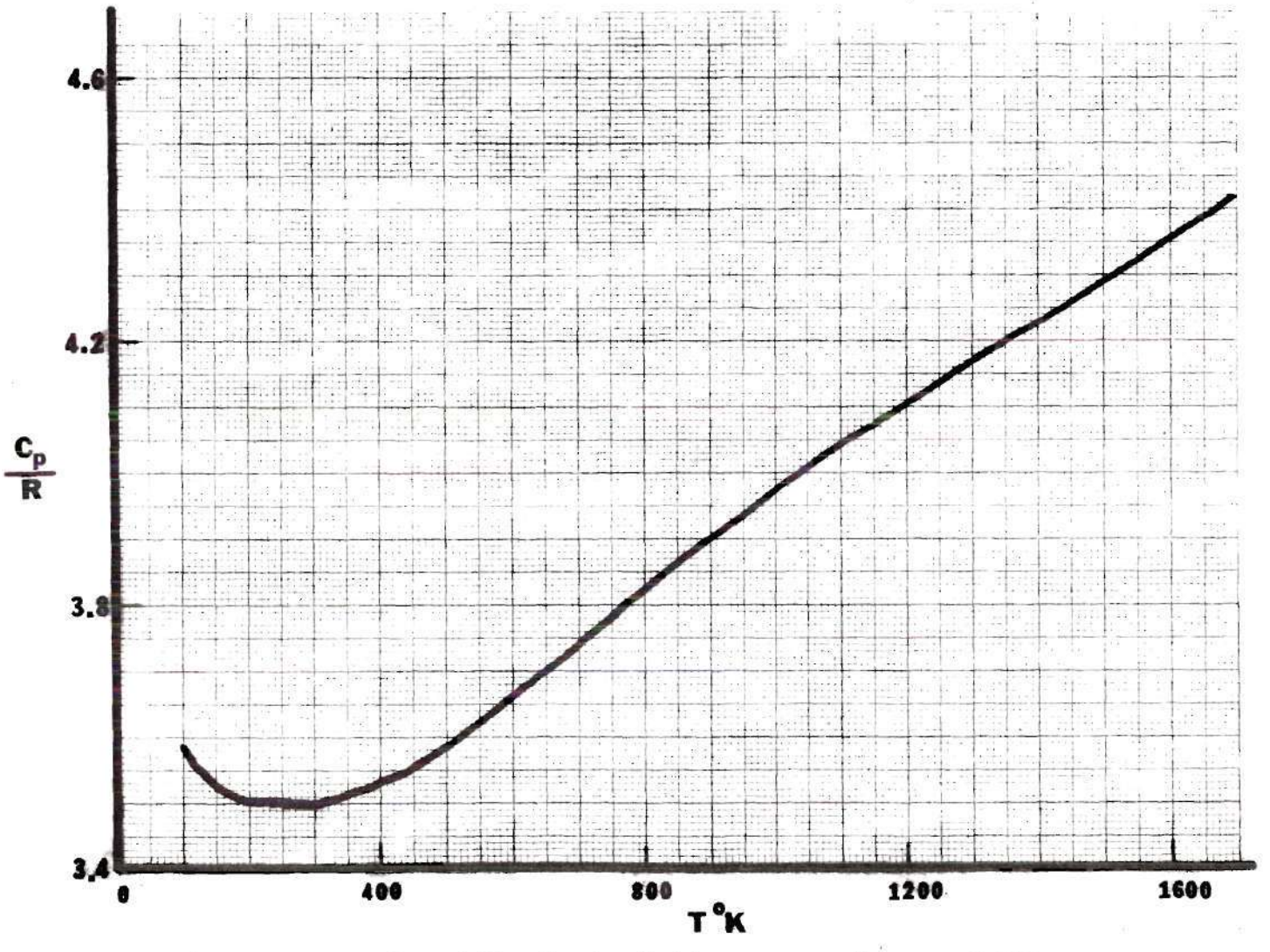

Figure D.1. Specific Heat of Air versus Temperature (R = 0.0686042 cal/g°K) [36]

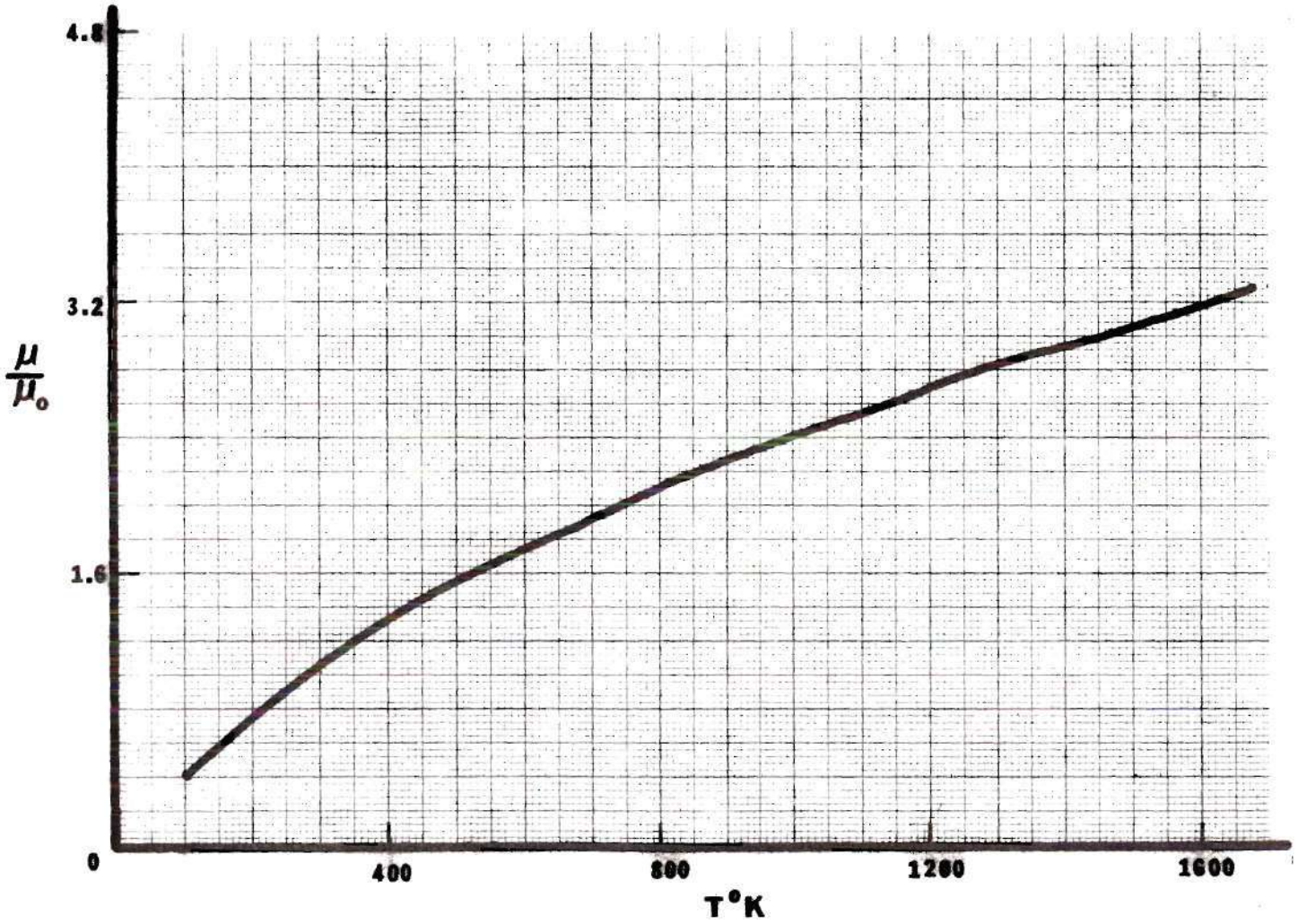

Figure D.2. Viscosity of Air versus Temperature (μ_o = 1.716 x 10^{-4} g/cm sec) [36]

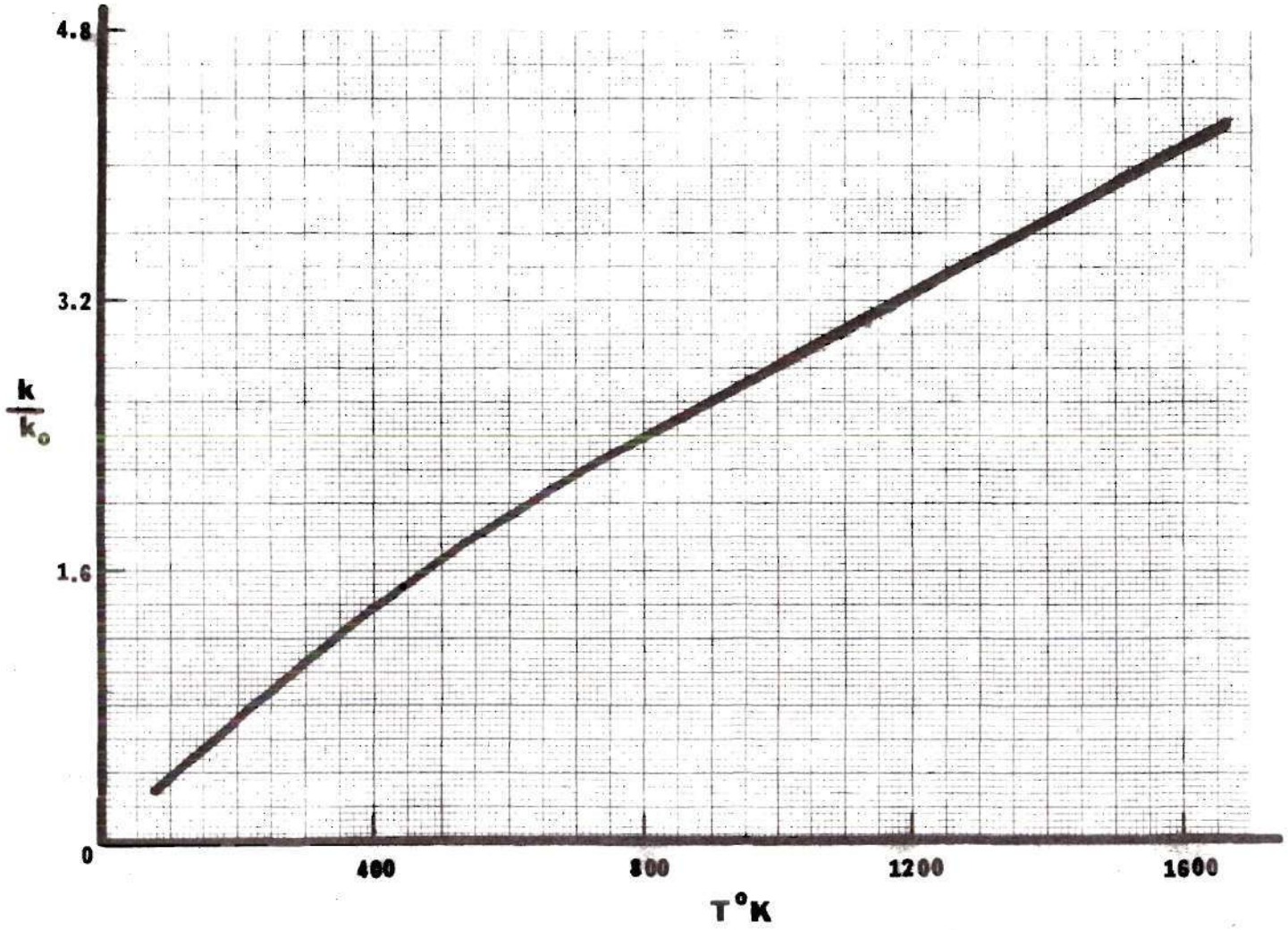

Figure D.3. Thermal Conductivity of Air versus Temperature (k_o = 2.414 x 10^{-4} W/cm°K) [35,36]

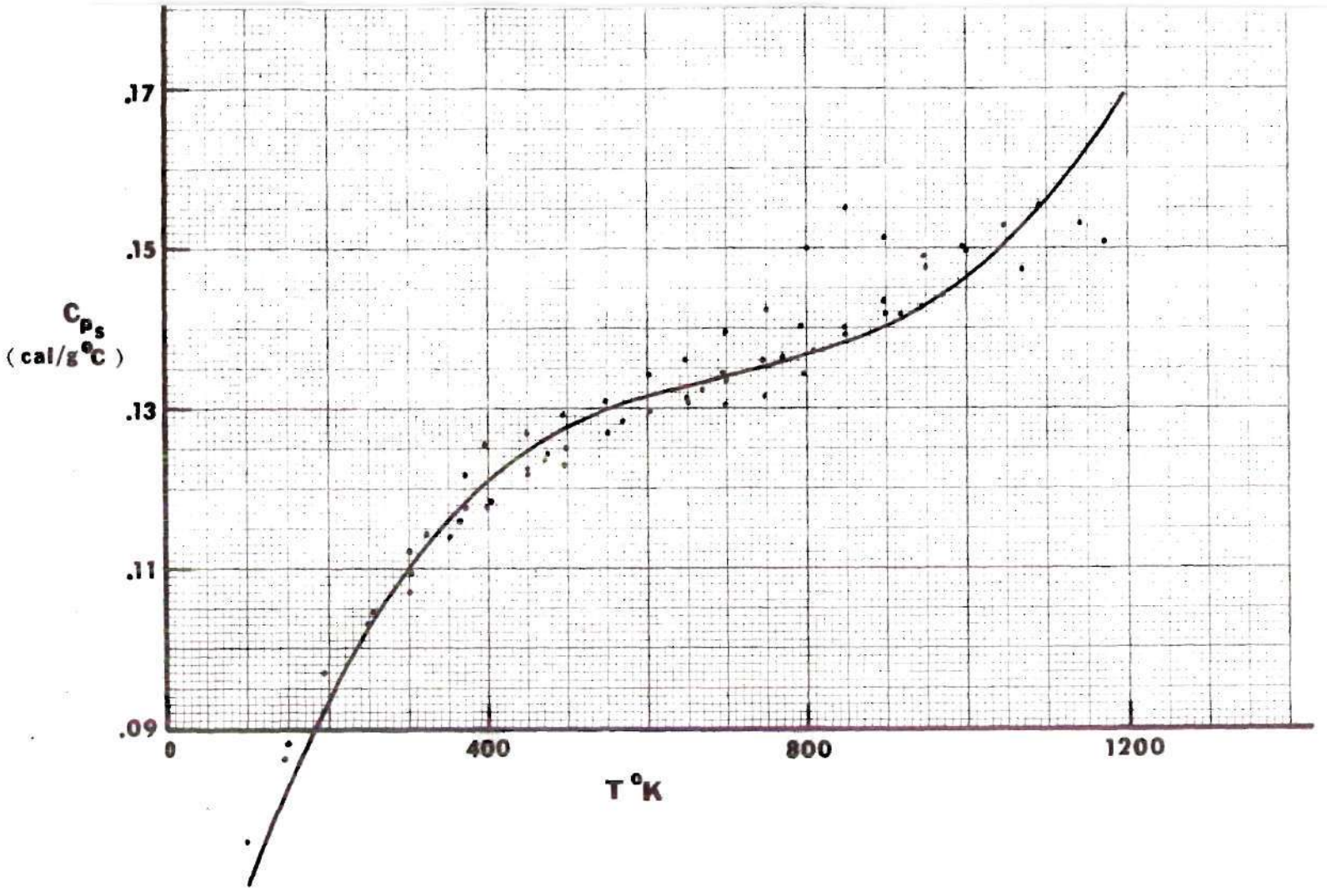

Figure D.4. Specific Heat of Stainless Steel 316 versus Temperature [37,38,39,40]

APPENDIX E

REAR SURFACE CONVECTIVE HEAT TRANSFER

The analysis of the free convection problem with a blowing boundary condition is given by Rohsenow and Hartnett [27]. The results of the numerical solution presented in Figure 3, page 612 of Reference [27] are given in Table E.1. A second degree polynomial which represents this analysis may be given as

$$\frac{Nu_x}{Gr_x^{1/4}} = f_n\left[\frac{v_o x^{1/4}}{4\nu C}\right]$$

where

f_n = polynomial coefficients

$$C = \left[\frac{g\beta(T_w - T_\infty)}{4\nu^2}\right]^{1/4}$$

This is integrated over x to obtain the average Nusselt number:

$$\frac{(hx/k)}{(g\beta\Delta T x^3/\nu^2)^{1/4}} = f_o + f_1\left(\frac{V_o x^{1/4}}{4\nu C}\right) + f_2\left(\frac{V_o x^{1/4}}{4\nu C}\right)^2$$

$$\int_o^{\ell} \frac{(h/k)x^{1/4}dx}{(g\beta\Delta T/\nu^2)} = \int_o^{\ell} \left[f_o + f_1\left(\frac{V_o x^{1/4}}{4\nu C}\right) + f_2\left(\frac{V_o x^{1/4}}{4\nu C}\right)^2\right]dx$$

Table E.1. Numerical Solution to the Blowing Natural Convection Problem

$\left(\frac{V_o x^{1/4}}{4\nu C}\right)$	$Nu_x/Gr_x^{1/4}$
-.75	1.555
-6.25	1.328
-.5	1.103
-.375	.863
-.25	.676
-.125	.5143
0	.375
.125	.250
.25	.152
.375	.080
.5	.032
.625	.0015
.75	.0010

$$\frac{(hL/k)}{(g\beta\Delta TL^3/\nu^2)^{1/4}} = \frac{5}{4L}\left[f_o\ell + f_1\left(\frac{V_o\ell^{1/4}}{4\nu C}\right)\ell\frac{4}{5} + f_2\left(\frac{V_o\ell^{1/4}}{4\nu C}\right)^2\frac{4\ell}{6}\right]$$

$$\frac{Nu}{Gr^{1/4}} = 5\left[\frac{f_o}{4} + \frac{f_1}{5}\left(\frac{V_o^{1/4}}{4\nu C}\right) + \frac{f_2}{6}\left(\frac{V_o\ell^{1/4}}{4\nu C}\right)^2\right]$$

Introducing the approximation of the characteristic length given by Kreith [26],

$$\ell = 0.9\ D_s = 1.8R$$

$$\frac{Nu}{(Gr)^{1/4}} = \left\{g_o + g_1\left(\frac{V_oR^{1/4}}{4\nu C}\right) + g_2\left(\frac{V_oR^{1/4}}{4\nu C}\right)^2 \quad \text{for } \left(\frac{V_oR^{1/4}}{4\nu C}\right) \leq 0.75\right.$$

$$\text{for } \left(\frac{V_oR^{1/4}}{4\nu C}\right) > 0.75$$

where $g_i = 5\ f_i\ (1.8)^{(i-1)/4}/(i+4)$.

The coefficients f_i and g_i are given in Table E.2.

Table E.2. Polynomial Coefficients Representing the Numerical Solution

i	f_i	g_i
0	.372330069926	.4018093
1	-1.050628571420	-1.0506300
2	.734420779241	.7088949

APPENDIX F

FABRIC THERMOPHYSICAL PROPERTIES

Summarized in the following tables are the thermophysical properties and the reaction kinetics parameters for several selected fabrics. These properties were taken from Reference [3]. The activation energy E_g and frequency factor k_g were determined by McCarter [41].

Table F.1. Fabric Thermophysical Properties [3,41]

GIRCFF Fabric Number	$\rho\delta$ g/cm^2	T_i °C	k/δ W/m^2K	C_p Ws/gK	k_g 1/s	E_g kWs/g mole	n_g
1	.02349	416	173	1.494	1.28 ex27	365.5	2.1
4	.02963	297	150	1.424	--- See GIRCFF No. 5 ---		
5	.01371	311	95	1.761	.92 ex12	142.6	1.1
6	.02357	416	183	1.545	1.28 ex27	365.5	2.1
8	.01619	450	112	2.045	1.28 ex27	365.5	2.1
9	.02648	308	50	1.558	3.07 ex21	206.9	1.4
10	.00665	443	360	2.398	.285 ex14	228.3	1.1
15	.02282	426	210	1.624	--	--	-
16	.01314	473	150	1.500	--	--	-
17	.00855	480	290	1.840	.18 ex20	310.3	1.6
18	.01288	311	75	1.735	.498 ex14	229.6	1.2
19	.01489	497	110	2.132	.533 ex50	603.0	2.1
20	.01993	480	75	1.270	--	--	-

APPENDIX G

SCREEN THERMOCOUPLE CALIBRATION

Three screens were calibrated as outlined in Chapter IV, and the results of the 5th degree least-square fit polynomial for the screen thermocouple and for the reference iron-constantan thermocouple [42] are given in Table G.1 and shown in Figure G.1. A least-square fit quadratic was obtained by Champion [6] for a similar 200 mesh stainless steel screen and constantan wire. These coefficients are also given in Table G.1. The screen calibration curves differ by a maximum of 5°C over the range of 0 to 500°C. For each calibration polynomial

$$T(°C) = \sum_{n=o}^{5} b_n (emf, mV)^n$$

Table G.1. Thermocouple-emf Polynomial Coefficients

	Iron-Constantan	Screen-Constantan	Screen-Constantan, Ref. [6]
b_0	.046559698000	-.7922292669 ex+1	-.466141655000
b_1	19.751133411400	.2737347650 ex+2	.234839290784 ex+2
b_2	-.190938952723	-.64689638712	-.138178833174
b_3	.9330944558800 ex-2	.268350881006 ex-1	0
b_4	-.190685801004 ex-3	-.705346166825 ex-3	0
b_5	.115635581696 ex-5	.822123493823 ex-5	0

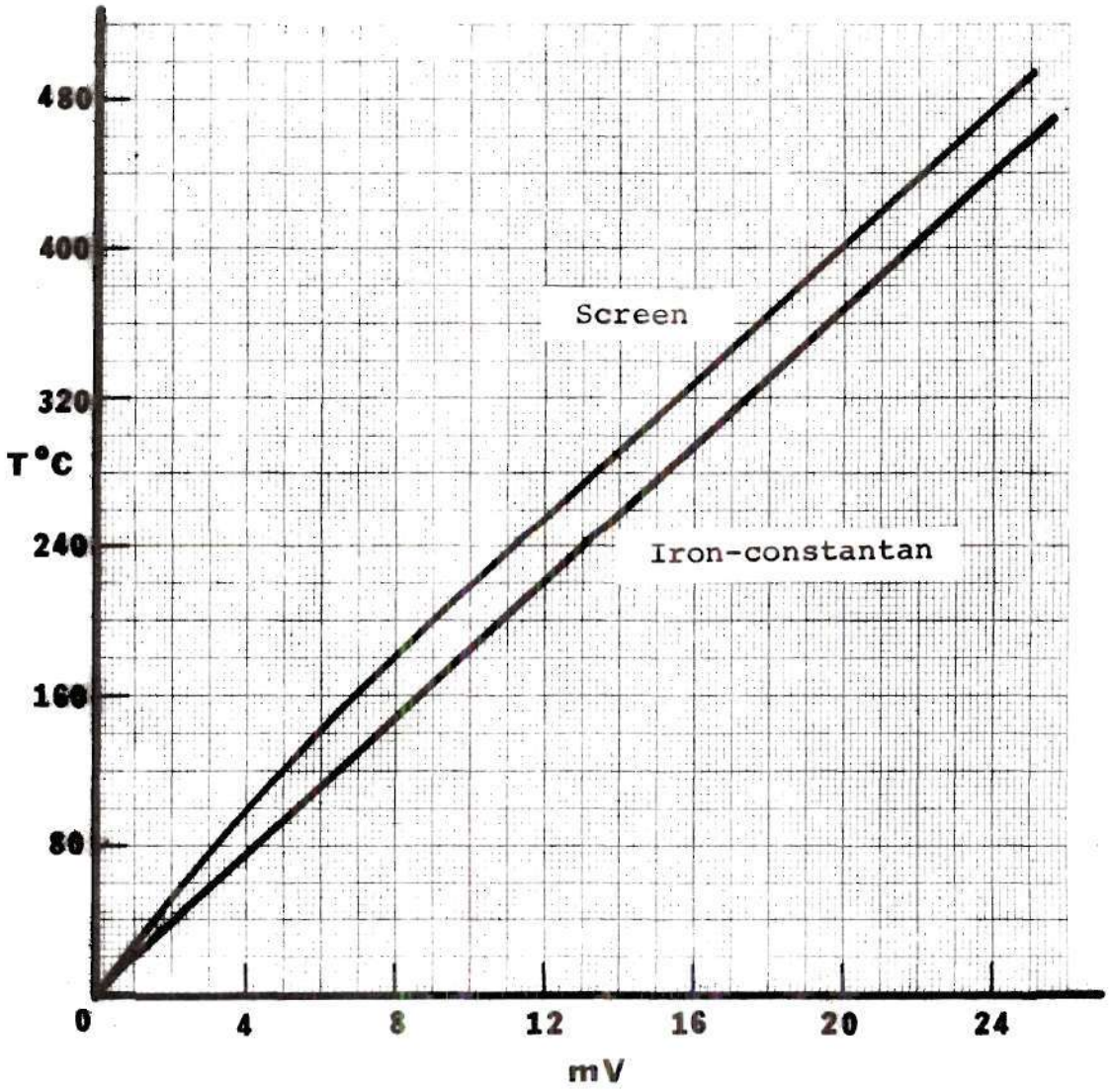

Figure G.1. Thermocouple Temperatures versus emf (Reference Junction = 0°C)

APPENDIX H

FLAME TEMPERATURES

The flame temperatures are listed in Table H.1 as a function of burner mass flow rate and position above the burner. These temperatures are the results of averages taken over several fabric ignition time tests in which the steady state flame temperature was measured in the plane of the fabric holder after the fabric had been burned or melted away [3]. Each of these tests were experimentally confirmed by repeating the flame temperature measurements and additional data taken where needed.

Table H.1. Flame Temperatures $\phi = 0.86$

L		$\dot{m}_{mix}$	T_f
in.	cm	g/hr	°C
4 1/8	10.5	1265	1165
		2158	1287
		2951	1257
3	7.6	1265	1205
		2158	1319
		2951	1320
1 3/4	4.4	1265	1256
		2158	1351
		2951	1359
3/4	1.9	1265	1290
		2158	1347
		2951	1352

APPENDIX I

CONVECTIVE HEAT TRANSFER TESTS

Listed in Table I.1 is the reduced data for all of the film coefficient determination tests. Table I.2 contains the reduced data for the freely suspended screen tests of Reference [6]. The last three tests listed are the tests which were repeated to check repeatability.

An asterisk (*) designates those tests for which $\phi \neq 0.86 \pm 0.01$. A cross hatch (#) designates those tests which were found to be defective.

Table I.1 Convective Heat Transfer - Similarity Parameters

Exp.	T_s(°C)	T_f(°C)	h(W/cm^2°C)	Nu	$(Re)_o$	Re	Pr	L/D	M	V_o(cm/s)
1	38.2	1290	.0029852	9.68	19.32	227.6	.683	.514	200	2.950
2 *	40.3	1290	.0029682	9.63	19.17	228.1	.683	.514	200	2.947
3 *	38.2	1352	.0060385	18.94	19.80	517.1	.681	.514	200	3.088
4 *	38.6	1352	.0058241	18.26	19.80	518.0	.681	.514	200	3.092
5	38.3	1352	.0055423	17.38	19.80	516.8	.681	.514	200	3.089
6 *	40.1	1347	.0046522	14.63	19.40	380.3	.681	.514	200	3.038
7 *	38.6	1347	.0043764	13.76	19.89	382.3	.681	.514	200	3.101
8	38.9	1347	.0043943	13.82	19.87	385.3	.681	.514	200	3.101
9 *	38.2	1347	.0046955	14.76	19.87	382.4	.681	.514	200	3.094
10 *	38.9	1290	.0027881	9.04	19.82	228.1	.683	.514	200	3.032
11	38.7	1290	.0026114	8.47	20.27	227.3	.683	.514	200	3.099
12 *	38.1	1290	.0030990	10.05	9.65	226.5	.683	.514	200	1.489
13	38.7	1290	.0032607	10.58	9.67	227.2	.683	.514	200	1.478
14	37.9	1347	.0050836	15.99	9.47	381.2	.681	.514	200	1.488
15	38.4	1352	.0060540	18.99	9.44	517.8	.681	.514	200	1.489
16 *	38.0	1290	.0036537	11.85	.00	225.9	.683	.514	200	.000

Table I.1 Convective Heat Transfer - Similarity Parameters (continued)

Exp.	T_s(°C)	T_f(°C)	h(W/cm^2°C)	Nu	$(Re)_o$	Re	Pr	L/D	M	V_o(cm/s)
17	38.2	1290	.0037722	12.24	.00	226.7	.683	.514	200	.000
18	38.5	1347	.0056902	17.89	.00	381.6	.681	.514	200	.000
19 *	38.7	1347	.0060193	18.93	.00	382.8	.681	.514	200	.000
20	37.9	1352	.0068964	21.63	.00	515.9	.681	.514	200	.000
21	154.0	1290	.0026956	8.74	15.61	225.7	.683	.514	200	3.304
22	154.0	1290	.0027358	8.87	15.68	227.0	.683	.514	200	3.286
23	154.9	1290	.0028809	9.34	14.49	226.0	.683	.514	200	3.053
24	154.3	1290	.0028515	9.25	14.54	226.0	.683	.514	200	3.059
25 *	153.9	1347	.0043276	13.61	14.24	379.8	.681	.514	200	3.053
26	154.2	1347	.0044966	14.14	14.25	381.4	.681	.514	200	3.057
27	154.4	1347	.0045157	14.20	14.25	381.0	.681	.514	200	3.059
28	154.2	1352	.0057994	18.19	14.22	512.9	.681	.514	200	3.055
29 *	155.2	1352	.0052323	16.41	14.22	517.0	.681	.514	200	3.064
30	154.2	1290	.0034954	11.34	7.36	226.0	.683	.514	200	1.549
31	154.5	1347	.0050547	15.89	7.22	382.2	.681	.514	200	1.550
32	154.5	1352	.0064218	20.14	7.20	512.5	.681	.514	200	1.549

Table I.1 Convective Heat Transfer - Similarity Parameters (continued)

Exp.	T_s(°C)	T_f(°C)	h(W/cm^2°C)	Nu	$(Re)_o$	Re	Pr	L/D	M	V_o(cm/s)
33	154.5	1290	.0041964	13.61	2.38	226.0	.683	.514	200	.504
34	154.8	1347	.0056410	17.74	2.33	381.1	.681	.514	200	.504
35	154.9	1352	.0060186	18.88	2.32	514.1	.681	.514	200	.503
36	302.5	1290	.0033239	10.78	10.63	226.0	.683	.514	200	3.028
37	302.7	1347	.0045950	14.45	10.42	383.8	.681	.514	200	3.029
38 #	303.2	1352	.0045611	14.30	10.43	514.9	.681	.514	200	3.037
39	18.6	1290	.0038408	12.46	.00	226.4	.683	.514	200	.000
40	20.3	1347	.0052354	16.46	.00	385.3	.681	.514	200	.000
41	21.2	1352	.0065159	20.44	.00	514.1	.681	.514	200	.000
42	19.5	1290	.0038655	12.54	.00	227.3	.683	.514	200	.000
43	20.2	1347	.0054322	17.08	.00	382.1	.681	.514	200	.000
44 #	21.1	1352	.0052886	16.59	.00	517.1	.681	.514	200	.000
45	23.7	1290	.0035225	11.43	7.10	227.1	.683	.514	200	1.030
46	24.1	1347	.0050611	15.91	6.96	383.2	.681	.514	200	1.032
47	24.9	1352	.0062207	19.51	6.95	516.8	.681	.514	200	1.034
48	25.5	1290	.0029943	9.71	14.03	227.1	.683	.514	200	2.048

Table I.1 Convective Heat Transfer - Similarity Parameters (continued)

Exp.	T_s(°C)	T_f(°C)	h(W/cm^2°C)	Nu	$(Re)_o$	Re	Pr	L/D	M	V_o(cm/s)
49	25.6	1347	.0047263	14.86	13.75	381.5	.681	.514	200	2.048
50 #	26.2	1352	.0042368	13.29	13.73	515.6	.681	.514	200	2.052
51	23.1	1352	.0059665	18.71	13.71	518.2	.681	.514	200	2.027
52 #	20.6	1352	.0051415	16.12	.00	516.8	.681	.514	200	.000
53	22.5	1352	.0058205	18.25	13.67	515.7	.681	.514	200	2.021
54	299.9	1352	.0057929	18.17	8.10	514.9	.681	.514	200	2.344
55	300.8	1352	.0056721	17.79	6.05	516.6	.681	.514	200	1.752
56	300.2	1352	.0059194	18.56	4.07	515.6	.681	.514	200	1.177
57	301.1	1352	.0063329	19.86	1.75	514.6	.681	.514	200	.509
58	294.6	1352	.0049028	15.38	18.93	515.1	.681	.514	200	5.423
59	24.5	1320	.0043950	14.02	3.44	519.4	.682	2.059	200	.508
60	28.0	1320	.0037436	11.94	10.36	520.3	.682	2.059	200	1.547
61	30.1	1320	.0030300	9.67	19.11	520.6	.682	2.059	200	2.872
62	31.5	1320	.0026954	8.60	25.24	519.8	.682	2.059	200	3.812
63	32.5	1320	.0029382	9.37	22.44	520.2	.682	2.059	200	3.400
64	34.6	1320	.0035320	11.27	14.93	519.8	.682	2.059	200	2.278

Table I.1 Convective Heat Transfer - Similarity Parameters (continued)

Exp.	T_s(°C)	T_f(°C)	h(W/cm^2°C)	Nu	$(Re)_o$	Re	Pr	L/D	M	V_o(cm/s)
65	23.8	1257	.0048675	16.09	3.51	531.5	.684	2.831	200	.509
66	25.7	1257	.0042075	13.90	10.48	531.3	.684	2.831	200	1.532
67	26.8	1257	.0035802	11.83	19.43	531.2	.684	2.831	200	2.851
68	27.7	1257	.0032356	10.69	25.66	531.1	.684	2.831	200	3.776
69	28.4	1257	.0036372	12.02	22.81	531.0	.684	2.831	200	3.364
70	29.1	1257	.0002846	.94	15.03	531.4	.684	2.831	200	2.221
71	24.0	1320	.0038001	12.12	14.82	518.9	.682	2.059	200	2.134
72	26.7	1319	.0033730	10.77	14.82	383.0	.682	2.059	200	2.152
73	27.9	1205	.0036794	12.53	15.45	230.5	.686	2.059	200	2.162
74	28.9	1257	.0037691	12.45	15.15	528.8	.684	2.831	200	2.169
75	30.0	1287	.0029750	9.67	14.99	386.7	.683	2.831	200	2.177
76	31.0	1165	.0028074	9.78	15.67	234.0	.688	2.831	200	2.182
77	31.2	1359	.0044485	13.90	3.37	511.4	.681	1.201	200	.504
78	33.5	1351	.0042126	13.22	10.11	513.0	.681	1.201	200	1.519
79	34.8	1256	.0032780	10.84	25.61	530.8	.684	1.201	200	3.736
80	154.8	1320	.0032153	10.26	14.93	512.5	.682	2.059	200	3.202

Table I.1 Convective Heat Transfer - Similarity Parameters (continued)

Exp.	T_s(°C)	T_f(°C)	h(W/cm^2°C)	Nu	$(Re)_o$	Re	Pr	L/D	M	V_o(cm/s)
81	156.6	1320	.0031805	10.15	14.91	511.3	.682	2.059	200	3.213
82	157.0	1319	.0032102	10.25	14.91	377.8	.682	2.059	200	3.214
83	157.2	1205	.0028419	9.67	15.54	228.0	.686	2.059	200	3.216
84	156.9	1320	.0028845	9.20	20.25	511.3	.682	2.059	200	4.366
85	26.1	1290	.0039464	12.80	14.99	224.3	.683	.514	150	2.229
86	27.6	1347	.0063173	19.87	14.70	379.8	.681	.514	150	2.240
87	30.5	1352	.0077273	24.24	14.67	513.7	.681	.514	150	2.261
88	32.6	1352	.0069910	21.93	19.61	513.0	.681	.514	150	3.044
89	34.4	1352	.0072992	22.89	6.87	512.4	.681	.514	150	1.072
90 #	26.1	1290	.0007549	2.44	14.99	224.0	.683	.514	250	2.229
91	23.6	1352	.0082708	25.94	3.40	513.6	.681	.514	150	.509
92	26.7	1352	.0072256	22.66	10.15	513.6	.681	.514	150	1.538
93	28.9	1352	.0064483	20.22	24.86	513.6	.681	.514	150	3.792
94	30.8	1347	.0068707	21.61	3.40	379.8	.681	.514	150	.521
95	32.9	1347	.0065576	20.62	10.16	380.6	.681	.514	150	1.569
96	33.5	1347	.0057929	18.22	24.89	380.1	.681	.514	150	3.849

Table I.1 Convective Heat Transfer - Similarity Parameters (continued)

Exp.	T_s(°C)	T_f(°C)	n(W/cm^2°C)	Nu	$(Re)_o$	Re	Pr	L/D	M	V_o(cm/s)
97	34.3	1290	.0047995	15.57	3.47	225.7	.683	.514	150	.527
98	35.9	1290	.0042062	13.64	10.36	225.4	.683	.514	150	1.584
99	35.2	1290	.0031043	10.07	25.39	225.7	.683	.514	150	3.871
100	22.1	1359	.0044227	13.82	3.32	506.1	.681	1.201	200	.519
101	24.5	1359	.0040865	12.77	9.93	506.2	.681	1.201	200	1.563
102	27.0	1359	.0029445	9.20	24.34	505.7	.681	1.201	200	3.864
103	29.8	1319	.0040773	13.02	3.36	378.7	.682	2.059	200	.532
104	31.8	1319	.0036096	11.52	10.06	372.7	.682	2.059	200	1.601
105	32.0	1319	.0025422	8.11	24.68	378.6	.682	2.059	200	3.928
106	33.0	1205	.0038035	12.95	3.51	228.5	.686	2.059	200	.538
107	34.3	1205	.0034796	11.85	10.48	228.5	.686	2.059	200	1.614
108	33.8	1205	.0024882	8.47	25.69	228.5	.686	2.059	200	3.949
109 #	33.0	1287	.0026359	8.56	3.40	383.3	.683	2.831	200	.538
110	35.8	1287	.0032757	10.64	10.17	382.9	.683	2.831	200	1.622
111	35.3	1287	.0030808	10.01	24.94	382.4	.683	2.831	200	3.968
112	36.1	1165	.0041314	14.40	3.56	232.4	.688	2.831	200	.543

Table I.1 Convective Heat Transfer - Similarity Parameters (continued)

Exp.	T_s(°C)	T_f(°C)	h(W/cm^2°C)	Nu	$(Re)_o$	Re	Pr	L/D	M	V_o(cm/s)
113	36.6	1165	.0032331	11.27	10.64	232.4	.688	2.831	200	1.625
114	35.7	1165	.0029881	10.41	26.10	232.4	.688	2.831	200	3.974
115	31.9	1205	.0038821	13.22	3.51	228.5	.686	2.059	200	.536
116	35.4	1287	.0027696	9.00	24.95	382.4	.683	2.831	200	3.972
117	29.1	1352	.0064078	20.10	-3.41	512.2	.681	.514	200	-.524
118	26.7	1352	.0070033	21.96	-3.39	510.6	.681	.514	200	-.517
119	28.2	1352	.0070715	22.18	-7.45	512.2	.681	.514	200	-1.142
120	27.7	1352	.0072636	22.78	-10.19	511.0	.681	.514	200	-1.559
121	26.1	1352	.0073773	23.14	-19.14	511.8	.681	.514	200	-2.890
122	29.3	1352	.0084615	26.54	-25.71	510.5	.681	.514	200	-3.923
123	31.3	1347	.0063201	19.87	-10.22	378.4	.681	.514	200	-1.568
124	29.8	1347	.0069210	21.76	-25.70	379.3	.681	.514	200	-3.921
125	34.4	1290	.0042730	13.86	-3.45	225.5	.683	.514	200	-.524
126	30.8	1290	.0046245	15.00	-10.38	225.5	.683	.514	200	-1.559
127	28.5	1290	.0051074	16.57	-19.66	225.2	.683	.514	200	-2.928
128	28.5	1290	.0053156	17.24	-26.57	225.2	.683	.514	200	-3.959

Table I.2 Convective Heat Transfer - Similarity Parameters
Freely Suspended Screen

Exp.	T_s(°C)	T_f(°C)	h(W/cm^2°C)	Nu	$(Re)_o$	Re	Pr	L/D	M	V_o(cm/s)
15	41.0	1287	.0067847	22.05	.00	382.2	.683	2.831	200	.000
65	24.4	1352	.0097309	30.52	.00	512.0	.681	.514	200	.000
67	23.0	1290	.0056933	18.47	.00	221.2	.683	.514	200	.000
68	27.7	1257	.0088090	29.11	.00	529.3	.684	2.831	200	.000
69	22.6	1165	.0036470	12.71	.00	231.8	.688	2.831	200	.000
70	23.1	1205	.0053637	18.26	.00	228.2	.686	2.059	200	.000
71	22.8	1319	.0067398	21.52	.00	377.9	.682	2.059	200	.000
73	25.7	1347	.0074428	23.41	.00	374.3	.681	.514	200	.000
74	22.7	1256	.0040437	13.37	.00	224.0	.684	1.201	200	.000
75	26.3	1351	.0064245	20.16	.00	373.8	.681	1.201	200	.000
76	32.7	1308	.0078480	25.21	.00	519.8	.682	1.201	200	.000
77	23.6	1320	.0071295	22.75	.00	517.7	.682	2.059	200	.000
1	30.2	1352	.0083099	26.06	.00	511.4	.681	.514	200	.000
2	32.2	1257	.0081960	27.09	.00	529.3	.684	2.831	200	.000
3	32.7	1257	.0080392	26.57	.00	529.3	.684	2.831	200	.000

APPENDIX J

SUMMARY OF FABRIC DESTRUCTION TIMES

Listed in Tables J.1 to J.13 is the reduced data for the ignition time measurements of the igniting GIRCFF fabrics [6]. The ignition times were corrected for the exposure time delay and the overall convective film coefficients used to normalize the heat flux were evaluated using the results of this thesis.

Table J.1. Summary of Fabric Destruction Times with CITA, GIRCFF Fabric No. 1

GIRCFF FABRIC NO. 1 (Polyester Cotton)

k/δ = .017300 W/cm^2K

C_p = 1.494 Ws/gK

$\rho\delta$ = .023490 g/cm^2

T_i = 416.00 °C

Exp. No.	L cm	$\dot{m}_{mix}$ g/h	T_o °C	T_f °C	θ_f	τ s	$\bar{\tau}^{\circ}_i$	$\bar{\tau}_i$	θ_m	$\bar{2h}$ W/cm^2	Fo	q*
25	10.50	2929	22.2	1255	3.130	6.985	.384	0.908	.531	.004563	3.443	0.685
28	10.50	1262	22.7	1082	2.693	9.826	.464	1.210	.538	.004324	4.843	0.538
32	7.60	2176	22.2	1310	3.270	6.401	.364	0.805	.530	.004415	3.155	0.699
33	7.60	1265	22.2	1220	3.041	9.066	.398	1.069	.533	.004139	4.469	0.600
39	1.90	2948	23.0	1352	3.381	3.315	.350	0.618	.529	.006550	1.634	1.080

Table J.2. Summary of Fabric Destruction Times with CITA, GIRCFF Fabric No. 4

GIRCFF FABRIC NO. 4 (Cotton)

k/δ = .015000 W/cm^2K

C_p = 1.424 Ws/gK

$\rho\delta$ = .029630 g/cm^2

T_i = 297.00 °C

Exp. No.	L cm	$\dot{m}_{mix}$ g/h	T_o °C	T_f °C	θ_f	τ s	$\bar{\tau}^o_i$	$\bar{\tau}_i$	θ_m	$\bar{2h}$ W/cm^2	Fo	q*
4	10.50	1263	22.2	1165	4.158	9.382	.275	0.961	.522	.004322	3.335	1.047
8	10.50	2933	22.2	1257	4.493	7.874	.251	0.851	.520	.004560	2.799	1.207
12	7.60	1262	22.2	1226	4.380	10.512	.259	1.030	.521	.004137	3.737	1.064
31	7.60	1264	22.2	1220	4.358	9.513	.260	0.932	.521	.004137	3.381	1.058
34	7.60	2170	22.8	1307	4.683	8.568	.240	0.895	.519	.004412	3.046	1.224
38	1.90	2945	23.0	1348	4.835	5.385	.231	0.835	.519	.006548	1.914	1.884

Table J.3. Summary of Fabric Destruction Times with CITA, GIRCFF Fabric No. 5

GIRCFF FABRIC NO. 5 (Cotton)

k/δ = .009500 W/cm^2K

C_p = 1.761 Ws/gK

$\rho\delta$ = .013710 g/cm^2

T_i = 311.00 °C

Exp. No.	L cm	$\dot{m}_{mix}$ g/h	T_o °C	T_f °C	θ_f	τ s	$\bar{\tau}^{\circ}_i$	$\bar{\tau}_i$	θ_m	$\bar{2h}$ W/cm^2K	Fo	q*
21	7.60	1306	22.7	1205	4.100	4.376	.279	.753	.523	.004158	1.721	1.565
35	7.60	2204	23.6	1319	4.507	3.406	.250	.626	.520	.004439	1.340	1.862
39	10.50	2925	24.1	1257	4.297	2.950	.264	.561	.522	.004562	1.160	1.824
64	10.60	1266	22.7	1165	3.962	3.826	.290	.688	.524	.004342	1.505	1.571
93	1.90	1261	24.4	1327	4.545	2.818	.248	.455	.520	.003906	1.108	1.654
94	1.90	2190	21.9	1351	4.597	2.663	.245	.604	.520	.005483	1.047	2.353
95	1.90	2965	21.9	1346	4.580	2.435	.246	.662	.520	.006572	0.958	2.808

Table J.4. Summary of Fabric Destruction Times with CITA, GIRCFF Fabric No. 6

GIRCFF FABRIC NO. 6 (Polyester Cotton)

k/δ = .018300 W/cm^2K

C_p = 1.545 Ws/gK

$\rho\delta$ = .023570 g/cm^2

T_i = 416.00 °C

Exp. No.	L cm	$\dot{m}_{mix}$ g/h	T_o °C	T_f °C	θ_f	τ s	τ_i°	$\bar{\tau}_i$	θ_m	$\bar{2h}$ W/cm^2K	Fo	q*
35	7.60	1266	23.0	1172	2.923	6.166	.418	.700	.534	.004139	3.098	0.540
63	7.60	2183	22.8	1293	3.230	5.734	.370	.695	.530	.004415	2.881	0.651
66	10.50	2988	22.8	1272	3.177	5.542	.377	.694	.531	.004563	2.785	0.659
68	10.50	1264	23.0	1154	2.877	6.226	.426	.739	.535	.004324	3.128	0.553
71	1.90	2968	22.8	1347	3.367	3.335	.352	.599	.529	.006550	1.675	1.015

Table J.5. Summary of Fabric Destruction Times with CITA, GIRCFF Fabric No. 8

GIRCFF FABRIC NO. 8 (Polyester Cotton)

k/δ = .011200 W/cm^2K

C_p = 2.045 Ws/gK

$\rho\delta$ = .016190 g/cm^2

T_i = 450.00 °C

Exp. No.	L cm	$\dot{m}_{mix}$ g/h	T_o °C	T_f °C	θ_f	τ s	$\bar{\tau}^{\circ}_i$	$\bar{\tau}_i$	θ_m	$\bar{2h}$ W/cm^2K	Fo	q*
41	7.60	1261	24.4	1176	2.705	2.346	.461	.294	.538	.004155	.793	0.804
43	1.90	2937	24.4	1338	3.086	0.745	.391	.147	.532	.006569	.252	1.497
45	10.50	2955	22.2	1314	3.019	0.875	.402	.121	.533	.004588	.295	1.018
47	10.50	1257	22.2	1165	2.671	2.436	.468	.319	.538	.004339	.824	0.826
56	7.60	2176	22.2	1343	3.087	1.036	.391	.138	.532	.004435	.350	1.011
119	1.90	3025	22.2	1282	2.944	1.185	.414	.235	.534	.006569	.400	1.413
123	1.90	2951	22.5	1367	3.145	0.857	.382	.170	.531	.006569	.289	1.532

Table J.6. Summary of Fabric Destruction Times with CITA, GIRCFF Fabric No. 9

GIRCFF FABRIC NO. 9 (Cotton)

k/δ = .005000 W/cm^2K

C_p = 1.558 Ws/gK

$\rho\delta$ = .026480 g/cm^2

T_i = 308.00 °C

Exp. No.	L cm	$\dot{m}_{mix}$ g/h	T_o °C	T_f °C	θ_f	τ s	$\bar{\tau}^o_i$	$\bar{\tau}_i$	θ_m	$\bar{2h}$ W/cm^2K	Fo	q*
1	10.50	1271	21.6	1165	3.992	6.270	.288	.659	.523	.004342	0.759	3.011
9	10.50	2138	22.2	1303	4.481	4.154	.252	.470	.521	.004670	0.503	3.699
13	7.60	1264	22.2	1226	4.212	8.290	.271	.835	.522	.004158	1.004	3.068
14	7.60	2067	22.2	1340	4.610	4.845	.244	.521	.520	.004439	0.587	3.631
29	1.90	2947	21.4	1352	4.642	3.318	.242	.528	.520	.006572	0.402	5.418

Table J.7. Summary of Fabric Destruction Times with CITA, GIRCFF Fabric No. 10

GIRCFF FABRIC NO. 10 (Cotton)

k/δ = .036000 W/cm^2K

C_p = 2.398 Ws/gK

$\rho\delta$ = .006650 g/cm^2

T_i = 443.00 °C

Exp. No.	L cm	$\dot{m}_{mix}$ g/h	T_o °C	T_f °C	θ_f	τ s	$\bar{\tau}_i^o$	$\bar{\tau}_i$	θ_m	$\bar{2h}$ W/cm^2K	Fo	q*
65	10.50	1266	22.7	1165	2.717	1.396	.458	.383	.538	.004382	3.151	.265
75	10.50	2939	23.8	1257	2.941	0.974	.415	.284	.534	.004658	2.200	.311
76	7.60	1262	22.5	1205	2.812	1.396	.439	.367	.536	.004199	3.151	.265
78	7.60	2181	22.6	1319	3.083	1.376	.391	.387	.532	.004492	3.106	.318
118	1.90	2990	22.2	1316	3.074	1.245	.393	.516	.532	.006620	2.810	.467
122	1.90	2951	22.5	1357	3.173	0.885	.378	.367	.531	.006620	1.997	.485

Table J.8. Summary of Fabric Destruction Times with CITA, GIRCFF Fabric No. 15

GIRCFF FABRIC NO. 15 (Polyester Cotton)

k/δ = .02100 W/cm^2K

C_p = 1.624 Ws/gK

$\rho\delta$ = .022820 g/cm^2

T_i = 426.00 °C

Exp. No.	L cm	$\dot{m}_{mix}$ g/h	T_o °C	T_f °C	θ_f	τ s	$\bar{\tau}^{\circ}_i$	$\bar{\tau}_i$	θ_m	$\bar{2h}$ W/cm^2K	Fo	q*
41	10.50	2953	22.7	1257	3.060	2.930	.395	.364	.532	.004608	1.660	.554
42	10.50	1269	22.7	1165	2.832	2.882	.435	.338	.536	.004351	1.633	.475
44	7.60	1268	22.8	1205	2.932	3.846	.417	.432	.534	.004168	2.179	.475
46	7.60	2177	22.8	1319	3.214	3.096	.372	.371	.530	.004451	1.754	.568
56	1.90	2950	22.8	1397	3.408	2.013	.347	.357	.528	.006584	1.140	.902

Table J.9. Summary of Fabric Destruction Times with CITA, GIRCFF Fabric No. 16

GIRCFF FABRIC NO. 16 (Polyester Cotton)

k/δ = .015000 W/cm^2K

C_p = 1.500 Ws/gK

$\rho\delta$ = .013140 g/cm^2

T_i = 473.00 °C

Exp. No.	L cm	$\dot{m}_{mix}$ g/h	T_o °C	T_f °C	θ_m	τ s	$\bar{\tau}^o_i$	$\bar{\tau}_i$	θ_m	$2\bar{h}$ W/cm^2K	Fo	q*
17	7.60	2174	21.9	1294	2.819	2.346	.437	.527	.536	.004432	1.785	0.674
18	7.60	1269	21.9	1219	2.653	2.068	.472	.435	.539	.004153	1.573	0.585
26	10.50	2945	22.2	1267	2.761	2.542	.449	.591	.537	.004585	1.934	0.679
27	10.50	1264	22.7	1165	2.536	2.826	.501	.621	.541	.004337	2.150	0.576
30	1.90	2949	21.6	1352	2.947	1.874	.414	.624	.534	.006566	1.426	1.056

Table J.10. Summary of Fabric Destruction Times with CITA, GIRCFF Fabric No. 17

GIRCFF FABRIC NO. 17 (Polyester Cotton)

k/δ = .029000 W/cm^2K

C_p = 1.840 Ws/gK

$\rho\delta$ = .008550 g/cm^2

T_i = 480.00 °C

Exp. No.	L cm	$\dot{m}_{mix}$ g/h	T_o °C	T_f °C	θ_f	τ s	$\bar{\tau}_i^o$	$\bar{\tau}_i$	θ_m	$\bar{2h}$ W/cm^2K	Fo	q*
66	10.50	1267	22.7	1165	2.497	1.736	.511	.480	.542	.004355	3.200	.293
77	7.60	1262	22.6	1205	2.585	1.696	.489	.449	.540	.004171	3.126	.294
79	7.60	2179	22.7	1285	2.760	1.341	.449	.379	.537	.004456	2.471	.341
80	10.50	2954	22.7	1257	2.699	0.835	.462	.244	.538	.004613	1.539	.343
117	1.90	2958	22.2	1340	2.878	0.995	.426	.416	.535	.006587	1.834	.532
121	1.90	2941	22.5	1381	2.969	1.075	.410	.450	.534	.006587	1.981	.553

Table J.11. Summary of Fabric Destruction Times with CITA, GIRCFF Fabric No. 18

GIRCFF FABRIC NO. 18 (Cotton)

k/δ = .007500 W/cm^2K

C_p = 1.735 Ws/gK

$\rho\delta$ = .012880 g/cm^2

T_i = 311.00 °C

Exp. No.	L cm	$\dot{m}_{mix}$ g/h	T_o °C	T_f °C	θ_f	τ s	$\bar{\tau}^{\circ}_i$	$\bar{\tau}_i$	θ_m	$2\bar{h}$ W/cm^2K	Fo	q*
60	10.50	1258	23.5	1165	3.970	3.580	.290	.695	.524	.004342	1.201	1.995
82	10.50	2958	23.0	1257	4.284	2.824	.265	.580	.522	.004593	0.947	2.304
83	7.60	1260	22.8	1198	4.077	3.596	.281	.669	.523	.004158	1.206	1.970
84	7.60	2168	23.0	1315	4.486	2.551	.252	.506	.520	.004439	0.865	2.346
116	1.90	2949	22.2	1353	4.608	2.745	.244	.807	.520	.006572	0.921	3.581
120	1.90	2952	22.5	1381	4.708	2.010	.238	.591	.519	.006572	0.674	3.670

Table J.12. Summary of Fabric Destruction Times with CITA, GIRCFF Fabric No. 19

GIRCFF FABRIC NO. 19 (Cotton, Fire Rtd)

k/δ = .011000 W/cm^2K

C_p = 2.132 Ws/gK

$\rho\delta$ = .014890 g/cm^2

T_i = 497.00 °C

Exp. No.	L cm	$\dot{m}_{mix}$ g/h	T_o °C	T_f °C	θ_f	τ s	$\bar{\tau}^o_i$	$\bar{\tau}_i$	θ_m	$\bar{2h}$ W/cm^2K	Fo	q*
58	10.50	2946	22.2	1301	2.693	2.335	.464	.337	.538	.004584	0.809	0.897
59	10.50	1257	23.5	1165	2.410	2.646	.535	.361	.544	.004337	0.916	0.735
61	7.60	1258	23.5	1186	2.455	2.931	.523	.383	.543	.004153	1.015	0.721
62	7.60	2166	23.6	1325	2.749	2.391	.452	.333	.537	.004432	0.828	0.891
105	1.90	2953	21.6	1363	2.821	1.641	.437	.339	.536	.006566	0.568	1.364

Table J.13. Summary of Fabric Destruction Times with CITA, GIRCFF Fabric No. 20

GIRCFF FABRIC NO. 20 (Wool)

k/δ = .007500 W/cm^2K

C_p = 1.270 Ws/gK

$\rho\delta$ = .019930 g/cm^2

T_i = 480.00 °C

Exp. No.	L cm	$\dot{m}_{mix}$ g/h	T_o °C	T_f °C	θ_f	τ s	$\bar{\tau}^{\circ}_i$	$\bar{\tau}_i$	θ_m	$2\bar{h}$ W/cm^2K	Fo	q*
16	7.60	2175	21.9	1334	2.864	2.568	.429	.449	.535	.004432	.760	1.376
19	7.60	1270	21.9	1208	2.589	2.290	.488	.375	.540	.004153	.678	1.134
2	10.50	1263	21.6	1029	2.197	2.826	.607	.484	.550	.004337	.837	0.952
10	10.50	2948	22.2	1291	2.771	1.875	.447	.339	.537	.004585	.555	1.365
36	7.60	1263	23.0	1196	2.566	2.958	.493	.485	.540	.004153	.876	1.121
37	7.60	1265	23.0	1229	2.638	3.013	.476	.494	.539	.004153	.892	1.162
61	1.90	2950	22.8	1366	2.937	1.595	.416	.413	.534	.006566	.472	2.104

BIBLIOGRAPHY

1. "America Burning," National Commission on Fire Prevention and Control, U. S. Government Printing Office, Washington, D. C., Stock Number 5200-00004, May, 1973.

2. "Studies of Death, Injuries, and Economic Losses Resulting from Accidental Burning of Products, Fabrics or Related Materials," U. S. Department of Health, Education and Welfare, Fourth Annual Report, U. S. Government Printing Office, Washington, D. C., 1972.

3. Alkidas, A., Champion, E. R., Giddens, W. E., Hess, R. W., Kumar, B., Naveda, O. A. A., Durbetaki, P., Williams, P. T., and Wulff, W., "Study of Hazards from Burning Apparel and the Relation of Hazards to Test Methods," Second Final Report, NSF Grant GI-31882, Georgia Institute of Technology, Atlanta, Georgia, December, 1972, National Technical Information Access No. COM-10956.

4. Alkidas, A., Hess, R. W., Wulff, W., and Zuber, N., "Study of Hazards from Burning Apparel and the Relation of Hazards to Test Methods," Final Report, NSF Grant No. GK-27189, Georgia Institute of Technology, Atlanta, Georgia, December, 1971, National Technical Information Access No. COM-73-10954.

5. Tribus, M., "Decision Analysis Approach to Satisfying the Requirements of the Flammable Fabrics Act," Paper presented at the Textile and Needle Trades Division, American Society of Quality Control, Greensboro, North Carolina, February 12, 1970.

6. Champion, E. R., "Determination of Fabric Ignition Times Through Use of a Convective Heat Source Apparatus," M.S. Thesis, Georgia Institute of Technolgy, Atlanta, Georgia, 1973.

7. Heskestad, G., "Ease of Ignition of Fabrics Exposed to Flaming Heat Sources," First Quarterly Progress Report, Factory Mutual Research, FMRC Ser. No. 19967, April 1, 1972.

8. Heskestad, G., "Ease of Ignition of Fabrics Exposed to Flaming Heat Sources," Second Quarterly Progress Report, Factory Mutual Research, FMRC Ser. No. 19967, July 1, 1972.

9. Gardon, R., "A Transducer for the Measurement of Heat-Flow Rate," Journal of Heat Transfer, Trans. ASME, Vol. 82, 1960, pp. 396-398.

10. Wolf, L., Jr., Obremski, H. J., and Christian, W. J., "Transpiration Cooling in an Arc-Jet Environment," AIAA Journal, Vol. 4, 1966, pp. 747-749.

11. Eckert, E., Drake, R., and Soehngen, E., "Manufacture of a Zehnder-Mach Interferometer," USAF, Air Material Command, Dayton, Ohio, Technical Report 5721, 1948.

12. Vickers, J. M. F., "Heat Transfer Coefficients Between Fluid Jets and Normal Surfaces," Industrial and Engineering Chemistry, Vol. 51, 1959, pp. 967-972.

13. Friedman, S. J., and Mueller, A. C., "Heat Transfer to Flat Surfaces," Inst. Mech. Engr. and ASME Proceedings of the General Discussion on Heat Transfer, 1951, pp. 138-142.

14. Perry, K. P., "Heat Transfer by Convection from a Hot Gas Jet to a Plane Surface," Proceedings, the Institution of Mechanical Engineers, Vol. 168, 1954, pp. 775-780.

15. Gardon, R., and Cobonpue, J., "Heat Transfer Between a Flat Plate and Jets of Air Impinging on It," International Developments in Heat Transfer, Proceedings, 2nd International Heat Transfer Conference, ASME, New York, 1962, pp. 454-460.

16. Daane, R. A., and Han, S. T., "An Analysis of Air-Impingement Drying," TAPPI, Vol. 44, 1961, pp. 73-80.

17. Gardon, R., and Akfirat, J. C., "The Role of Turbulence in Determining the Heat Transfer Characteristics of Impinging Jets," Int. J. of Heat Mass Transfer, Vol. 8, 1965, pp. 1261-1272.

18. Hrycak, P., Lee, D. T., Gauntner, J. W., and Livingood, J. N. B., "Experimental Flow Characteristics of a Single Turbulent Jet Impinging on a Flat Plate," NASA TN D-5690, 1970.

19. Gardon, R., and Akfirat, J. C., "Heat Transfer Characteristics of Impinging Two-Dimensional Air Jets," Journal of Heat Transfer, Trans. ASME, Vol. 88, 1966, pp. 101-108.

20. Schlichting, H., Boundary Layer Theory, 6th Ed., McGraw-Hill, New York, 1968, pp. 681-687.

21. Corrsin, S., "Investigation of Flow in an Axially Symmetrical Heated Jet of Air," NACA Wartime Report, Series WR-92, 1943.

22. Alkidas, A., Champion, E. R., Giddens, W., Hess, R. W., Durbetaki, P., and Wulff, W., "Study of Hazards from Burning Apparel and the Relation of Hazards to Test Methods," Progress Report No. 5, Georgia Institute of Technology, July 1, 1972.

23. Slattery, J. C., Momentum, Energy and Mass Transfer in Continua, McGraw-Hill, New York, 1972.

24. Streeter, V. L., Handbook of Fluid Dynamics, 1st Ed., McGraw-Hill, New York, 1961, p. 16-21.

25. Fishenden, M., and Saunders, O. A., An Introduction to Heat Transfer, Oxford University Press, London, 1950, pp. 89-101.

26. Kreith, F., Principles of Heat Transfer, 2nd Ed., International Textbook, Scranton, Pennsylvania, 1965.

27. Rohsenow, W. M., and Hartnett, J. P., Handbook of Heat Transfer, McGraw-Hill, New York, 1973, pp. 1-3, 6-1 to 6-16, 7-15 to 7-163.

28. Sparrow, E. M., and Cess, R. D., "Free Convection with Blowing or Suction," Journal of Heat Transfer, Vol. 83, 1961, pp. 387-389.

29. Eichhorn, R., "The Effect of Mass Transfer on Free Convection," Journal of Heat Transfer, Trans. ASME, Series C., Vol. 82, 1960, pp. 260-263.

30. Fluid Meters: Their Theory and Application, Report of ASME Research Committee on Fluid Meters, 5th Ed., 1959, p. 87.

31. Eckert, E. R. G., and Drake, R. M., Analysis of Heat and Mass Transfer, McGraw-Hill, New York, 1972, pp. 445-453.

32. McNaughton, K. J., and Sinclair, C. G., "Submerged Jets in Short Cylindrical Flow," Journal of Fluid Mechanics, Vol. 25, 1966, pp. 367-375.

33. Acree, R. L., Champion, E. R., Durbetaki, P., Lee, C., Naveda, O. A. A., Wedel, G. L., Williams, P. T., and Wulff, W., "Fabric Ignition," Third Annual Report, NSF Grant GI-31882, Georgia Institute of Technology, Atlanta, Georgia, March, 1974.

34. Multi-Metal Wire Cloth, Inc., Catalog, 1973, pp. 26-27.

35. Croom, B., and Leyke, E. W., "Thermodynamic, Transport, and Flow Properties for the Products of Methane Burned in Oxygen Enriched Air," NASA SP-3035, 1966.

36. Hilsenrath, J., Beckett, C. W., Benedict, W. S., Fano, L., Hodge, H. J., Masi, J. F., Nuttal, R. L., Touloukian, Y. S., and Wooley, H. W., Tables of Thermodynamic and Transport Properties of Air, Argon, Carbon Dioxide, Carbon Monoxide, Hydrogen, Nitrogen, Oxygen, and Steam, Pergamon Press, New York, 1960.

37. Griffiths, E., "The Physical Properties of a Series of Steels--Part II," The Journal of the Iron and Steel Institute, Vol. CLIV, 1946, pp. 82-96.

38. Eldridge, H. W., and Deem, H. W., "Report on Physical Properties of Metal and Alloys from Cryogenic to Elevated Temperature," ASTM Special Technical Publication No. 296, 1961, pp. 62-63.

39. Touloukian, Y. S., Thermophysical Properties of High Temperature Solid Materials, Volume 3: Ferrous Alloys, MacMillan, New York, 1967, pp. 155-156 and 161-162.

40. Douglas, T. B., and Victor, A. C., "Enthalpy and Specific Heat of Nine Corrosion--Resistant Alloys at High Temperature," Journal of Research of the National Bureau of Standards, Vol. 65C, 1961, pp. 65-69.

41. McCarter, R. J., "Report on the Thermal Analysis of GIRCFF Fabrics," NBS Report 10846, May 11, 1972.

42. "The Omega Temperature Measurement Handbook," Omega Engineering, Inc., Stanford, Connecticut, 1973.

43. Bird, R. B., Stewart, W. E., and Lightfoot, E. N., Transport Phenomena, John Wiley, New York, 1960.

44. Reid, R. C., and Sherwood, T. K., The Properties of Gases and Liquids, McGraw-Hill, New York, 1958.